Title
Investigating the roles of ribosome-associated proteins in translational regulation of gene expression

Author
Riepe, Celeste

Publication Date
2019

Peer reviewed|Thesis/dissertation

Investigating the roles of ribosome-associated proteins in translational regulation of gene expression

By

Mary Celeste Riepe

A dissertation submitted in partial satisfaction of the

requirements for the degree of

Doctor of Philosophy

in

Molecular and Cell Biology

in the

Graduate Division

of the University of California, Berkeley

Committee in charge:

Professor Nicholas Ingolia, Co-Chair
Professor Jacob Corn, Co-Chair
Professor Gloria Brar
Professor Jamie Cate
Professor Daniel Nomura

Spring 2019

Abstract

Investigating the roles of ribosome-associated proteins in translational regulation of gene expression

by

Mary Celeste Riepe

Doctor of Philosophy in Molecular and Cell Biology

University of California, Berkeley

Professor Nicholas Ingolia, Co-Chair

Professor Jacob Corn, Co-Chair

The ribosome has long been regarded as the protein producing center of the cell, yet we are still defining its role as a target of gene regulation in the cell. Towards this end, I developed a proteomics-based approach to uncover novel ribosome-associated proteins that regulate translation in the cell. I also worked with the Kopito Lab at Stanford University to understand why a core ribosomal protein, RPL26, is post-translationally modified by a ubiquitin-like protein, UFM1. Additionally, I collaborated with the Corn Lab at UC Berkeley and ETH Zurich to describe how double-stranded DNA damage leads to the depletion of core ribosomal proteins, RPL40 and RPS27A. These projects demonstrate that ribosome composition is neither static nor homogeneous but can be altered depending on the environmental and cellular context.

Table of Contents

Dedication

To Elena Zelin.

Thank you for letting me follow up with your serendipitous discoveries about translation and genome editing for my thesis project. Your patience with my continuous stream of emails and experimental mishaps has been greatly appreciated.

Chapter 1: Specialized Ribosomes and Their Role in Translational Regulation of Gene Expression

The composition of the ribosome is remarkably well-conserved: in all walks of life, two ribosomal subunits made of RNA and protein join together on a messenger RNA to decode nucleotide codons into functional proteins. In humans, the ribosome is made of large and small subunits that are composed of 80 core ribosomal proteins and 4 ribosomal RNAs. The remarkable evolutionary conservation of ribosomal proteins and rRNAs from bacteria to humans has informed our textbook model of the ribosome as unvarying molecular machine with identical structure, composition, and function.

My work seeks to upend this textbook version of the ribosome. We first developed a proteomics-based method to establish that other proteins beyond the 80 core ribosomal proteins are key constituents of the translation machinery of the cell (*Chapter 3: A Proteomics-Based Approach to Identifying Novel Ribosome-Associated Proteins*). Secondly, we investigate why the human ribosome is post translationally modified by ubiquitin-like protein, UFM1, at the endoplasmic reticulum (*Chapter 4: UFMylation of Ribosomal Protein RPL26 Regulates Expression of Extracellular Matrix Proteins*). And lastly, we demonstrate that ribosomes lose two core ribosomal proteins, RPS27A and RPL40, after dsDNA damage (*Chapter 5: Double-Stranded DNA damage triggers ribosome remodeling and translational shutdown*).

In the following section, we will discuss evidence of ribosomal heterogeneity. The subsequent section, *Chapter 2: Translational Regulation of Gene Expression during the DNA Damage Response*, details the role of translation and ribosomal proteins in the DNA damage response, setting the stage for our work describing the changes in ribosome composition in response to DNA damage in *Chapter 5*.

Ribosomes protein composition can change in response to stress

The concept of ribosome heterogeneity was introduced in the 1950s after electron micrographs revealed ribosomes with unique shapes and sizes (Society. et al., 1958). Soon after, Francis Crick promoted the "one gene-one ribosome-one-protein" hypothesis (Crick, 1958), yet this theory was debunked when it was shown that phage messenger RNAs are translated in *E. coli* even though no new ribosomes are synthesized after infection (Brenner and Crick, 1961). This observation led the authors to conclude that the ribosome is a non-specialized molecular machine that translates the genetic information stored in messenger RNA into proteins. This model of a ribosomes as a molecular machine with uniform structure and function has held for decades and is our prevailing textbook model for protein synthesis in the cell. Yet during the 1970s, evidence emerged that *Escherichia coli* ribosomes had different ribosome protein compositions under different growth conditions (Deusser, 1972; Deusser and Wittmann, 1972). While most of the ribosomal proteins remained consistent between growth conditions, ribosome proteins S6, S21, and L12 showed over two fold increase in rich media compared to their levels in when bacteria were grown in nutrient poor media (Deusser, 1972). Thus it was hypothesized that organisms alter their ribosome composition in response to stress.

Ribosome protein composition alters during cellular differentiation

In the 1980s, evidence emerged that ribosomal composition can differ over the course of an organism's life cycle. The first pieces of evidence that cells modify ribosome protein composition came from studies of slime mold life cycle (Ramagopal and Ennis, 1981). Using 2D

electrophoresis of ribosomes, the authors identified 12 proteins that change expression as *Dictyostelium discoideum* differentiates from vegetative growth to spores. This observation led the authors to hypothesize that the specialization of the ribosome population under different conditions lead to changes in protein synthesis rate and gene expression between cell types. In accordance with this hypothesis, (Gunderson et al., 1987) found that that the parasite *Plasmodium berghei* expresses two different rRNA genes depending on whether the organism is in the sporozite form in mosquitos or the asexual form in humans. In the decades following these observations, changes in ribosome protein expression over the course of cellular differentiation has been documented in budding yeast during meiosis (Eisenberg et al., 2018), in *Arabidopsis* cells during embryogenesis (Weijers et al., 2001), and in mouse cells during tissue differentiation (Genuth and Barna, unpublished work).

Transcripts encoding ribosomal proteins are differentially expressed between tissue types

Transcripts encoding ribosomal proteins have been observed to have heterogeneous expression levels between tissue types. In the early 2000s, bioinformatics studies of ribosomal protein EST abundance in human tissue cDNA libraries revealed that 13 genes had heterogeneous expression between human tissue types (Bortoluzzi et al., 2001). (Kondrashov et al., 2011) later observed through microarray analysis that that ribosome protein transcripts exhibit up to a 250 fold difference in expression between mouse embryonic tissue types. Another study (Guimaraes and Zavolan, 2016) analyzed promoter data from the FANTOM Consortium (FANTOM Consortium and the RIKEN PMI and CLST (DGT) et al., 2014) for human ribosome protein and paralog genes from different tissues, primary cell lines, and tumor cells and found that about a quarter of ribosomal proteins showed tissue-specific expression differences. Some of these tissue specific differences in ribosome protein expression even showed evolutionarily conserved between different species. for example, elevated levels of ribosome protein paralog *RPL3L* was observed in skeletal muscle tissues both Rhesus monkeys and chickens, which diverged 300 million years ago.

As these tissue-specific differences are observed at the transcript level, it is still an open question as to whether or not tissues have ribosomes with different protein compositions that are specialized to regulate translation in a tissue-specific manner. (Kondrashov et al., 2011) found that mice haploinsufficient for *RPL38* exhibit homeotic transformations. It was found that RPL38 deficiency leads to decreased translation *Hox* mRNAs and that this decrease appears to be a function of RPL38 at the ribosome, as the protein is not observed in non-ribosomal fractions in the cell. In a follow up study, (Xue et al., 2015) identified regulatory elements in *Hox* mRNAs that require RPL38 for productive translation. Thus it appears that tissues can tailor their ribosome compositions to promote the translation of mRNA elements that are important for tissue-specific functions.

Ribosome protein transcript abundance is altered in cancer

Alterations in ribosome protein transcript levels has been observed in various forms of cancer (Bee et al., 2006; Guo et al., 2011; Henry et al., 1993; Kim et al., 2004; Pogue-Geile et al., 1991; Wong et al., 2014). When comparing ribosome protein transcript expression in malignant tissues versus matched normal tissues, (Guimaraes and Zavolan, 2016) found that dysregulation of ribosomal proteins was a common feature of cancer cells, with cancer cells having an ~30% increase in median ribosome protein expression. Certain types of ribosomal proteins were consistently increased across cancers whereas others exhibited decreased

expression. Many of the ribosomal proteins with decreased expression in cancer cells have been reported to activate cell-cycle regulator p53 (Wang et al., 2015b), suggesting that their decrease in cancer promotes cell growth and proliferation. In other cases, specific ribosomal proteins appeared to be markers of particular cancer types; for example, *RPL26L1* and *RPS27L* were found to be upregulated in breast and thyroid carcinomas but not other cancers. Observations that ribosome protein abundance changes during cancer has led to the hypothesis that cancer cells make specialized ribosomes that promote growth and proliferation. However, most of these observations were made from promoter and transcriptomics datasets, so we cannot rule out the possibility that the changes reflect extraribosomal functions of ribosomal proteins. Thus it remains an open question as to whether or not cancers produce specialized ribosomes that alter the protein production landscape of the cell.

Species differentially express ribosome protein paralogs

Both prokaryotes and eukaryotes can encode different paralogs of ribosomal proteins in their genomes (Sauert et al., 2015). For example, the bacteria *Bacillus subtilis* has paralogs for L31 and S14 that are either with or without zinc binding domains, and *B. subtilis* alternates between these paralogs depending on the presence or absence of zinc (Natori et al., 2007). In *Arabidopsis thaliana,* ribosomal proteins are encoded by two to seven paralogs (Barakat et al., 2001), and some of these paralogs are differentially expressed during development. One paralog, *RPS5A*, is found in dividing cells while the other paralog, *RPS5B*, is expressed in differentiating cells (Weijers et al., 2001). Humans have only one set of paralogous ribosomal genes, *RPS4X*, *RPSY1*, and *RPS4Y2* (Fisher et al., 1990; Lopes et al., 2010). In human males, Y-linked *RPS4Y2* is only expressed in the testis and prostate whereas the other two genes are ubiquitously expressed, suggesting that these organs have ribosomes that are tailored to translate sex-specific mRNAs.

In yeast, 59 ribosomal proteins have paralogs, and 70% of these pairs are asymmetrically expressed (Parenteau et al., 2011). (Komili et al., 2007) compared 12 paralog pairs, and found that strains with null mutations in ribosome protein paralogs have different mRNA localization patterns, resistance to stress, and transcriptional profiles. Paralogous ribosomal proteins were also observed to have different cellular localization and assembly patterns. Based on these observations, the authors proposed that cells have a "ribosome code" in which ribosomes with different protein compositions, post-translational modifications, and rRNA molecules are created to regulate gene expression during translation.

Ribosome proteins are not equimolar in translating ribosomes

Given the heterogeneity of ribosomal protein transcript abundance between different tissues, (Slavov et al., 2015) asked if there was fixed, equimolar stoichiometry between ribosomal proteins in mouse ES and yeast cells. Ribosomal proteins were isolated from different polysome profiling fractions and their relative abundance was compared using a tandem mass tag (TMT) proteomic approach. The authors found that the ratio of ribosomal proteins was different between monosomes and polysomes and that polysomes had different amounts of certain ribosomal proteins depending on the number of ribosomes per transcript. Ribosome protein ratios were different between mouse ES cells and isogenic neural precursor cells. Moreover, ribosome protein ratios between monosomes and polysomes were different between yeast cells under different nutrient conditions. Thus the composition of the ribosome depends on the ratio of mRNA to ribosome as well the growth conditions of the cell.

In another study, (Shi et al., 2017) asked the same question as (Slavov et al., 2015) but quantified absolute protein abundance using selective reaction monitoring (SRM)-based proteomics of mouse ES cell polysomes. Of the 15 ribosomal proteins assayed using this method, 6 were found to exhibit less than 1:1 stoichiometry in ribosomes. The authors also quantified the relative abundance of 76 core ribosomal proteins between free 40S and 60S subunits and polysome fractions using TMT labeling, and they found that 7 proteins that did not have equimolar stoichiometry, suggesting that cells have different populations of ribosomes with varying core ribosomal populations. This led the authors to hypothesize that cells have different populations of ribosomes that are specialized to translate different subsets of transcripts.

Ribosomal proteins can associate with different subsets of mRNAs

As they observed that ribosomes have different stoichiometries of ribosomal proteins, Shi et al., (2017) affinity purified ribosomes with tagged core ribosomal proteins that were found to be substoichiometric and sequenced the associated ribosomes footprints to see if there were differences in associated mRNAs. The authors endogenously tagged RPL10A and RPS25 with the 3X FLAG tag, and when they performed ribosome profiling on the footprints associated with these proteins, they found that there was significant enrichment or depletion of specific mRNAs, including transcripts that were important for cell cycle, metabolism, and development. When the authors performed the same experiment with RPL22, a protein that is not substoichiometric in polysomes, they found that there were few genes that showed significant changes between RPL22 pulldowns and whole cell lysates. This led the authors to conclude that cells have different subpopulations of ribosomes that preferentially translate certain classes of mRNAs.

Ribosomes have different subcellular compositions

Protein expression in the cell can be regulated spatially and temporally through localized translation of mRNAs (Martin and Ephrussi, 2009). The localization of specific mRNAs in subcellular compartments has led to the hypothesis that ribosomes may have specialized compositions in different subcellular regions (Genuth and Barna, 2018). Recent transcriptomics studies found enrichment of ribosomal protein transcripts in axons. This finding came as a surprise given that ribosomes are assembled in the nucleus (Andreassi et al., 2010; Saal et al., 2014; Zivraj et al., 2010). Consequently, (Shigeoka et al.) performed SILAC analysis of newly synthesized proteins in *Xenopus laevis* retinal ganglion cell (RGC) axons and confirmed that ribosomal proteins are actively being synthesized. The authors found that ribosomal proteins at the surface of the ribosome as well as ribosome assembly factors are newly synthesized in axons. Enrichment of certain core ribosomal proteins in axons compared with the whole neuron was also observed, leading the authors to hypothesize either that neurons synthesize ribosomal proteins that are easily lost or damaged in the axon or that axons produced ribosomes are specialized to translate a particular subclass of mRNAs.

Although subcellular mRNA localization is well documented in the field, subcellular ribosome heterogeneity and its functional role in local translation is still an emerging area of research. In *Chapter 4*, we will discuss our recent publication with the Kopito Lab at Stanford in which we found that ribosomes at the endoplasmic reticulum have a unique, conserved post-translational modification, UFM1 (Walczak et al., 2019). We find that modulating this modification leads to global changes in gene expression, particularly for proteins synthesized at the endoplasmic reticulum membrane, suggesting that ribosomes at the endoplasmic reticulum are modified to perform a particular function important for membrane protein synthesis.

Post-translational modifications of ribosomes and their role in gene regulation

As seen in our UFMylation study, differences in auxiliary binding factors like post-translational modifications can contribute to heterogeneity in ribosome structure and function. The first post translational modification of a ribosomal protein was observed over 40 years ago when radioactive phosphorus was shown to modify RPS6 in mouse liver ribosomes (Gressner and Wool, 1974). RPS6 has since been shown to have five different phosphorylation sites, and these sites are phosphorylated through multiple pathways including mTORC1 and PI3K signaling (Meyuhas, 2015). Despite the fact that this modification has long been studied, the exact function of these phosphorylation events remains unknown. Mice lacking the five RPS6 phosphorylation sites are still viable, but have reduced cell size, reduced glucose tolerance, and increased bulk protein synthesis (Ruvinsky et al., 2005).

In another study, ribosomal proteins were found to be the targets of LRRK2, a kinase implicated in familial and sporadic Parkinson's disease (Martin et al., 2014). Ribosomal proteins were identified using mass spectrometry analysis of LRRK2 tandem affinity purifications. *In vitro* kinase assays revealed that LRRK2 phosphorylates 19 of 67 ribosomal proteins, with pathogenic LRRK2 mutants hyperphosphorylating RPS15, RPS11, and RPS27. LRRK2 associates with ribosome fractions *in vivo*, suggesting that these phosphorylation events occur at the ribosome, and expressing pathogenic LRRK2 mutants led to increased bulk translation in human cancer cell lines. Remarkably, mutating the phosphorylated RPS15 residue rescued the neurotoxicity of the LRRK2 pathogenic mutant in flies. However, the exact function of LRRK2-mediated phosphorylation of the ribosome still remains unknown.

Ribosomes are also modified with ubiquitin. Ubiquitin is a 76-amino acid protein that is covalently linked at its C-terminus to lysine residues of other proteins. Ubiquitins have different types of linkages that signal different biological processes: the K48 linkage targets proteins for degradation while other linkages (K6, K11, K27, K29, K33, K63, and M1) are involved in a diverse set of processes such as cell cycle regulation and cytokine signaling (Akutsu et al., 2016). In a screen for proteins with the K63 linkage in yeast, (Silva et al., 2015) found that ribosomal proteins and translation elongation factors were enriched with K63 linkages after oxidative stress. These modifications appeared to stabilize the 80S structure, as yeast mutants lacking these modification had a marked decrease in bulk translation after oxidative stress. The exact biological role of these linkages after oxidative stress has yet to be fully determined, but it is thought that these linkages might recruit trans acting factors that help stabilize the ribosomes.

Ribosomes were also shown to be ubiquitinated after the unfolded protein response (UPR) is activated in mammalian cells (Higgins et al., 2015). The mammalian proteome was screened for ubiquitin modifications that increase with treatment with DTT or tunicamycin, and RPS2 and RPS3 were found to be monoubiquitinated in monosomes and polysomes after these drugs activated the unfolded protein response. When the RPS2 monoubiqutination site was mutated to arginine, cells were more sensitive to tunicamycin- and thapsigargin-induced cell death, suggesting that this modification conferred a cytoprotective effect during the unfolded protein response.

Numerous other ribosomal protein phosphorylation and ubiquitin modifications have been documented in high throughput mass spectrometry studies (www.phosphositeplus.com), yet the vast majority of these events remain unvalidated and are of unknown function. Possible functional roles for these modifications include recruitment of trans-acting regulatory factors to the ribosome or spatial-temporal regulation of translation within the cell (Simsek and Barna,

2017). Future studies will have to tease apart the functional relevance of these modifications and their role in translational regulation of gene expression.

Organisms differentially express rRNA genes in response to their environment

As shown with *Plasmodium berghei* (Gunderson et al., 1987), species can alter their ribosomes by changing rRNA composition. Species from bacteria to humans have multiple copies of rRNA genes in their genome (Sauert et al., 2015), and different expression of rRNA sequence variants has been described in bacteria (Kim et al., 2008; Kurylo et al., 2018; López-López et al., 2007; Song et al., 2019), plants (Cloix et al., 2002), frogs (Wegnez et al., 1972), and sea urchins (Dimarco et al., 2012). The halophilic archean, *Haloarcula marismortui,* was found to increase expression of one of its three 16S operons at high temperatures but decrease its expression at low temperatures, suggesting that the archaea has evolved to produce specialized ribosomes at high temperatures (López-López et al., 2007). *Streptomyces coelicolor*, a gram positive bacteria with a morphologically complex life cycle, was found to differentially express six large subunit rRNA operons over the course of germination to sporulation (Kim et al., 2008), suggesting that these bacteria synthesize distinct ribosomes during development. Differential expression of rRNA operons was also observed in *E. coli* when bacteria were moved from nutrient rich to nutrient poor media (Kurylo et al., 2018). Of the seven rRNA operons in *E. coli*, *rrnH* expression increased the most after the shift. This operon encodes a 16S rRNA variant that increases the translation of RpoS sigma factor, a transcription factor responsible for upregulating stress response genes. Expression of 16S rRNA variant appears to influence antibiotic resistance, cell motility, and biofilm formation. Thus bacteria have evolved a mechanism to influence translation of stress response genes via altering rRNA composition within the ribosome.

Recent work has identified intraspecies and intraindividual heterogeneity in human rRNA sequence, copy number, and expression (Parks et al., 2018). rRNA sequence variance and copy number tracks with human populations, and tissue specific expression patterns were observed for certain operons. Nucleotide variants mapped to functional centers of the ribosomes, suggesting that humans have different ribosomal populations that can have different functional roles in translation. Determining the impact of these nucleotide variants on translation could have interesting implications for human health and disease.

rRNAs are modified in response to environmental cues

Alternative modifications to rRNA molecules can also contribute to ribosome heterogeneity. rRNA molecules are one of the most modified types of RNA in the cell, with 2% of the rRNA nucleotides harboring chemical modifications (Sloan et al., 2017). The most common rRNA modifications are 2'-O-methylation of ribose and isomerization of uridine to pseudouridine (Ψ). These events are directed by small nucleolar RNAs (snoRNAs) that associate and guide proteins that catalyze the modifications. rRNA modifications have roles in ribosome biogenesis and stabilizing the ribosome structure with modifications occurring in close proximity to the functional center of the ribosome. Dysregulation of rRNA modifications has been linked to human disease such as X-linked Dyskeratosis congenita (Heiss et al., 1998) and Bowen-Conradi syndrome (Armistead et al., 2009), and loss-of-function mutations in snoRNAs lead to severe developmental defects in zebrafish (Higa-Nakamine et al., 2012).

The majority of rRNA modifications are constitutive, but a subset have been found to be substoichiometric or modulated in response to stress (Taoka et al., 2015, 2016). Deep sequencing of pseudouridylated *Saccharomyces cerevisiae* rRNAs revealed that the majority of the rRNA

modifications do not change expression after changes in nutrient conditions; however, pseudouridylation of U2314 of the 25S rRNA was observed to shift two fold after post-diauxic growth (Carlile et al., 2014). (Taoka et al., 2015) developed Stable Isotope-Labeled riboNucleic Acid as an internal Standard (SILNAS) mass spectrometry to identify and quantify rRNA modifications *in vivo*, and found that 6 pseudouridine modifications in the yeast *Schizosaccharomyces pombe* varied when yeast were grown at different temperatures. For example, pseudouridylation of U76 in the 5.8S rRNA increased from 44% to 90% when yeast were transferred from 17 °C to 35 °C. A later study found that while the majority (94/112) of *S. cerevisiae* rRNA modifications (Taoka et al., 2016) are constitutive, 18 exhibit ~5-80% modification under normal growth conditions, suggesting the existence of heterogeneous populations of ribosomes with different rRNA modifications.

Methylation of a specific rRNA nucleotide was implicated in aging and oxidative stress response (Schosserer et al., 2015). Reduced levels of the RNA methyltransferase NSUN5 was found to increase lifespan and oxidative stress resistance in yeast, worms, and flies. This methyltransferase was found to modify 25S rRNA C2278 in yeast, and yeast lifespan greater when 25S rRNA carried the C2278G mutation. In NSUN5 null cells, yeast were found to have decreased translational fidelity and increased translation of stress response genes. Interestingly, this protein decreased expression with age in yeast and human cell lines, suggesting that decreasing this protein may be a way for organisms to modulate rRNA composition to cope with the oxidative stress over time. Further functional studies of rRNA modifications that change in response to environmental cues will be necessary for us to understand their functional roles.

Conclusions

As we have detailed above, cells can alter their ribosome composition in response to biological stimuli. Changes to ribosome structure can occur at the protein level with ribosomal proteins assembling into translation machinery at different stoichiometries, or at the rRNA sequence level with different rRNA molecules assembling into the ribosome in response to different environmental conditions. Ribosomes can also be altered post-translationally through phosphorylation and ubiquitination, and post-transcriptionally via pseudouridylation and methylation. Although a wealth of ribosome heterogeneity has been described in the literature, the functional role of the majority of these changes to ribosome composition is still poorly understood. Thus it remains a major challenge of the ribosome field to understand how these modifications contribute to translational regulation of gene expression.

Chapter 2: The Ribosomal Response to DNA Damage

In this chapter, we discuss current literature about the translational response to DNA damage. We will also discuss known roles of ribosomal proteins in the DNA damage response and p53 signaling.

DNA damage response inhibits translation via eIF2 alpha phosphorylation and dephosphorylation of 4E-BP

Studies in both yeast and mammalian cells have shown that translation is decreased after DNA damage. Translational shutdown was found to be mediated by both eukaryotic initiation factor 2 alpha phosphorylation (eIF2α) and hypo-phosphorylation of eIF4 binding protein, 4E-BP. Phosphorylation of eIF2α inhibits translation initiation by preventing the recruitment of the initiator methionine tRNA to mRNA while the lack of phosphorylation of 4E-BP leads to the inhibition of initiation factor eIF4 and cap-dependent translation. There are four eIF2α kinases in mammals: the dsRNA-sensing kinase, Protein Kinase R (PKR); the unfolded protein response kinase, PKR-like endoplasmic reticulum kinase (PERK); the nutrient-response kinase, General Control Non-Depressible 2 (GCN2); and the heme-sensing kinase, heme-regulated inhibitor (HRI). Of these four kinases, three have been implicated in the DNA damage response. PKR has been shown to phosphorylate eIF2α after ionizing radiation (von Holzen et al., 2007) and doxorubicin treatment (Peidis et al., 2011). PERK, on the other hand, has been shown to be activated after UV irradiation (Jiang and Wek, 2005; Wu et al., 2002) and ionizing radiation (Kim et al., 2014) while GCN2 has been implicated after UV irradiation (Deng et al., 2002; Jiang and Wek, 2005; Robert et al., 2009). Other studies have identified that ionizing radition causes translational shutdown through the hypophosphorylation of 4E-BP, leading to the protein binding to eIF4E and thus decreasing cap-dependent translation (Braunstein et al., 2009a; Kumar et al., 2000a; Schneider et al., 2005a).

Because chemical and radiation-based methods of DNA damage often induce multiple types of genomic lesions, it is unclear if the diversity of translational inhibition pathways activated after DNA damage is due to the activation of one response pathway or a multitude of pathways activated in tandem. Furthermore, it is unclear if these pathways are a a direct response to DNA damage, or if the accumulation of multiple DNA lesions causes secondary effects that involve multiple translation pathways. To complicate matters even further, brute-force DNA damaging methods like ionizing radiation often have other deleterious effects like damaging RNA or producing harmful radical oxygen species, so DNA damage may or may not be the principal driver of the translational response. Consequently, in our study of translation after dsDNA damage (see *Chapter 5*), we used an agent known to cause dsDNA damage, etoposide, to see whether or not this drug caused inhibition of translation. We also asked whether a single Cas9-induced DSB was enough to cause a translational response, or if this translational shutdown was due to the accumulation of lesions. We also asked if one or both of the canonical translation inhibition pathways is activated after dsDNA damage, and we worked to identify the signaling kinases that play a role in the damage response.

Ribosome biogenesis is inhibited after DNA damage

Ribosome biogenesis is also disrupted after dsDNA damage. rRNA transcription in the nucleoli, the site of ribosome biogenesis in the cell, decreases after laser microirradiation or etoposide treatment in mouse embryonic fibroblasts (Kruhlak et al., 2007). This decrease was

dependent on DNA damage response kinase ATM and repair factors NBS1 and MDC1. These factors displaced RNA polymerase I (PolI) at the site of DNA damage, leading to reduced rRNA transcription and ribosome biogenesis. ATM-mediated inhibition of PolI transcription was also observed when I-PpoI or Cas9 endonucleases targeting rDNA repeats in the cell (van Sluis and McStay, 2015). This response was found to inhibit rRNA synthesis in trans, as NBS1 was found to translocate into nucleoli lacking damage after other nucleoli were irradiated (Ciccia et al., 2014; Larsen et al., 2014). These observations suggest that cells decrease the production of ribosomes in response to DNA damage.

Ribosomal proteins are involved in DNA damage response

A number of studies have documented extraribosomal functions of core ribosomal proteins in the DNA damage pathways. RPL26 was found to bind to the 5'UTR of p53 mRNA and stimulate p53 translation after DNA damage (Takagi et al., 2005). Knocking down *RPL26* did not change global translation but decreased translation of p53, demonstrating that this decrease was not due to impaired ribosome function. Other ribosomal proteins (RPL11, RPL23, RPL5 RPS27, RPS27A, RPS27L, and RPS7) have been shown to bind and inhibit the function of MDM2, an E3 ligase that regulates p53 levels in the cell (Chen et al., 2007; Dai and Lu, 2004; Jin et al., 2004; Lohrum et al., 2003; Sun et al., 2011; Xiong et al., 2011; Zhang et al., 2003; Zhu et al., 2009). Ribosomal protein RPL37 was found be proteasomally degrade in the nucleoplasm after DNA damage, and its degradation led to the upregulation of p53 in an RPL11-dependent manner, suggesting that DNA-damage induced ribosomal stress is communicated from the nucleolus to the cytoplasm through ribosomal protein signalling (Llanos and Serrano, 2010).

Recently, a core ribosomal protein was directly implicated in DNA repair. (Yang et al., 2019) found that that RPL6 is directly recruited to histone H2A at sites of DNA damage in a poly(ADP-ribose) polymerase-dependent manner. When RPL6 was knocked down in U2OS cells, there was impaired recruitment of key DNA repair factors like MDC1, RNF168, and BRCA1 to the site of DNA damage. These cells also experienced defects in DNA damage–induced G_2–M checkpoint, and cell survival was decreased after DNA damage.

Ribosomal proteins are ubiquitinated in response to DNA damage

Ribosomal and nucleolar proteins were identified in a proteomics screen for proteins ubiquitinated after doxorubicin-induced DNA damage. (Halim et al., 2018) isolated peptides that contain diglycyl-remnants, the chemical linkages that remain when ubiquitin is digested off a protein with trypsin, after U2OS cells were treated with doxorubicin. Using Ingenuity Pathway Analysis of proteins that experience greater than two-fold change in ubiquitination after DNA damage, the authors found that ribosomal and DNA damage response proteins are the most represented protein classes. Moreover, ubiquitination of ribosomal and nucleolar proteins after DNA damage was mitigated in the presence of ATM or ATR inhibitors, confirming that these changes were specific to the DNA damage response. As these analyses were performed on whole cell lysates, it remains an open question whether or not these proteins are ubiquitinated at the ribosome surface, before they assemble into ribosomal subunits in the nucleolus, or as free proteins in the cytoplasm. In *Chapter 5*, we will explore this question by demonstrating how cells change ribosome composition in response to double-stranded DNA damage.

Chapter 3: A Proteomics-Based Approach to Identifying Novel Ribosome-Associated Proteins

Abstract

The ribosome has long been studied as the protein production machine within the cell, yet we are still exploring how this molecular machine regulates protein expression during translation. Towards this end, we sought to characterize the human riboproteome, the set of proteins and the post-translational modifications that comprise the translation apparatus within human cells. We developed a method to purify ribosomes using an ectopically expressed, SBP-tagged core ribosomal protein, RPL10A-SBP, and we analyzed the proteins found in our purified ribosomes using mass spectrometry. We identified only 66 of the 79 ribosomal proteins expressed in HEK cells, yet the low peptide yield from our purifications suggested that our method needed to be scaled up to improve protein identification. We did, however, identify proteins previously unknown to be associated with the ribosome like CCDC124, which was later described to interact with the GTPase center of the ribosome in yeast (Wang et al., 2018). Our results give us hope that our method can be revisited in the future to identify other novel ribosome associated proteins.

Introduction

The riboproteome is composed of the core and auxiliary ribosomal proteins that associate with the translation machinery in the cell. These proteins have roles as diverse as directing mRNA transcripts to different subcellular locations to aiding in the folding of nascent polypeptide chains. Regulation of gene expression at the ribosome is an emerging area in biology, and the identification of novel ribosome-associated factors has the potential to provide us with a new repertoire of proteins that regulate protein production in the cell. Consequently, we sought to identify and characterize members of the human riboproteome.

At the time this study was conducted, there were two publications describing the eukaryotic riboproteome: (Fleischer et al., 2006) and (Reschke et al., 2013). Fleischer et al. (2006) performed mass spectrometry on proteins purified from yeast polysome profiling fractions and discovered 77 previously unknown translation-machinery associated (TMA) proteins. Yeast TMA null mutants exhibited a broad range of phenotypes including aberrant polysome profiles, decreased translational efficiency, and poor translational fidelity. TMA22 (DENR) and TMA20 (MCT-1) were later found to regulate re-initiation after translation of upstream open reading frames (uORFs) in flies (Schleich et al., 2014) and to facilitate 40S subunit recycling after stop codons in yeast (Young et al., 2018). Reschke et al. (2013), on the other hand, conducted mass spectrometry analysis on proteins from polysome fractions from different human prostate cell lines and mouse embryonic fibroblasts (MEFs). The authors used stable isotope labeling with amino acids in cell culture (SILAC) to compare the relative abundances of riboproteome proteins between cancerous and normal human prostate lines, prostate lines treated with mTORC1 inhibitors, and MEFs harboring wildtype and null versions of the ribosome biogenesis gene *Npm1*. The authors identified 1,499 riboproteome proteins from these experiments with 363 proteins appearing in all datasets; these proteins included 79 of the 80 core ribosomal proteins, RNA binding proteins, and proteins previously unknown to have a role in translation. The authors also observed differential protein abundance between different experimental conditions and noted that many proteins associated with the riboproteome are genetically amplified during cancer.

There were three limitations to the Fleischer et al., (2006) and Reschke et al., (2013) papers that we sought to address in our work. (1) Mass spectrometry was performed on ribosomal fractions isolated using sucrose gradient ultracentrifugation. Thus protein complexes of molecular weights to similar to that of the ribosome contaminate the ribosome fractions, leading certain proteins to be improperly identified as translation machinery associated. (2) These papers did not distinguish between ribosome-associated proteins and RNA binding proteins. Therefore it is unclear if these proteins colocalize with the ribosome or are mRNA binding proteins that are associated with mRNAs as they are translated. (3) It is unclear how many of the proteins identified in these proteomics datasets represent nascent polypeptide chain contaminants rather than fully-formed ribosome-associated proteins. In our study, we planned to address these limitations by (1) purifying ribosomes using affinity-tagged core ribosomal proteins to distinguish between ribosome proteins and proteins that co-sediment with ribosomes after ultracentrifugation, (2) comparing RNase treated purified ribosomes with untreated purified ribosomes to distinguish between ribosome-associated proteins and RNA binding proteins, and (3) treating ribosomes with puromycin to release nascent chains to determine how much contamination from nascent peptide chains is found in our riboproteome datasets. The following

results section details my progress in developing a ribosome-purification technique for mass spectrometry and the first round of mass spectrometry data.

Results

Development of SBP Purification Method for Ribosome Pulldowns

We first sought to optimize an affinity purification method for ribosome pulldowns. We chose RPL10A as our molecular handle because RPL10A-Avi had been used to pull down ribosomes and their associated transcripts for ribosome profiling (Ingolia et al., 2014). We tested six different peptide tags (**Table 1**) by transiently transfecting C-terminally tagged RPL10A in HEK 293T cells, pulling down tagged RPL10A from lysates using magnetic beads, and assaying the purity and efficacy of the pulldowns using silver staining and Western blotting (data not shown).

Table 1. Affinity tags for ribosome purifications with RPL10A

Tag	Length	Binding	Elutable?
His	6	Non-covalent	Yes – imidazole
Avi	15	Non-covalent	No – requires TEV
3X FLAG	22	Non-covalent	Yes – FLAG peptide
SBP	38	Non-covalent	Yes – biotin
SNAP	181	Covalent	No – requires TEV
Halo	297	Covalent	No – requires TEV

We found that we could obtain pure ribosomes using a three-step purification method in which ribosomes were pelleted using ultracentrifugation, affinity purified using the streptavidin binding protein (SBP) affinity tag, and eluted from streptavidin beads with biotin (**Figure 1A**). Ribosomes could only be purified from ribosome pellets; pulldowns with whole cell lysates lead to the purification of free RPL10A-SBP without the rest of the ribosome. This was likely because the binding of RPL10A-SBP is more kinetically favorable than binding of RPL10A-SBP incorporated in the ribosome (**Figure 1B**). We created stable HEK Flp In cell lines expressing *pCMV-RPL10A-SBP*, and we validated that the majority of RPL10A-SBP gets incorporated into the ribosome (**Figure 1C**). We also created SBP-tagged constructs for RPS8, RPS2, RPS17, RPL36, and RPL22, and we tested to see if these proteins co-purified with the ribosome pellet and if they could be bound and subsequently eluted off streptavidin beads (**Figure 1C**). We found that the incorporation of the tagged ribosomal protein into the ribosome was dependent on the specific identity of the core protein, but all of our ribosomal protein constructs could be bound and eluted off of streptavidin beads. The efficacy of these constructs as molecular handles for ribosome purification was variable (**Figure 1D**), and these preliminary results were

confounded by the high background in the untagged control lysates. Nevertheless, we were confident that our method could be used for isolating purified ribosomes for mass spectrometry analysis.

Figure 1. Validation of SBP Purification Method for Ribosome Pulldowns

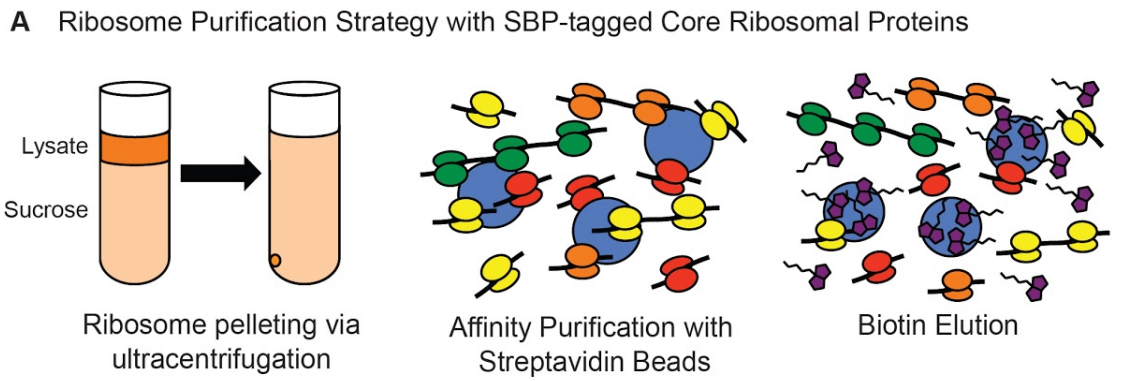

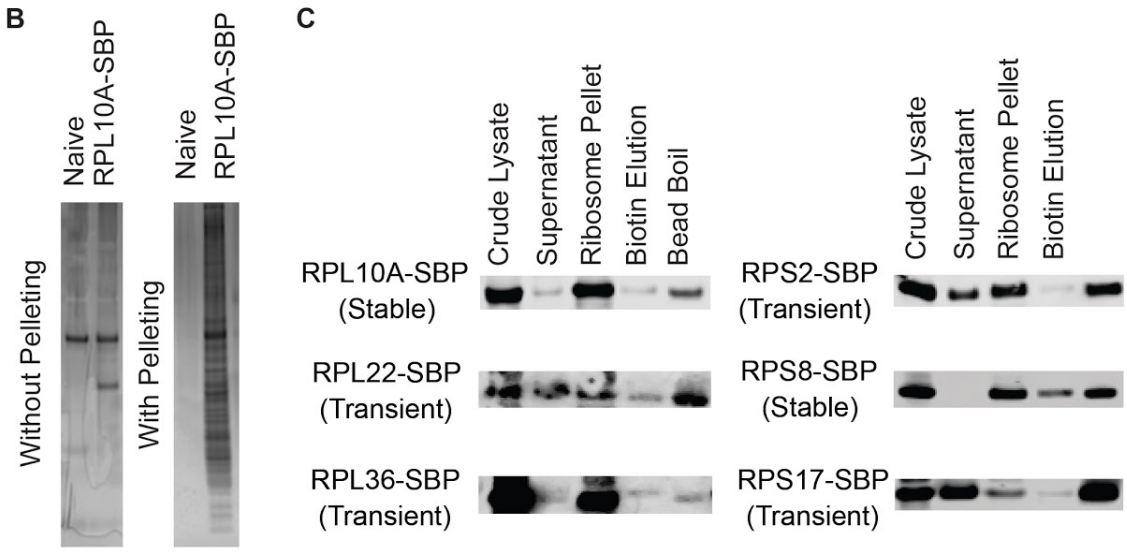

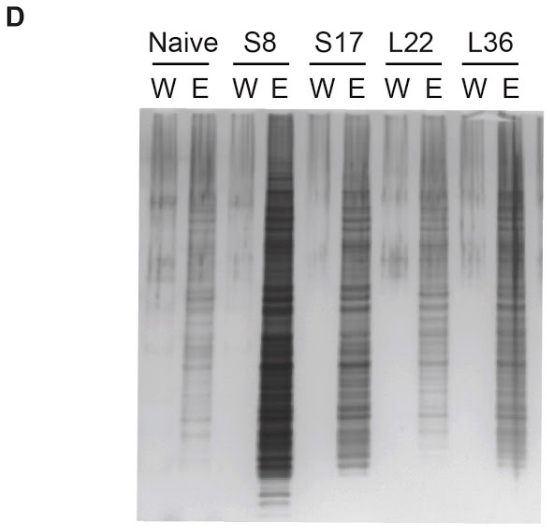

Figure 1. SBP Purification Method for Ribosome Pulldowns

(A) Schematic of the three-step purification method for affinity purifying ribosomes with SBP-tagged core ribosomal proteins. HEK cells ectopically expressing SBP-tagged core ribosomal proteins were lysed, and lysates were layered on top of a 1 M sucrose layer and spun at 541,000 x *g* for 1 hour. Pellets were resuspended in lysis buffer and ribosomes were affinity purified using streptavidin beads. SBP-tagged ribosomes were eluted off of the streptavidin beads using 5 mM biotin in lysis buffer.
(B) Silver stains of ribosome purifications with and without the ribosome pelleting step. *pCMV-RPL10A-SBP* was transiently transfected into HEK Flp-In cells 24 hours prior to lysis.
(C) anti-SBP Westerns of tagged core ribosomal proteins at different stages of the ribosome purification scheme. RPL10A-SBP and RPS8-SBP pulldowns were conducted with lysates from stable HEK Flp-In cell lines while RPS17, RPS2, and RPL36 constructs were transiently transfected. (Experiments performed by Phil Frankino).
(D) Silver stains of ribosome pulldowns with different molecular handles. (Experiments performed by Phil Frankino.) W: Final wash. E: Biotin elution fractions.

Mass Spectrometry Analysis of Affinity Purified Ribosomes

To uncover novel ribosome-associated proteins, we performed mass spectrometry on ribosomes purified from HEK Flp-In T-Rex RPL10A-SBP cell lines. We also prepared samples from naive HEK Flp-In T-Rex cells lacking the RPL10A-SBP transgene to gauge the level of contamination in our affinity purifications. We digested our purifications with trypsin/LysC and analyzed peptides by LC-MS/MS. Using X! Tandem with a human proteomics database from the Global Proteome Machine (GPM), we identified 148 proteins in our RPL10A-SBP pulldowns (**Table 2**), with 89 proteins identified in both samples. We only identified 10 proteins in our negative control samples, with trypsin, LysC, and lipoamide acyltransferase being the major contaminants (**Table 3**). Lipoamide acyltransferase contains a biotin-lipoyl binding domain, and based on the molecular weight of the enzyme, we speculate that the biotinylated version of the protein is the background band observed in our negative control purifications (**Figure 1B**). Importantly, we did not observe mitochondrial ribosomal proteins in our datasets, indicating that we were able to separate cytosolic ribosomes from the mix of cytosolic and mitochondrial ribosomes that are isolated in ribosome pellets.

We only observed 66 of 79 ribosomal proteins in our RPL10A-SBP datasets (**Table 2**), suggesting that we did not capture the full riboproteome in our dataset. We attribute this discrepancy to low protein yield after our affinity purifications, as the total number of spectra was fewer than what we observed in a ribosome pellet experiment that used the same peptide preparation protocol and LC-MS/MS system (~20,000 spectra versus ~300). We thus believe that scaling up this experiment will improve the detection of ribosome-associated proteins.

Table 2. List of proteins and their spectral counts from replicate L10A-SBP pulldown MS datasets. OS = organism. GN = gene name. SV = Splice variant.

Protein name	L10A-SBP (1)	L10A-SBP (2)
Lysyl endopeptidase OS=Pseudomonas aeruginosa (strain ATCC 15692 / PAO1 / 1C / PRS 101 / LMG 12228) GN=prpL SV=1	191	155
Heterogeneous nuclear ribonucleoprotein M OS=Homo sapiens GN=HNRNPM SV=3	54	36
Nucleophosmin OS=Homo sapiens GN=NPM1 SV=2	36	21
40S ribosomal protein S3a OS=Homo sapiens GN=RPS3A SV=2	34	16
60S ribosomal protein L4 OS=Homo sapiens GN=RPL4 SV=5	34	36
Trypsin OS=Sus scrofa SV=1	33	33
60S ribosomal protein L5 OS=Homo sapiens GN=RPL5 SV=3	32	20
Heterogeneous nuclear ribonucleoproteins C1/C2 OS=Homo sapiens GN=HNRNPC SV=1	32	32
60S ribosomal protein L13 OS=Homo sapiens GN=RPL13 SV=4	30	21
60S ribosomal protein L26 OS=Homo sapiens GN=RPL26 SV=1	28	9
40S ribosomal protein S18 OS=Homo sapiens GN=RPS18 SV=3	23	9
60S ribosomal protein L6 OS=Homo sapiens GN=RPL6 SV=3	23	15
40S ribosomal protein S19 OS=Homo sapiens GN=RPS19 SV=2	21	2
40S ribosomal protein S3 OS=Homo sapiens GN=RPS3 SV=2	21	9
60S ribosomal protein L29 OS=Homo sapiens GN=RPL29 SV=2	19	11

40S ribosomal protein S11 OS=Homo sapiens GN=RPS11 SV=3	16	6
60S ribosomal protein L31 OS=Homo sapiens GN=RPL31 SV=1	16	11
60S ribosomal protein L8 OS=Homo sapiens GN=RPL8 SV=2	15	10
40S ribosomal protein S21 OS=Homo sapiens GN=RPS21 SV=1	14	3
Plasminogen activator inhibitor 1 RNA-binding protein OS=Homo sapiens GN=SERBP1 SV=2	14	8
60S ribosomal protein L15 OS=Homo sapiens GN=RPL15 SV=2	13	7
Keratin, type II cytoskeletal 1 OS=Homo sapiens GN=KRT1 SV=6	13	15
60S acidic ribosomal protein P0 OS=Homo sapiens GN=RPLP0 SV=1	12	3
40S ribosomal protein S25 OS=Homo sapiens GN=RPS25 SV=1	12	5
40S ribosomal protein S14 OS=Homo sapiens GN=RPS14 SV=3	12	11
40S ribosomal protein S26 OS=Homo sapiens GN=RPS26 SV=3	11	0
60S ribosomal protein L11 OS=Homo sapiens GN=RPL11 SV=2	11	0
60S ribosomal protein L23a OS=Homo sapiens GN=RPL23A SV=1	11	1
60S ribosomal protein L7 OS=Homo sapiens GN=RPL7 SV=1	11	2
60S ribosomal protein L28 OS=Homo sapiens GN=RPL28 SV=3	11	7
40S ribosomal protein S15 OS=Homo sapiens GN=RPS15 SV=2	11	8

Insulin-like growth factor 2 mRNA-binding protein 1 OS=Homo sapiens GN=IGF2BP1 SV=2	11	9
Lipoamide acyltransferase component of branched-chain alpha-keto acid dehydrogenase complex, mitochondrial OS=Homo sapiens GN=DBT SV=3	11	15
Heterogeneous nuclear ribonucleoprotein U OS=Homo sapiens GN=HNRNPU SV=6	11	16
Nuclease-sensitive element-binding protein 1 OS=Homo sapiens GN=YBX1 SV=2	10	8
Nuclease-sensitive element-binding protein 1 OS=Homo sapiens GN=YBX1 SV=3	10	8
60S ribosomal protein L17 OS=Homo sapiens GN=RPL17 SV=3	9	0
Chromatin target of PRMT1 protein OS=Homo sapiens GN=CHTOP SV=2	9	3
60S ribosomal protein L7a OS=Homo sapiens GN=RPL7A SV=2	9	7
Guanine nucleotide-binding protein subunit beta-2-like 1 OS=Homo sapiens GN=GNB2L1 SV=3	9	9
40S ribosomal protein S28 OS=Homo sapiens GN=RPS28 SV=1	8	0
40S ribosomal protein S5 OS=Homo sapiens GN=RPS5 SV=4	8	0
Ribosomal protein L19 OS=Homo sapiens GN=RPL19 SV=1	8	4
ATP-dependent RNA helicase A OS=Homo sapiens GN=DHX9 SV=4	8	9
Histone H1.2 OS=Homo sapiens GN=HIST1H1C SV=2	8	12
60S acidic ribosomal protein P2 OS=Homo sapiens GN=RPLP2 SV=1	7	1
60S ribosomal protein L28 OS=Homo sapiens GN=RPL28 SV=1	7	2

60S ribosomal protein L18 OS=Homo sapiens GN=RPL18 SV=2	7	3
40S ribosomal protein S6 OS=Homo sapiens GN=RPS6 SV=1	7	5
Keratin, type I cytoskeletal 10 OS=Homo sapiens GN=KRT10 SV=6	7	5
40S ribosomal protein S4, X isoform OS=Homo sapiens GN=RPS4X SV=2	7	6
Double-stranded RNA-binding protein Staufen homolog 1 OS=Homo sapiens GN=STAU1 SV=2	7	6
Keratin, type I cytoskeletal 9 OS=Homo sapiens GN=KRT9 SV=3	7	10
Histone H1.4 OS=Homo sapiens GN=HIST1H1E SV=2	7	15
40S ribosomal protein S8 OS=Homo sapiens GN=RPS8 SV=2	6	0
40S ribosomal protein SA OS=Homo sapiens GN=RPSA SV=4	6	1
RNA-binding protein with serine-rich domain 1 OS=Homo sapiens GN=RNPS1 SV=1	6	9
40S ribosomal protein S23 OS=Homo sapiens GN=RPS23 SV=3	5	1
Polyadenylate-binding protein 1 OS=Homo sapiens GN=PABPC1 SV=2	5	1
Polyadenylate-binding protein OS=Homo sapiens GN=PABPC1 SV=1	5	1
60S ribosomal protein L13a OS=Homo sapiens GN=RPL13A SV=2	5	2
60S ribosomal protein L22 OS=Homo sapiens GN=RPL22 SV=2	5	3
RNA-binding protein EWS OS=Homo sapiens GN=EWSR1 SV=1	5	3
Nucleolar RNA helicase 2 OS=Homo sapiens GN=DDX21 SV=5	5	4

40S ribosomal protein S10 OS=Homo sapiens GN=RPS10 SV=1	4	0
40S ribosomal protein S7 OS=Homo sapiens GN=RPS7 SV=1	4	0
60S ribosomal protein L32 OS=Homo sapiens GN=RPL32 SV=1	4	0
Putative 40S ribosomal protein S10-like OS=Homo sapiens GN=RPS10P5 PE=5 SV=1	4	0
40S ribosomal protein S24 OS=Homo sapiens GN=RPS24 SV=1	4	2
60S ribosomal protein L10 OS=Homo sapiens GN=RPL10 SV=4	4	2
Regulator of nonsense transcripts 1 OS=Homo sapiens GN=UPF1 SV=2	4	2
60S ribosomal protein L23 OS=Homo sapiens GN=RPL23 SV=1	4	4
60S ribosomal protein L3 OS=Homo sapiens GN=RPL3 SV=2	4	5
Matrin-3 OS=Homo sapiens GN=MATR3 SV=2	4	5
Probable ATP-dependent RNA helicase DDX17 OS=Homo sapiens GN=DDX17 SV=2	4	5
60S ribosomal protein L27 OS=Homo sapiens GN=RPL27 SV=2	3	0
60S ribosomal protein L34 OS=Homo sapiens GN=RPL34 SV=3	3	0
60S ribosomal protein L36 OS=Homo sapiens GN=RPL36 SV=3	3	0
Catenin beta-1 OS=Homo sapiens GN=CTNNB1 SV=1	3	0
Chromosome 11 open reading frame 48, isoform CRA_c OS=Homo sapiens GN=C11orf98 SV=1	3	0
Histone H1.1 OS=Homo sapiens GN=HIST1H1A SV=3	3	0

Histone H1t OS=Homo sapiens GN=HIST1H1T SV=4	3	0
mRNA turnover protein 4 homolog OS=Homo sapiens GN=MRTO4 SV=2	3	0
RNA-binding protein FUS OS=Homo sapiens GN=FUS SV=1	3	0
60S ribosomal protein L12 OS=Homo sapiens GN=RPL12 SV=1	3	1
Double-stranded RNA-binding protein Staufen homolog 2 OS=Homo sapiens GN=STAU2 SV=1	3	1
Emerin OS=Homo sapiens GN=EMD SV=1	3	1
Eukaryotic initiation factor 4A-III OS=Homo sapiens GN=EIF4A3 SV=4	3	1
RNA-binding motif protein, X chromosome OS=Homo sapiens GN=RBMX SV=3	3	1
TATA-binding protein-associated factor 2N OS=Homo sapiens GN=TAF15 SV=1	3	1
40S ribosomal protein S2 OS=Homo sapiens GN=RPS2 SV=2	3	2
Insulin-like growth factor 2 mRNA-binding protein 3 OS=Homo sapiens GN=IGF2BP3 SV=2	3	2
Y-box-binding protein 3 OS=Homo sapiens GN=YBX3 SV=4	3	2
60S ribosomal protein L14 OS=Homo sapiens GN=RPL14 SV=4	3	3
60S ribosomal protein L24 OS=Homo sapiens GN=RPL24 SV=1	3	3
Keratin, type II cytoskeletal 2 oral OS=Homo sapiens GN=KRT76 SV=2	3	3
Ribosomal RNA processing protein 1 homolog B OS=Homo sapiens GN=RRP1B SV=3	3	7
40S ribosomal protein S17 OS=Homo sapiens GN=RPS17 SV=2	2	0

40S ribosomal protein S20 OS=Homo sapiens GN=RPS20 SV=1	2	0
60S acidic ribosomal protein P1 OS=Homo sapiens GN=RPLP1 SV=1	2	0
60S ribosomal protein L18a OS=Homo sapiens GN=RPL18A SV=1	2	0
Chromatin target of PRMT1 protein OS=Homo sapiens GN=CHTOP SV=1	2	0
Coiled-coil domain-containing protein 124 OS=Homo sapiens GN=CCDC124 SV=1	2	0
ELAV-like protein 1 OS=Homo sapiens GN=ELAVL1 SV=2	2	0
Histone H2B type 1-K OS=Homo sapiens GN=HIST1H2BK SV=3	2	0
Protein transport protein Sec31A OS=Homo sapiens GN=SEC31A SV=1	2	0
Ral GTPase-activating protein subunit alpha-2 OS=Homo sapiens GN=RALGAPA2 SV=2	2	0
RNA-binding motif protein, X chromosome OS=Homo sapiens GN=RBMX SV=1	2	0
60S ribosomal protein L21 OS=Homo sapiens GN=RPL21 SV=2	2	1
Insulin-like growth factor 2 mRNA-binding protein 2 OS=Homo sapiens GN=IGF2BP2 SV=2	2	1
Serine/arginine repetitive matrix protein 2 OS=Homo sapiens GN=SRRM2 SV=2	2	4
Interleukin enhancer-binding factor 3 OS=Homo sapiens GN=ILF3 SV=3	2	11
40S ribosomal protein S12 OS=Homo sapiens GN=RPS12 SV=3	1	0

40S ribosomal protein S13 OS=Homo sapiens GN=RPS13 SV=2	1	0
40S ribosomal protein S15a OS=Homo sapiens GN=RPS15A SV=2	1	0
40S ribosomal protein S30 OS=Homo sapiens GN=FAU SV=1	1	0
60S ribosomal protein L10a OS=Homo sapiens GN=RPL10A SV=2	1	0
60S ribosomal protein L36a OS=Homo sapiens GN=RPL36A SV=2	1	0
ATP-dependent RNA helicase DDX3X OS=Homo sapiens GN=DDX3X SV=1	1	0
Keratin, type I cuticular Ha2 OS=Homo sapiens GN=KRT32 SV=3	1	0
Keratin, type I cuticular Ha3-II OS=Homo sapiens GN=KRT33B SV=3	1	0
Keratin, type I cytoskeletal 24 OS=Homo sapiens GN=KRT24 SV=1	1	0
KH domain-containing, RNA-binding, signal transduction-associated protein 1 OS=Homo sapiens GN=KHDRBS1 SV=1	1	0
La-related protein 4 OS=Homo sapiens GN=LARP4 SV=3	1	0
Origin recognition complex subunit 2 OS=Homo sapiens GN=ORC2 SV=2	1	0
Putative ATP-dependent RNA helicase DHX30 OS=Homo sapiens GN=DHX30 SV=1	1	0
Ras GTPase-activating protein-binding protein 1 OS=Homo sapiens GN=G3BP1 SV=1	1	0
Suppressor of SWI4 1 homolog OS=Homo sapiens GN=PPAN SV=1	1	0
Serine/arginine-rich splicing factor 4 OS=Homo sapiens GN=SRSF4 SV=2	1	1

Zinc finger RNA-binding protein OS=Homo sapiens GN=ZFR SV=2	1	1
Bcl-2-associated transcription factor 1 OS=Homo sapiens GN=BCLAF1 SV=2	1	2
Ras GTPase-activating protein-binding protein 2 OS=Homo sapiens GN=G3BP2 SV=2	1	2
60S ribosomal protein L27a OS=Homo sapiens GN=RPL27A SV=2	1	3
Ribosomal L1 domain-containing protein 1 OS=Homo sapiens GN=RSL1D1 SV=3	1	3
Heterogeneous nuclear ribonucleoprotein A3 OS=Homo sapiens GN=HNRNPA3 SV=2	0	1
Heterogeneous nuclear ribonucleoprotein F OS=Homo sapiens GN=HNRNPF SV=3	0	1
Heterogeneous nuclear ribonucleoprotein H OS=Homo sapiens GN=HNRNPH1 SV=4	0	1
Histone H1x OS=Homo sapiens GN=H1FX SV=1	0	1
Pinin OS=Homo sapiens GN=PNN SV=4	0	1
Serine/arginine-rich splicing factor 6 OS=Homo sapiens GN=SRSF6 SV=2	0	1
Thyroid hormone receptor-associated protein 3 OS=Homo sapiens GN=THRAP3 SV=2	0	1
Transcription intermediary factor 1-beta OS=Homo sapiens GN=TRIM28 SV=5	0	1
Cellular tumor antigen p53 OS=Homo sapiens GN=TP53 SV=4	0	2
Serine/arginine-rich splicing factor 2 OS=Homo sapiens GN=SRSF2 SV=4	0	3
Beta-casein OS=Bos taurus GN=CSN2 SV=2	0	4
Protein Shroom3 OS=Homo sapiens GN=SHROOM3 SV=2	0	4
Keratin, type II cytoskeletal 4 OS=Homo sapiens GN=KRT4 SV=4	0	13

Table 3. List of spectral counts for proteins that appear in the negative, untagged control sample MS datasets. OS = organism. GN = gene name. SV = Splice variant.

Protein name	Naïve (1)	Naive (2)	L10A-SBP (1)	L10A-SBP (2)
Lysyl endopeptidase OS=Pseudomonas aeruginosa (strain ATCC 15692 / PAO1 / 1C / PRS 101 / LMG 12228) GN=prpL SV=1	262	232	191	155
Trypsin OS=Sus scrofa SV=1	40	45	33	33
Lipoamide acyltransferase component of branched-chain alpha-keto acid dehydrogenase complex, mitochondrial OS=Homo sapiens GN=DBT SV=3	29	26	11	15
Catenin beta-1 OS=Homo sapiens GN=CTNNB1 SV=1	12	12	3	0
Keratin, type I cytoskeletal 9 OS=Homo sapiens GN=KRT9 SV=3	5	4	7	10
Keratin, type II cytoskeletal 1 OS=Homo sapiens GN=KRT1 SV=6	3	0	13	15
Keratin, type I cytoskeletal 10 OS=Homo sapiens GN=KRT10 SV=6	3	1	6	5
Proto-oncogene tyrosine-protein kinase ROS OS=Homo sapiens GN=ROS1 SV=3	2	1	0	0
Uncharacterized protein KIAA1683 OS=Homo sapiens GN=KIAA1683 SV=1	1	0	0	0
Protein Shroom3 OS=Homo sapiens GN=SHROOM3 SV=2	0	1	0	2

Discussion

Ribosomes can be purified using affinity-tagged core ribosomal proteins

In this study, we developed a method to purify ribosomes using SBP-tagged core ribosomal proteins. To purify ribosomes, we isolated ribosomes by ultacentrifugation through a sucrose cushion, binding SBP-tagged ribosomes to streptavidin beads, and eluting SBP-tagged ribosomes from the beads using biotin. We were able to implement this strategy with multiple core ribosomal proteins including RPL10A, RPS2, RPS8, RPS17, RPL22, and RPL36, suggesting that we can use this purification strategy to investigate the specific functions of core ribosomal proteins and their associated factors.

Our ribosome purifications with RPL10A-SBP were clean, with very few contaminants being identified in the silver stains or mass spectrometry datasets of naive (untagged) cell lysates (**Figure 1B**, **Table 2**). Importantly, we did not observe any mitochondrial ribosomal proteins, which are contaminants of mass spectrometry experiments that rely on ultracentrifugation methods to purify cytosolic ribosomes (Reschke et al., 2013). Unfortunately, our protein yield was not high enough to provide a complete snapshot of the human riboproteome, but we are confident that this issue can be remedied by using more streptavidin beads or increasing the biotin elution time. We believe that with a bit more finessing, this method can be used for mass spectrometry analysis or ribosome-protein selective ribosome profiling.

Although our mass spectrometry data were less than ideal, we were heartened that the majority of our hits were factors that we would commonly associate with ribosomes and translated mRNAs. We observed several RNA binding proteins that are well known to associate with mRNAs such as the mRNA reader YTHDF1 and the polyadenylate binding protein PABPC1. We were a bit surprised by the large representation of histones, as these are nuclear proteins. However, we did not perform a nuclear removal step prior to our pulldowns, and it follows that we are likely isolating nucleolar ribosomal intermediates that contain RPL10A-SBP.

After we began our study, (Simsek et al., 2017) published their results characterizing the human riboproteome from affinity purifications of core ribosomal proteins. (Simsek et al., 2017) used Cas9 genome editing to edit mouse embryonic stem cells to introduce the FLAG tag at the *RPL36* or *RPS17* locus. Tagged ribosomes were affinity purified and submitted for TMT mass spectrometry analysis, and approximately 430 proteins were found to be both RNaseA and puromycin independent ribosome-associated proteins. These included expected proteins like core ribosome proteins, initiation factors, and elongation factors as well as unexpected proteins like cell cycle regulators and metabolic enzymes. The authors also identified UFM1 as a novel, post-translational modification of ribosomes (see *Chapter 4* for our work with the Kopito Lab on ribosome UFMylation), and characterized pyruvate kinase (PKM) as a translational activator. Their method clearly demonstrated that proteomics analysis of affinity-purified core ribosomal proteins uncovers novel ribosome-associated proteins, many of which still have unknown functions in translation.

Identification of novel ribosome-associated proteins from RPL10A-SBP pulldowns

Despite the lackluster quality of our mass spectrometry datasets, we did successfully identified proteins that were later described as novel ribosome-associated proteins. Two unique CCDC124 peptides were identified in one of our RPL10A-SBP datasets, and recently a yeast homolog of CCDC124, Lso2, was found to associate with 25S rRNA near the GTPase activation

center of ribosomes (Wang et al., 2018). This protein appears to have a role in recovery of translation after yeast transition from stationary to exponential phase, as *lso2Δ* yeast have reduced translational output and aberrant start codon pausing when the yeast enter the exponential growth phase. We are thus curious to know if unnamed genes that appeared in our RPL10A-SBP pulldowns like C11orf98 have important regulatory roles for translation. We hope that with a few more rounds of protocol development we can use our SBP pulldown method to uncover a human riboproteome that is complementary to those published by Simsek et al. (2017) and Reschke et al. (2013).

Materials and Methods

Cloning of affinity tagged ribosomal proteins

pNTI154 pcDNA5/FRT/pCMV-RPL10A-Avi (Ingolia et al, 2014) was modified to express ribosomal proteins with His, SBP, Halo, SNAP, or 3X FLAG C-terminal affinity tags using Gibson cloning. RPS2 and RPS8 were cloned from plasmids from Calvin Jan (Jonathan Weissman Laboratory, UCSF) while other ther ribosomal proteins were cloned from HEK Flp-In Cell Line cDNA generated using using SuperScript II Reverse Transcriptase (Thermo Fisher Scientific).

To transiently express tagged ribosomal proteins, plasmids were transfected using Mirus 293 reagent according to the manufacturer's protocol. Lysates were harvested 24 hours after transfection for Western blotting or affinity purifications. Stable HEK Flp-In T-Rex cell lines were generated by transfecting or nucleofecting pcDNA5/FRT plasmids and the pOG44 Flp-Recombinase Expression Vector (Invitrogen) and selecting for hygromycin resistant cells. To generate cell lines using transient transfections, HEK Flp-In cells were split 1:5 into a 6-well dish then transfected 24 hours later with 100 ul Optimem (Gibco), 0.1 µg pcDNA5/FRT vector, 0.9 µg pOG44, and 3 µl X-tremeGENE 9 DNA Transfection Reagent (Roche). Two days later, the cells were trypsinized and transferred to media containing 5 µg/ml blasticidin (Invitrogen) and 50 µg/ml Hygromycin B (Thermo Fisher Scientific). Cells were grown on selective media until all cells in a negative control transfection were dead. To generate cell lines using nucleofection, 1 x 10^6 HEK Flp-In T-Rex cells (Invitrogen) were nucleofected using a Lonza 4D nucleofector in according to the Amaxa 4D-Nucleofector™ Protocol for HEK293 (Lonza) with 1.8 µg pOG44 Flp-Recombinase Expression Vector and 0.2 µg pcDNA5/FRT vector per large nucleofection. Two days after nucleofection, cells were passaged and placed on media containing 5 µg/ml blasticidin and 10 µg/ml Hygromycin B until all cells from a control plate nucleofected with pmaxGFP™ Vector (Lonza) were dead. Flp-In cell lines were validated using Westerns against the affinity tag of interest.

Affinity purification of ribosomes using the SBP peptide tag

HEK cells were lysed in 140 mM KCl, 10 mM HEPES, 5 mM $MgCl_2$, 1% Triton-X, 1 mM TCEP, 25 U/ml TurboDNase (Invitrogen), and 2X protease inhibitor cocktail (Sigma). HEK cells were washed with DPBS (Gibco) and lysed in either 400 µl (10 cm dish) or 600 µl (15 cm dish) ice-cold lysis buffer. Lysates were incubated on ice for 10 minutes, and cell debris was removed by centrifuging lysates at 20,000 x *g* for 10 minutes. The supernatant was removed, and the centrifugation step was repeated twice to ensure that no cell debris would be pelleted with the ribosome in the subsequent ribosome pelleting step. Protein concentrations were measured using the Pierce 660 nm Protein Assay Kit.

Crude lysates were normalized such that each sample contained 3-6 mg protein, and 300-1500 µl cell lysate was transferred to 13 mm x 51 mm polycarbonate ultracentrifuge tubes (Beckman-Coulter). 900 ul 1 M sucrose in lysis buffer was layered under the lysate, and the tubes were ultracentrifuged at 100,000 rpm for 1 hour at 4°C in a TLA110 rotor in a Optima TLX Ultracentrifuge (Beckman). The supernatants were removed, and the ribosome pellet was resuspened in 600 µl lysis buffer by pipetting up and down 50 times.

To affinity purify SBP-tagged ribosomes, the resuspended ribosome pellet was incubated with 60 µl m270 Streptavidin Dynabeads (Invitrogen) in low binding microcentrifuge tubes at

4°C for 1 hour while shaking in a Tomy Micro Tube Shaker at the lowest setting. Tubes with the magnetic beads were placed on a DynaMag™ magnetic stand (Invitrogen) for 1 minute, and the flow through was removed. The beads were washed for 5 minutes shaking in 600 µl lysis buffer at 4°C, and this wash step was repeated four times for a total of five wash steps.

To elute the SBP-tagged proteins, we added 25 µl 5 mM biotin in lysis buffer to the magnetic beads, making sure not to elute the unspecifically bound proteins by pipetting the beads up and down, and incubated the beads for 1 hour at 4°C shaking on the Tomy Micro Tube Shaker. After the elution fraction was collected, we added 25 ul 1X NuPAGE LDS Sample Buffer (Invitrogen) in lysis buffer to the beads and boiled the beads for 10 minutes at 80 °C to obtain the bead boil fraction.

Analysis of affinity purifications with silver staining and Western blotting

The efficacy and cleanliness of our affinity purifications were assayed using silver staining and Western blotting. Protein fractions were boiled in 1X LDS Sample Buffer (Invitrogen) according to the manufacturer's protocol and run on 10% or 4-12% Bis-Tris Bolt (or NuPAGE) Protein Gels (Invitrogen) in MES SDS-PAGE buffer. To gauge the cleanliness of our purifictions, protein gels were stained using SilverQuest™ Silver Staining Kit according to the manufacturer's protocol. To assess the efficacy of our pulldowns, we immunoblotted against the SBP tag. We transferred proteins from protein gels to nitrocellulose membranes using the XCell II™ Blot Module (Thermo Fisher Scientific), blocked the membranes in 5% milk in TBST or Odyssey Blocking Buffer (PBS) (LI-COR) for 1 hour, and washed the membrane three times with TBST. The membranes were incubated with SBP Tag Mouse Monoclonal Antibody, Clone SB19-C4 (sc-101595, Santa Cruz Biotechnology) diluted 1:1000 in TBST for 1 hour at 4°C. Membranes were washed three times with TBST for 5 minutes then incubated with IRDye® 800CW Donkey anti-mouse Secondary Antibody (LI-COR) diluted 1:10,000 in TBST for 1 hour at 4°C. Membranes were washed three times with TBST for 5 minutes then imaged with a LI-COR Odyssey CLx Imager.

Proteomic analysis of SBP-tagged ribosomes

We affinity purified ribosomes from 15 cm plates of HEK Flp-In T-Rex cells stably expressing RPL10A-SBP. Purifications were performed in biological duplicate with two samples of naive HEK Flp-In T-Rex cells serving as the negative controls. After the final biotin elution step, we prepared our samples for shotgun proteomics according to the protocol written by Mela Mulvihill from Daniel Nomura's group at UC Berkeley. To precipitate proteins, we added 55 µl DPBS and 20 µl 100% TCA to each 25 µl sample. Samples were incubated at -80°C for 1 hour then spun at 20,000 x *g* for 10 minutes at 4°C in a microcentrifuge. Pellets were washed in ice cold 0.01M HCl 90% acetone three times then air dried and resuspended in 30 µl 8 M urea in DPBS and 30 µl 0.2% ProteaseMax (Promega) 100 mM ammonium bicarbonate then vortexed for several minutes. To reduce the samples, 40 µl 100 mM ammonium bicarbonate and 10 µl 110 mM TCEP were added to the samples, and the samples were incubated for 30 minutes at 60°C. To alkylate the samples, we added 2.5 µl 500 mM iodoacetimide and incubated the samples in the dark for 30 minutes. To digest the proteins, we added 120 µl DBPS, 1.5 µl 1% ProteaseMax (Promega) 100 mM ammonium bicarbonate, and 4 µl of 0.5 µg/µl Trypsin/LysC Mix, Mass Spectrometry Grade (Promega) to each sample. Peptides were digested overnight at 37 °C. To quench the tryptic digests, 24 µl 50% formic acid was pipetted into each sample, and

the sample was spun at 13200 rpm for 30 minutes. The supernatant was transferred to a new tube, and the sample were stored at -80°C.

Mass spectrometry analysis was performed at the UC Davis Proteomics Core Facility. Peptides were run on a Q-Exactive+ Mass Spectrometer with a Proxeon nano-spray source and Easy-LC II HPLC. Data was analyzed using Scaffold version 4.6.1 using X!Tandem version CYCLONE (2013.02.01.1) with a human proteome database from The Global Proteomics Machine (GPM) that was modified to include some common contaminant peptides. The search was conducted with a 20 PPM fragment tolerance with +57 + C (Carbamidomethyl) as a fixed modification and -18 on n (Glu->pyro-Glu), -17 on n (Ammonia-loss), -17 on n (Gln->pyro-Glu), +1 on NQ (Deamidated), +16 on MW (Oxidation), +32 on MW (Dioxidation), and +42 on n (Acetyl) as variable modifications. In our results section tables, we included peptides that were given an X! Tandem -log(expect scores) scores of greater than 1.5 and proteins that had at least 1 peptide mapping to them. We used a peptide FDR of 0.1% and a protein FDR of 1.2%.

Acknowledgements

I would like to thank Phil Frankino for his hard work cloning and testing out different ribosomal protein constructs during his rotation. I would also like to thank Dan Nomura for sharing his lab's proteomics protocol and for recommending that I get in touch with the UC Davis Proteomics Core, which resulted in numerous collaborations between their facility and the Ingolia Lab. Lastly, I would like to thank Brett Phinney and Michelle Salemi at the UC Davis Proteomics Core, who have been enormously supportive of my research over the course of the last four years.

Funding Sources

This work was supported by National Institute Health New Innovator Award (DP2 CA195768, Nicholas Ingolia). Celeste Riepe was supported by fellowships awarded through the The Shurl and Kay Curci Foundation and the National Science Foundation Graduate Research Fellowship Program (DGE 1106400 and DGE 1752814) while Phil Frankino was supported by the National Institute Health T32 Training Grant (4T32GM007232-40);

Chapter 4: Ribosomal protein RPL26 is the principal target of UFMylation

Contents of this chapter are excerpts from:

Walczak, C.P., Leto, D.E., Zhang, L., **Riepe, C.**, Muller, R.Y., DaRosa, P.A., Ingolia, N.T., Elias, J.E., and Kopito, R.R. (2019). Ribosomal protein RPL26 is the principal target of UFMylation. **Proc. Natl. Acad. Sci.** U. S. A. *116*, 1299–1308.

The results, figure, figure legend, and materials and methods for this chapter are the work of Celeste Riepe, Nicholas Ingolia, and Ryan Muller. The abstract and discussion section are the work of Christopher Walczak, Dara Leto, and Ron Kopito. References to supplemental datasets containing sequencing analysis were removed from the text, as the datasets are not included in the dissertation.

Abstract

Ubiquitin fold modifier 1 (UFM1) is a small, metazoan-specific, ubiquitin-like protein modifier that is essential for embryonic development. Although loss-of-function mutations in UFM1 conjugation are linked to endoplasmic reticulum (ER) stress, neither the biological function nor the relevant cellular targets of this protein modifier are known. [Walczak et al., 2019 shows] that a largely uncharacterized ribosomal protein, RPL26, is the principal target of UFM1 conjugation. RPL26 UFMylation and de-UFMylation is catalyzed by enzyme complexes tethered to the cytoplasmic surface of the ER and UFMylated RPL26 is highly enriched on ER membrane-bound ribosomes and polysomes. Biochemical analysis and structural modeling establish that UFMylated RPL26 and the UFMylation machinery are in close proximity to the SEC61 translocon, suggesting that this modification plays a direct role in cotranslational protein translocation into the ER. These data suggest that UFMylation is a ribosomal modification specialized to facilitate metazoan-specific protein biogenesis at the ER.

Results

Disruption of UFMylation Affects Transcription but Not Translation.

Because RPL26 is a core component of the ribosome, we wondered how UFMylation might influence translation. As RPL26 is UFMylated at the ER, we performed ribosome profiling on cytosolic and ER-enriched cellular fractions and compared the translational differences in $UFM1^{KO}$ and $UFSP2^{KO}$ cells relative to wild-type controls, in conjunction with mRNA-seq analysis from unfractionated lysates (**Figure 1A**). Both mutants had substantial effects on the translatome of HEK293 cells. Consistent with the ER localization of the UFMylation machinery, the membrane fraction changed much more than the cytosolic fraction. Overall, these changes were driven by mRNA abundance, however, and we observed little evidence of translational disruption. Likewise, examination of individual profiles did not reveal substantial changes in ribosome footprint distribution of membrane-associated transcripts in aggregate or on individual candidate genes. Taken together, these data argue against a model whereby UFMylation of RPL26 directly regulates translation of ER-associated mRNAs, and show that our profiling data reflect adaptive changes in the transcriptome that accompany the loss or constitutive gain in UFMylation.

These transcriptional changes provide some clues regarding the cellular role for RPL26 UFMylation, although they are indirect and likely adaptive effects. Broader gene expression changes were observed in $UFSP2^{KO}$ cells than in $UFM1^{KO}$ (**Figure 1B**), suggesting either that loss of de-UFMylation is more disruptive, or perhaps that UFSP2 has a secondary role beyond removing UFM1 from conjugates. We also observed a stronger effect on genes identified in membrane fractions of the ribosome profiling experiment than those in the cytosolic fraction (**Figure 1A**) consistent with the localization of the UFMylation and de-UFMylation machinery to the ER. The intersection of gene ontology (GO) terms associated with significantly up-regulated and down-regulated transcripts in $UFM1^{KO}$ and in $UFSP2^{KO}$ RNA-seq revealed a significant enrichment of transcripts encoding extracellular matrix (ECM) proteins, particularly those comprising the collagen-containing ECM (**Figure 1B–E**). While the ECM GO term was enriched in the down-regulated $UFM1^{KO}$ gene list, the ECM GO term was enriched in both up-regulated and down-regulated gene lists for $UFSP2^{KO}$, suggesting that constitutive UFMylation has opposing effects on different subsets of ECM genes.

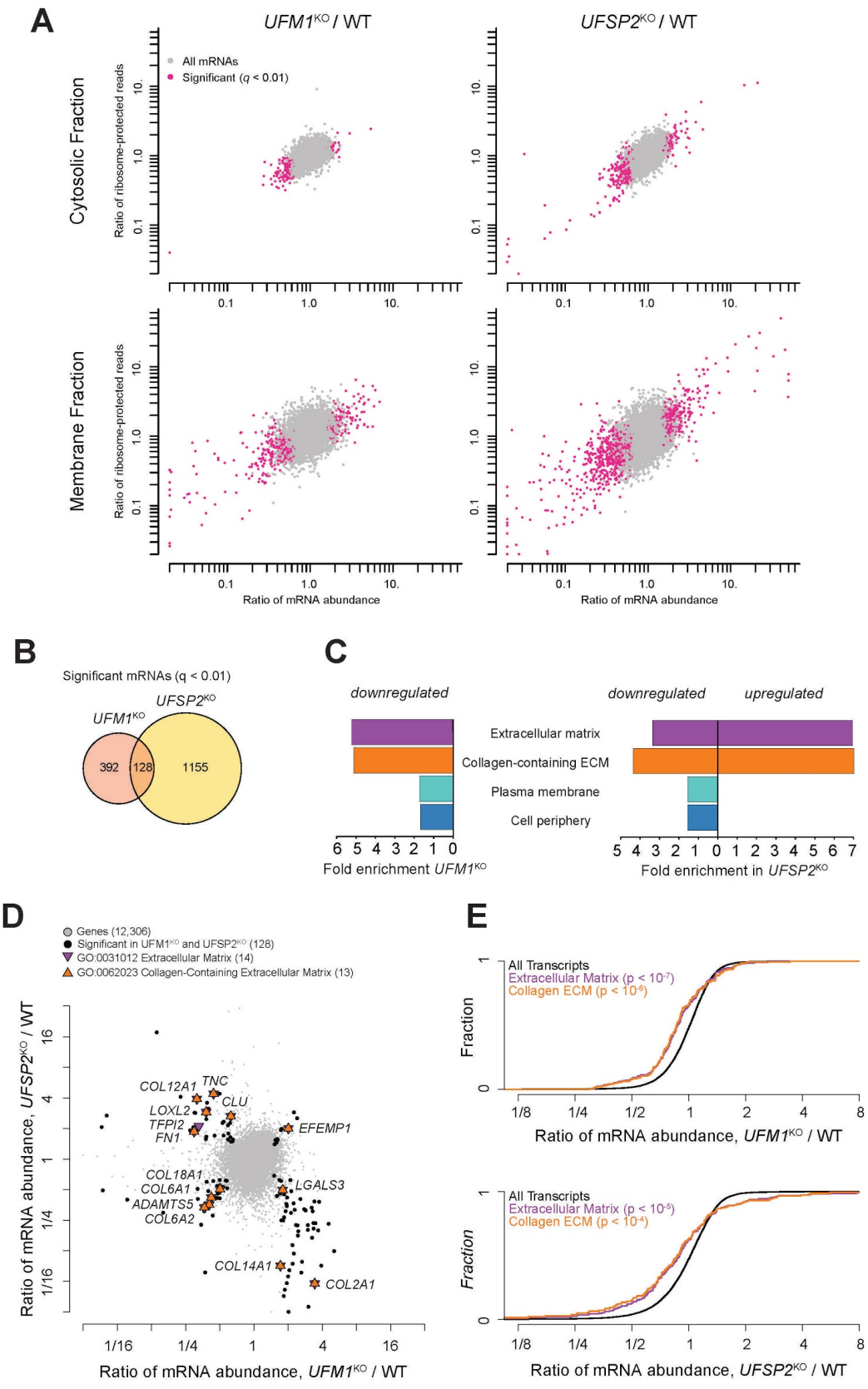
A
UFM1KO / WT
UFSP2KO / WT
All mRNAs
Significant (q < 0.01)
Cytosolic Fraction
Membrane Fraction
Ratio of ribosome-protected reads
Ratio of mRNA abundance
B
Significant mRNAs (q < 0.01)
UFM1KO
UFSP2KO
392
128
1155
C
downregulated
upregulated
Extracellular matrix
Collagen-containing ECM
Plasma membrane
Cell periphery
Fold enrichment UFM1KO
Fold enrichment in UFSP2KO
D
Genes (12,306)
Significant in UFM1KO and UFSP2KO (128)
GO:0031012 Extracellular Matrix (14)
GO:0062023 Collagen-Containing Extracellular Matrix (13)
COL12A1
TNC
CLU
LOXL2
TFPI2
FN1
EFEMP1
COL18A1
COL6A1
ADAMTS5
COL6A2
LGALS3
COL14A1
COL2A1
Ratio of mRNA abundance, UFSP2KO / WT
Ratio of mRNA abundance, UFM1KO / WT
E
All Transcripts
Extracellular Matrix (p < 10-7)
Collagen ECM (p < 10-6)
Extracellular Matrix (p < 10-5)
Collagen ECM (p < 10-4)
Fraction
Ratio of mRNA abundance, UFM1KO / WT
Ratio of mRNA abundance, UFSP2KO / WT

Figure 1. Disruption of UFMylation affects transcription but not translation.

(A) Scatterplots of the fold changes (knockout/wild type) in ribosome-protected reads in either cytosol or membrane fractions and of fold changes in RNA-seq reads from whole cell lysates. Pink dots represent genes that were statistically significant in the RNA-seq dataset only [false discovery rate (FDR) < 0.01].

(B) Venn diagram of genes with significantly different expression (FDR < 0.01) in $UFM1^{KO}$ and $UFSP2^{KO}$ HEK293 cells compared with wild type.

(C) GO analysis of $UFM1^{KO}$ and $UFSP2^{KO}$ expression changes. Genes up-regulated or down-regulated in knockout cells were analyzed separately to identify statistically overrepresented GO terms (FDR < 0.05, Fisher's exact test). GO cellular component terms shared in analysis of both knockouts are displayed. The terms "extracellular matrix" and "collagen-containing ECM" were overrepresented in both up-regulated and down-regulated genes in $UFSP2^{KO}$.

(D) mRNA expression differences for $UFSP2^{KO}$ and $UFM1^{KO}$ cells versus wild type. Black circles indicate genes with significant differential expression in both mutants. Colored symbols highlight significantly changed genes in GO component categories related to the ECM.

(E) Cumulative distribution of fold changes of genes with extracellular matrix or collagen-containing extracellular matrix annotations. P values were obtained by a Mann–Whitney–Wilcoxon U test.

Discussion

[...] Because our RNA-seq analysis was performed on stable cell lines that constitutively lack functional UFMylation or de-UFMylation pathways, the altered gene expression profile observed in these cells likely reflects secondary adaptive changes which compensate for a primary biogenesis defect in a subset of secretory proteins. The strong overrepresentation of ECM-associated genes in this adaptive response suggests the possibility that UFMylation may contribute to correct biosynthesis of one or more ECM components. Evolution of the ECM was a key event in the transition from unicellular to multicellular life (Özbek et al., 2010). The observation that UFMylation occurs on a metazoan-specific C-terminal extension of RPL26 suggests that this appendage likely also coevolved with emergence of the UFM1 system and the ECM. ECM proteins, particularly collagens, require an extensive set of specialized factors to fold, modify, assemble, secrete, process, and cross-link these large, rigid molecules (Ishikawa and Bächinger, 2013). The robust association of human UFMylation genes with abnormal brain development and microcephaly in humans (Colin et al., 2016; Hamilton et al., 2017; Muona et al., 2016; Nahorski et al., 2018) and with defective neuromuscular junction formation in *Drosophila* (Duan et al., 2016) suggests a role for UFMylation in tissue development, a process that is intimately dependent on cell–cell and cell–matrix interaction. [...]

Although further study is clearly required to elucidate the mechanistic relationship between UFMylation and tissue development and morphogenesis, our identification of RPL26 as the primary target of UFMylation, together with the physical proximity of UFM1-modified ribosomes to the machinery required for cotranslational protein translocation at the ER, points to a role for this ubiquitin-like modifier in the early steps of secretory protein biogenesis.

Materials and Methods

Ribosome profiling

Ribosome profiling was conducted in biological duplicate as detailed in (McGlincy and Ingolia, 2017) with the following modifications. *UFM1*^{KO}, *UFSP2*^{KO}, and wild-type HEK293 cells grown to 70-80% confluency on 10 cm dishes were washed once with cold PBS and 400 µL of cytosol extraction buffer (0.02% digitonin, 20 mM Tris pH 7.4, 150 mM NaCl, 5 mM MgCl, 1 mM DTT, 25 U/mL DNase, and protease inhibitor cocktail) was added directly to the plate. Cells were scraped, collected, and kept on ice for 10 mins. Lysates were cleared by centrifugation at 21,130x g for 10 mins to obtain the cytosolic fractions, snap frozen in liquid nitrogen and stored at -80°C. The pellets remaining after centrifugation were rinsed with PBS before solubilization in polysome lysis buffer (1% Triton X-100, 20 mM Tris pH 7.4, 150 mM NaCl, 5 mM MgCl, 1 mM DTT, 25 U/mL DNase, and protease inhibitor cocktail). After 10 mins on ice, lysates were cleared by centrifugation at 21,130x g for 10 mins to obtain the membrane fraction, snap frozen in liquid nitrogen and stored at -80°C. Instead of circularizing single-stranded cDNA with CircLigase II, we used CircLigase I (Epicentre) as detailed in (Ingolia et al., 2012) with a 2 h incubation step. In addition to depleting rRNA with RiboZero Gold (Illumina), we performed an rRNA depletion step after circularization as previously described in (Ingolia et al., 2012). Libraries were sequenced as 50 bp single-end reads on an Illumina HiSeq 4000.

RNA-seq sample preparation and sequencing

Biological duplicates of *UFM1*^{KO}, *UFSP2*^{KO}, and wild-type HEK293 cells were grown to 70-80% confluency on 10 cm dishes. Cells were washed once with cold PBS and 400 µL of cold polysome lysis buffer (1% Triton X-100, 20 mM Tris pH 7.4, 150 mM NaCl, 5 mM MgCl, 1 mM DTT, 25 U/mL DNase, and protease inhibitor cocktail) was added directly to the plate. Cells were scraped, collected, and kept on ice for 10 mins. Lysates were cleared by centrifuging at 21,130x g for 10 mins, then snap frozen in liquid nitrogen and stored at -80°C. Total RNA was isolated using the Direct-Zol RNA Miniprep Kit (Zymo), and sequencing libraries were prepared using the TruSeq Stranded Total RNA Library Prep Kit with Ribo Zero Gold (Illumina). Samples were sequenced on a HiSeq4000 (Illumina) with 50 base single-read sequencing.

Sequencing data processing and analysis

Sequencing reads were aligned to the Human GENCODE Gene Release GRCh38.p7 release 25 using TopHat (Trapnell et al., 2009). Alignment files were converted, sorted, and indexed using Samtools (Li et al., 2009) and the number of reads per transcript was counted using fp-count (Ingolia et al., 2014) with the basic gene annotations from GRCh38.p7. Differential changes in gene expression were calculated using DESeq2 (Love et al., 2014) with a cutoff of FDR < 0.01 for per-gene significance. Gene expression and ribosome profiling data are available in the Gene Expression Omnibus (GEO) under accession number GSE123539.

GO Analyses

Significant GO component categories were identified using PANTHER (Mi et al., 2013, 2017) by comparing lists of genes that were significantly up-regulated or down-regulated in *UFM1*^{KO} and *UFSP2*^{KO} cells with a background list of genes identified in the RNA-seq experiment (Fisher's exact test, FDR < 0.05). GO component terms identified in both *UFM1*^{KO}

and *UFSP2*^{KO} were selected for further discussion with the exception of "Plasma Membrane Part" (GO: 0044459), a category that is largely redundant with "Plasma Membrane" and cannot be used for direct manual annotation (Quick GO database, (Binns et al., 2009)). Cumulative distribution plots were drawn using lists of genes per GO term that PANTHER identified from the background dataset and the genes' corresponding log2 fold changes calculated during the DESeq2 analysis. Significant changes in distribution between the log2 fold changes for the genes per GO term and those of all transcripts identified in the RNA-seq dataset for each knockout cell line were calculated using the Mann-Whitney-Wilcoxon test with $P < 0.01$.

Chapter 5: Double Stranded DNA Damage Triggers Ribosome Remodeling and Translational Shutdown

Contents of this chapter were originally posted as a preprint on bioRxiv on December 5, 2018 as:

Riepe, C.*, Zelin, E.*, Wyman, S.K., Nguyen, D.N., Liang, J.R., Frankino, P.A., Meacham, Z.A., Vu, J.T., Marson, A., Ingolia, N.T., Corn, J.E. (2018). Double Stranded DNA Damage and Genome Editing Trigger Ribosome Remodeling and Translational Shutdown. **bioRxiv**. https://doi.org/10.1101/486704.

References to supplemental tables containing sequencing analysis were removed from the text, as the datasets are not included in the dissertation.

Summary

DNA damage activates a robust transcriptional stress response, but much less is known about how DNA impacts translation. The advent of genome editing via a Cas9-induced DNA double-strand break has intensified interest in understanding cellular responses to DNA damage. Here we find that DNA double-strand breaks (DSBs) induced by Cas9 or other damaging agents lead to a reduction of core ribosomal proteins, RPS27A and RPL40, and that the loss of these proteins is post-transcriptional and p53-independent. DSBs furthermore lead to the shutdown of translation through phosphorylation of eukaryotic initiation factor 2 alpha, and altering these signals affects genome editing outcomes. This DSB translational response is widespread and precedes the transcriptional response. Our results demonstrate that even a single double-strand break can lead to ribosome remodeling and reduced translational output, and suggest caution in interpreting cellular phenotypes measured immediately after genome editing.

Introduction

Unrepaired DNA damage can lead to lethal mutations and contributes to cancer initiation and progression. Cells have thus evolved a variety of responses to protect their genomes from a myriad of chemical and environmental insults. Double-strand breaks pose a particularly acute danger, as they may cause the wholesale loss of genetic information and require dramatic repair processes. In humans, cells with double-strand breaks arrest until repair is completed and undergo programmed cell death if repair is unsuccessful.

Double-strand breaks provoke a distinctive transcriptional response. Activation of the transcription factor p53 is a hallmark of the DSB response, leading to transcriptional reprogramming, cell cycle arrest, or in cases of severe damage, apoptosis (Joerger and Fersht, 2016). Deficiency in p53 signaling is also pivotal to the progression of many cancers, allowing neoplasms to accumulate DNA damage that results in mutations rapid tumor evolution. In addition to its critical role in maintaining genomic integrity, the cellular response to DSBs is essential to genome editing methods like CRISPR-Cas9. Cas9 editing relies on introducing a targeted double-strand break within a genome, which the cell repairs through error-prone non-homologous end joining (NHEJ) or through templated, homology directed repair (HDR). HDR from even a single Cas9-mediated DSB can induce low levels of p53 signaling, which can have negative consequences for cell fitness and genome editing outcomes (Haapaniemi et al., 2018; Ihry et al., 2018).

Although DSBs are known to initiate transcriptional changes, less is understood about the role of translation in the DNA damage response. A purely transcriptional reaction to a genetic insult leaves a gap in response, potentially exposing a cell to the impact of damaged DNA during a critical time window in which damage had raised an alarm but newly transcribed mRNAs have not accumulated. While transcriptional changes can modulate protein abundance hours or days after a genomic insult, translational control can enact regulatory programs within minutes of an environmental stress (Andreev et al., 2015; Sidrauski et al., 2015).

We thus sought to characterize how cells respond to DNA damage at the translation level, and in particular, how cells respond to a single double-strand break during Cas9-mediated genome editing. We serendipitously found that cells temporarily deplete core ribosomal proteins, RPS27A and RPL40, in response to dsDNA damage. RPS27A and RPL40 are regulated post-transcriptionally and in a p53-independent manner, and their depletion persists days after the initial genomic lesion with Cas9. We also found that both non-specific double-strand breaks as well as single, targeted double-strand breaks reduce translation via eukaryotic initiation factor 2 alpha (eIF2α) phosphorylation, and that modulating the downstream effects of eIF2α phosphorylation during Cas9 editing leads to different repair outcomes. Ribosome profiling and RNA-seq data from Cas9-edited cells suggest that cells mount a translation response to dsDNA damage that precedes transcriptional changes. Our data demonstrate that Cas9-mediated genome editing can trigger temporary ribosome remodeling and translational shutdown in response to DNA double-strand breaks.

Results

Ribosome proteins RPS27A and RPL40 are downregulated after genome editing with Cas9

While investigating changes in ubiquitin gene expression after DNA damage, we serendipitously observed that the two ribosomal proteins encoded as fusion proteins with ubiquitin, RPS27A (eS31) and RPL40 (eL40), are downregulated after Cas9-guide RNA (gRNA) ribonucleoprotein (RNP) nucleofection (**Figure 1A**). This downregulation was apparent as late as 48-72 hours after nucleofection, even though at this point Cas9 was largely absent from the cell (**Figure 1B**) and genomic formation of indels was completed (**Figure 1C**). We found that RPS27A levels recovered 96 hours after nucleofection and RPL40 levels were beginning to increase within 72 hours (**Figure 1A**), suggesting that the cell resets protein expression three to four days after editing (**Figure S1A**).

Downregulation of RPS27A and RPL40 depended on the DNA double-strand break, as catalytically inactive dCas9 did not provoke a similar response (**Figure 1A**). The guide RNA used in this experiment targeted a non-coding region of the *JAK2* gene (sgIntron), and *JAK2* levels remain unchanged after Cas9 nucleofection (**Figure S1B**). Our data therefore suggest that the loss of ribosomal subunits was due to the break itself and not disruption of *JAK2*. This days-long response was striking, as Cas9-mediated genome editing is often assumed to be relatively benign beyond the effects of the genomic sequence change itself.

We next asked whether ribosomal protein depletion was a specific response to DSBs versus other genomic lesions. We found that the loss of RPS27A and RPL40 does not occur after non-DSB DNA damage such as alkylation (methyl methanesulfonate), oxidative damage (hydrogen peroxide), thymine dimers (ultraviolet radiation), or replication fork stalling (hydroxyurea) (**Figure 1D**). By contrast, both single, targeted DSBs caused by Cas9 RNP nucleofection and multiple, unspecific DSBs induced by the topoisomerase II inhibitors etoposide or doxorubicin reduced RPS27A and RPL40 levels. Therefore, the loss of RPL40 and RPS27A we observed after genome editing is caused by multiple DSB-inducing agents and is specific to DSBs.

As RPS27A and RPL40 are core components of the ribosome, we wondered whether intact ribosomes lacked these core components or if the reduction in levels of these proteins reflected changes in the pool of free ribosomal subunits. We used Western blotting of polysome profiling fractions to measure the abundance of different ribosomal proteins in small (40S) and large (60S) ribosome subunits, 80S monosomes, and polysomes from cells treated with DMSO or etoposide (**Figure 1E-F**). Strikingly, etoposide caused an accumulation of 80S monosomes and a reduction of actively translating polysomes. We found that RPS27A and RPL40 were absent from 80S monosomes and other ribosomal subunits after etoposide treatment, while the control ribosomal proteins RPS10 (eS10) and RPL10A (uL1) remained. The lack of RPS27A and RPL40 in 80S monosomes and polysomes suggests that they are absent from actively translating ribosomes, but we cannot rule out the hypothesis that monosomes are not translationally competent after DSBs and that actively translating ribosomes require RPS27A and RPL40. In sum, we observe that DSBs cause an increase in 80S monosomes and reduction in translating polysomes, while RPS27A and RPL40 are lost from the translation machinery of etoposide-treated samples. Before investigating the DSB-induced accumulation of monosomes, we examined the mechanism by which RPS27A and RPL40 are lost after double-stranded DNA damage.

Figure 1. Ribosome proteins RPS27A and RPL40 are downregulated after genome editing with Cas9

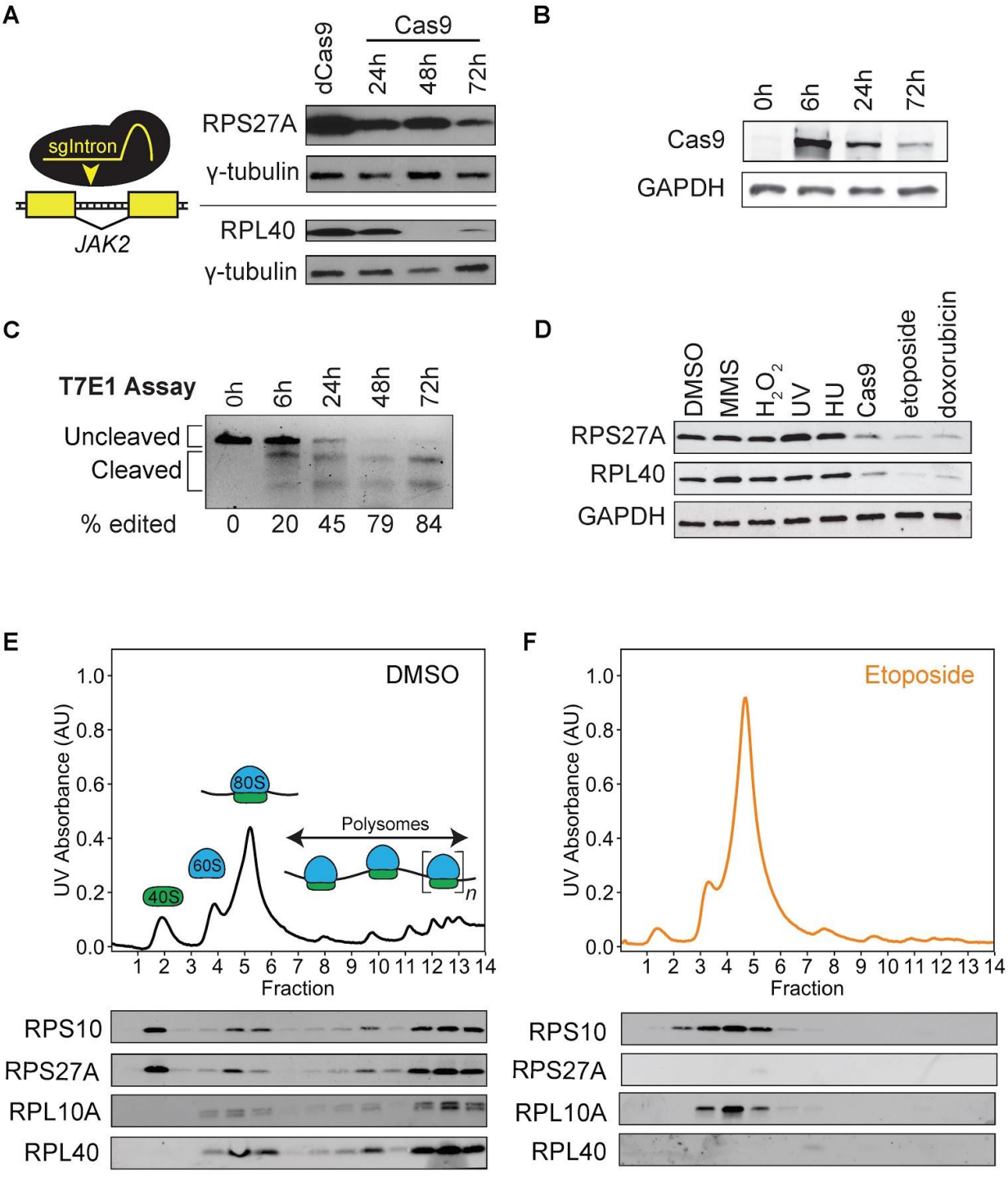

Figure 1. Ribosome proteins RPS27A and RPL40 are downregulated after genome editing with Cas9

(A) Western blots reveal that RPS27A and RPL40 are depleted in HEK cells after nucleofection with Cas9 RNP complexes targeting intron 12 of *JAK2*(sgIntron). HEK cells harvested 72 hours post dCas9-sgIntron nucleofection served as the negative control.

(B) Western blots depict rapid loss of Cas9 protein after RNP nucleofection.

(C) T7 endonuclease 1 assay of JAK2 editing after Cas9-sgIntron nucleofection demonstrates that editing is largely complete after 24 hours. Band intensities were calculated using ImageJ, and percent edited was computed as 100% x (1-(1-fraction cleaved)$^{1/2}$), where fraction cleaved = (sum of cleavage product intensities)/(sum of uncleaved and cleaved product intensities).

(D) Western blots of HEK cell lysates treated with different DNA damaging agents show that RPS27A and RPL40 are depleted after DNA double-strand breaks (DSB) and not other forms of DNA damage. MMS: methyl methanesulfonate, 0.03%, 1 hour. Cas9: Cas9-sgIntron nucleofection, 72 hr recovery. H_2O_2: hydrogen peroxide. UV: UV irradiation, 20 J/m^2, 6 hour recovery. HU: hydroxyurea, 10 mM, 16 hours. Etoposide: 5 μM, 16 hours. Doxorubicin: 10 μM, 16 hours. DMSO: 0.01%, 16 hours.

(E) Polysome profiles and ribosome protein Western blots of polysome profiling fractions from HEK cells treated with DMSO or (F) 5 μM etoposide for 16 hours reveal that RPL40 and RPS27A are lost from ribosome subunits after DSBs. UV absorbance = UV absorbance at 254 nm.

Figure S1. Ribosome proteins RPS27A and RPL40 are downregulated after Cas9 genome editing

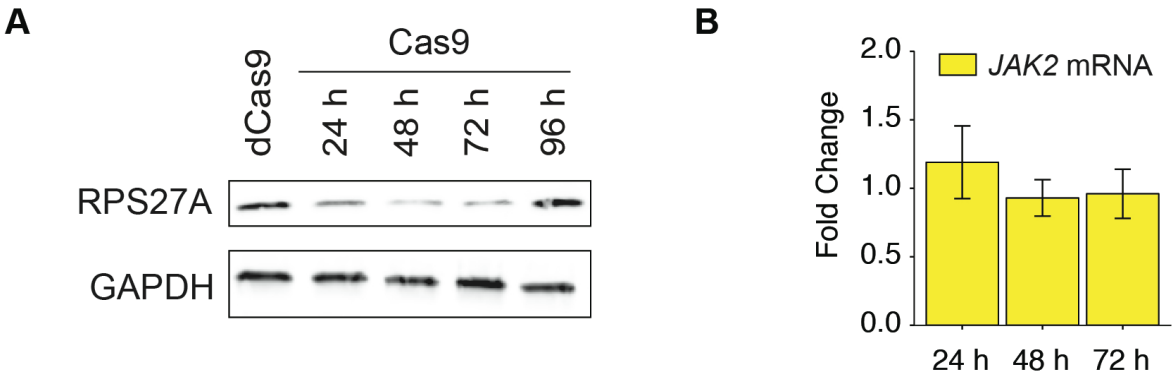

Figure S1 (Related to Fig. 1). Ribosome proteins RPS27A and RPL40 are downregulated after genome editing with Cas9

(A) As in Figure 1A, showing recovery of RPS27A at 96 hours post-nucleofection.

(B) Genome editing does not affect *JAK2* mRNA abundance. Fold changes were calculated using the $2^{-\Delta\Delta Ct}$ method with Cas9 without sgIntron (apo Cas9) as the control and *GAPDH* as the reference gene (n = 3, error bars = SD).

Ubiquitins translated from *RPS27A* and *RPL40* decrease after dsDNA breaks

Since RPS27A and RPL40 are translated as polypeptide fusions between an N-terminal ubiquitin moiety and a C-terminal ribosomal protein, we asked if ubiquitin moieties associated with RPS27A and RPL40 are depleted from dsDNA-damaged cells. The ubiquitin-ribosomal protein fusions are post-translationally processed into separate polypeptides, and cleavage presumably occurs prior to incorporation of RPL40 and RPS27A into the ribosome, as the N-termini of RPL40 and RPS27A are positioned near the elongation factor binding site and the A site of the decoding center, respectively (Ben-Shem et al., 2010; Rabl et al., 2011). Ubiquitins translated from the four human ubiquitin genes, *RPL40* (also known as *UBA52*), *RPS27A*, *UBC*, and *UBB* are indistinguishable at the amino acid level, and consequently, we employed Cas9-mediated genome engineering to introduce unique epitope tags to the N-terminal ubiquitins associated with these loci. We created endogenously-tagged clonal cell lines for three of the four human ubiquitin genes: *V5-RPL40, HA-RPS27A*, and *Myc-UBC* (**Figure 2A**). Each of the ubiquitins encoded by these genes has an identical amino acid sequence, but the unique tag allows us to individually track them.

Western blotting for each tag confirmed that the ubiquitin species from each edited locus could be uniquely tracked and incorporated into polyubiquitin chains (**Figure S2A**). We found that induction of either multiple DSBs with etoposide or a single DSB with a Cas9 RNP greatly reduced the abundance of the epitope-tagged ubiquitins translated from *V5-RPL40* and *HA-RPS27A* but had no effect on the ubiquitin associated with *Myc-UBC* (**Figure 2B**). By tracking tagged ubiquitin after a single Cas9 DSB, we found that the time course of *RPS27A* and *RPL40* ubiquitin depletion mirrored that of the RPS27A and RPL40 proteins, including recovery of the proteins several days after a DSB (**Figure 2C, Figure S2B**). Nucleofection of a targeted but catalytically inactive dCas9 RNP had no effect on the levels of the ubiquitins derived from *RPL40* or *RPS27A* (**Figure S2B**), confirming that the formation of a DSB was critical for loss of *RPS27A* and *RPL40*. Other forms of DNA damage such as MMS or UV radiation did not change the levels of ubiquitins associated with *RPL40* or *RPS27A* (**Figure S2C**). This mirrors the specificity to a double stranded DNA break we observed for the ribosomal proteins (**Figure 1D**), suggesting that the translation products of *RPL40* and *RPS27A* are repressed in tandem after dsDNA damage. Notably, DSBs had no gross effect on the total ubiquitin pool (**Figure 2E**), suggesting that cells are not modulating overall ubiquitin abundance.

Figure 2. Ubiquitins translated from *RPS27A* and *RPL40* decrease after dsDNA breaks

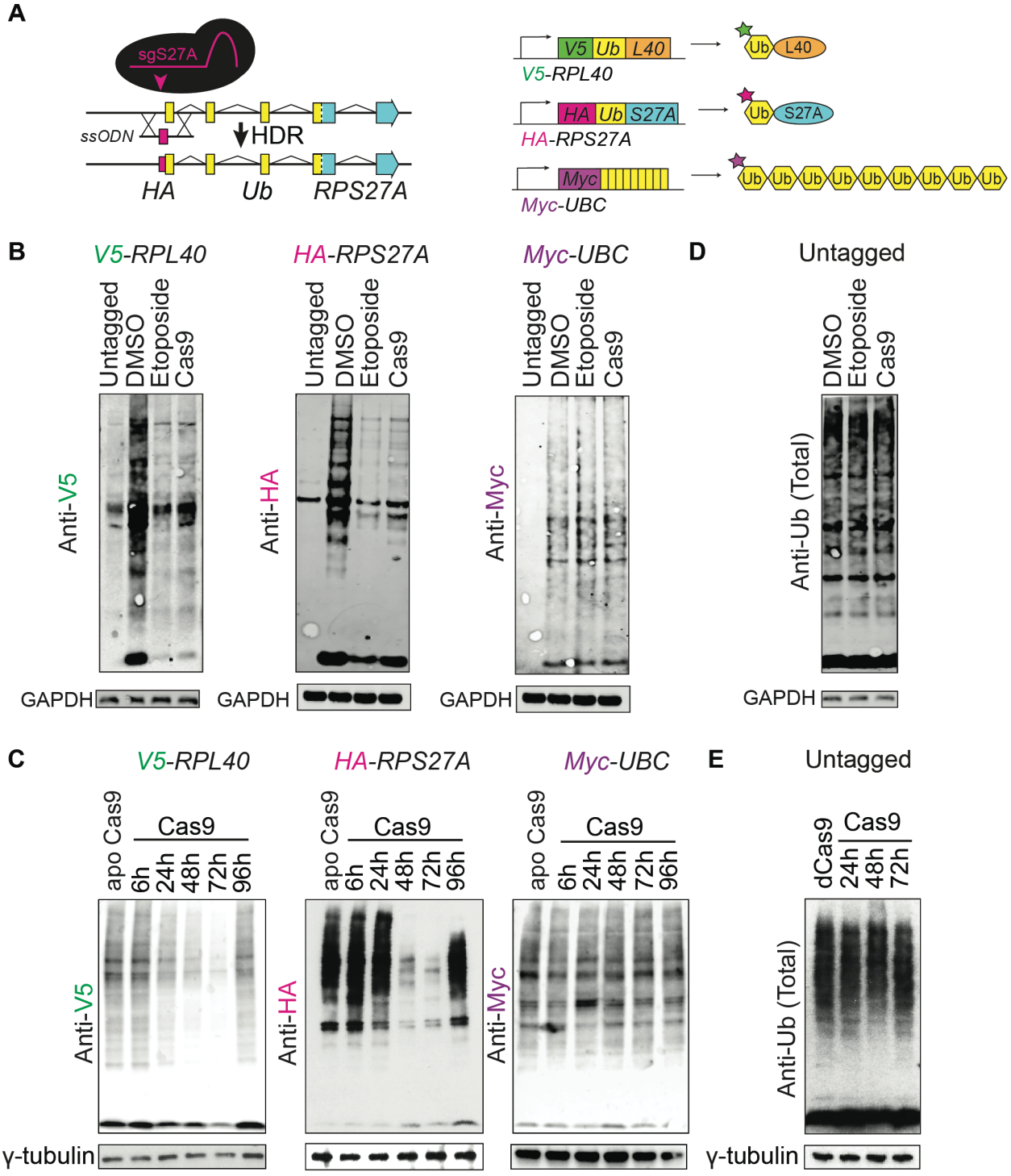

Figure 2. Ubiquitins translated from *RPS27A* and *RPL40* decrease after dsDNA breaks

(A) Schematic of Cas9 genome editing strategy for introducing the HA epitope tag at the N-terminus of the ubiquitin translated from *RPS27A,* and a schematic of edited *HA-RPS27A, V5-RPL40,* and *Myc-UBC* and their primary translation products. *V5-RPL40* and *Myc-UBC* were edited in a similar fashion as *HA-RPS27A*. (ssODN = single-stranded oligodeoxyncleotide donor.)

(B) Western blots depicting reduction of epitope-tagged ubiquitin translated from *V5-RPL40, HA-RPS27A*, but not *Myc-UBC,*16 hours after treatment with 5 μM etoposide or 72 hours after Cas9-sgIntron nucleofection.

(C) Western blots depicting the time course of depletion and recovery of epitope-tagged ubiquitin after Cas9-sgIntron nucleofection. apo Cas9 indicates Cas9 nucleofection without an sgRNA 72 hours post nucleofection.

(D) Western blots show that total ubiquitin levels are unchanged after treatment with 5 μM etoposide or 72 hours after Cas9-sgIntron nucleofection.

(E) Western blots show that there is no change in total ubiquitin levels 1-3 days after Cas9-sgIntron nucleofection. dCas9-sgIntron 72 hours after nucleofection served as the negative control.

Figure S2 (Rel. to Fig. 2). Ubiquitins translated from *RPS27A* and *RPL40* decrease after dsDNA breaks

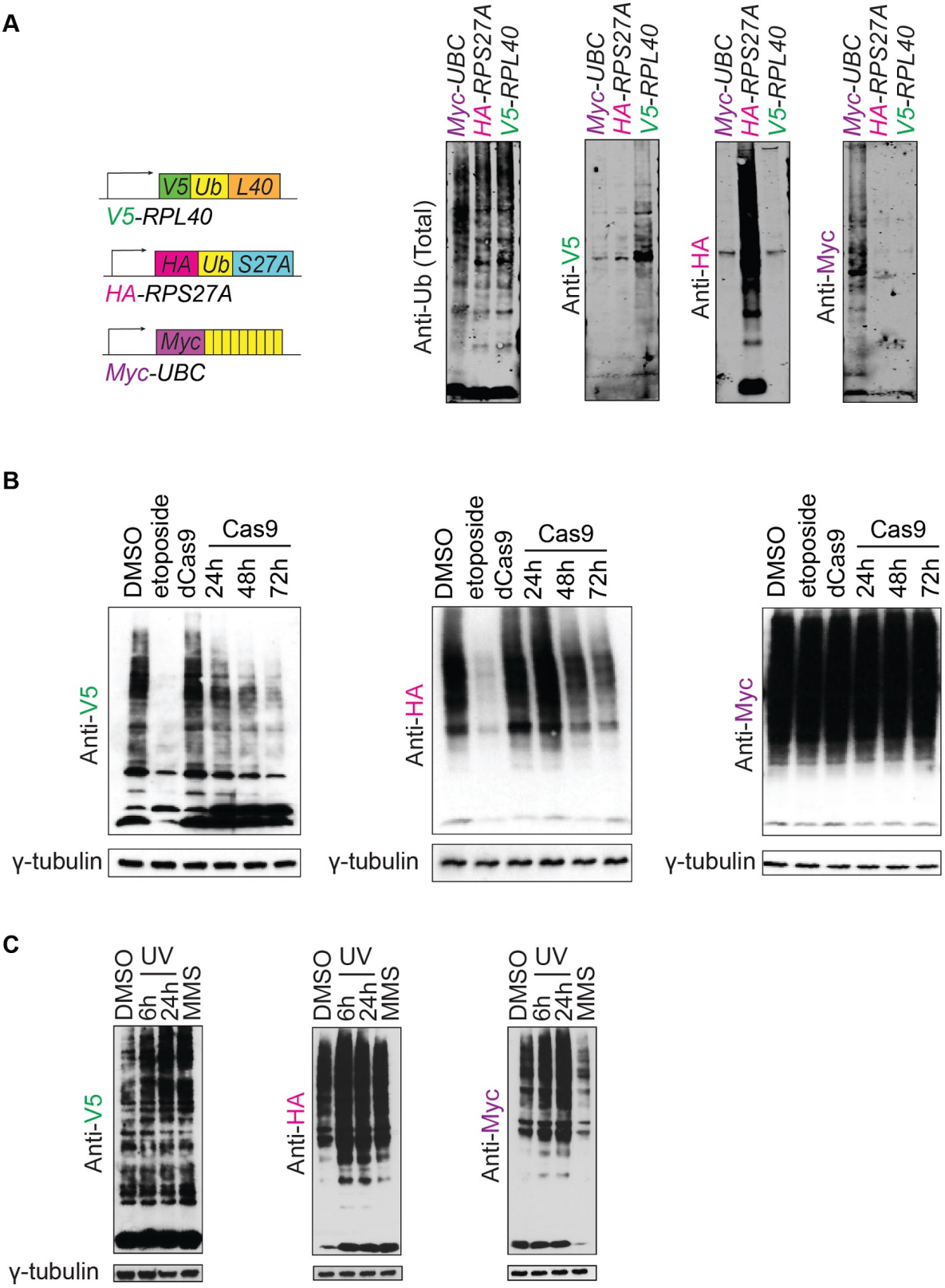

Figure S2 (Related to Fig. 2). Ubiquitins translated from *RPS27A* and *RPL40*d ecrease after dsDNA breaks

(A) Western blotting of HEK 293 cell lines edited to introduce epitope tags at the endogenous *RPL40, RPS27A*, and *UBC* loci.

(B) As in **Figure 2C**, nucelofection with dCas9 RNPs (72 hours) does not lead to depletion of V5-Ub and HA-Ub, demonstrating that their depletion is due to Cas9 DSBs.

(C) Tagged ubiquitin expression in edited HEK cells after UV radiation (20 J/m^2) or treatment with 0.03% MMS for 1 hour.

RPS27A is proteasomally degraded after dsDNA breaks

We next worked to identify the mechanism underlying the reduction in RPS27A and RPL40 after DSBs. We determined that loss of these proteins occurred post-transcriptionally, as qRT-PCR showed that DSBs induced by either etoposide or Cas9 did not affect the mRNA levels of *RPS27A* or *RPL40* (**Figure 3A-B**). In light of the key role played by ubiquitin signaling in proteasomal degradation, we wondered whether proteasomal degradation could explain the loss of RPS27A or RPL40. Indeed, we found that proteasome inhibition by epoxomicin treatment rescues the loss of RPS27A after DNA damage (**Figure 3C**). By contrast, the loss of RPL40 is unaffected, indicating that RPL40 is not proteasomally degraded after etoposide treatment (**Figure 3D**). Proteasome inhibition on its own increased basal RPS27A and RPL40 levels, suggesting some amount of constitutive degradation. The levels of other ribosomal proteins, including RPL22 and RPL10A, were unchanged by etoposide or epoxomicin treatment (**Figure 3E**). DSB-induced, proteasome-dependent degradation is therefore specific for RPS27A and does not globally affect the entire ribosome.

Next, we wanted to test whether the proteasome-dependent loss of RPS27A reflected direct proteasomal degradation of RPS27A. We generated HEK Flp-In cell lines with single copy *Ub-RPS27A-SBP* or *RPS27A-SBP* transgenes lacking the endogenous promoter, introns, and UTR sequences. Both *RPS27A-SBP* and *Ub-RPS27A-SBP* generate protein products of the same molecular weight (**Figure S3A**), consistent with prior reports that the ubiquitin moiety is rapidly cleaved from RPS27A (Baker et al., 1992; Grou et al., 2015; Larsen et al., 1998). Since these transgenes are expressed in a non-native genomic context without most regulatory RNA elements, their loss after induction of a DSB further suggests post-transcriptional regulation.

We affinity purified RPS27A-SBP in denaturing conditions and used ubiquitin chain-specific antibodies to determine that RPS27A-SBP is basally modified with Lys48 polyubiquitin chains that signal for proteasomal degradation (Newton et al., 2008). Lys48 chain modification of RPS27A increases upon induction of DSBs with etoposide (**Figure S3B**). In contrast, we did not observe substantial modification of RPS27A-SBP by Lys63 or Met1 (linear) polyubiquitin chains, which generally do not target proteins to the proteasome. Taken together, our data indicate that cells lose mature RPS27A through proteasome-mediated degradation after dsDNA damage.

We next sought identify the DNA damage response pathway that triggers the degradation of RPS27A. Consistent with our observation that RPS27A is not regulated through transcription, we found that RPS27A degradation is independent of expression of p53; RPS27A is lost after DSBs in both p53-positive (HEK293) and p53-negative (K562) cell lines (**Figure 3F**). Using small molecule inhibitors, we found that the RPS27A response is not mediated through the activity of ATM or ATR, two of the master kinases that recognize damage at the site of the DSB and initiate a DNA damage response through a phosphorylation signaling cascade (Blackford and Jackson, 2017; Maréchal and Zou, 2013) (**Figure 3G-H**). Thus the upstream molecular signals that link DSB signaling with the depletion of RPS27A remain unclear.

Proteasomal degradation is initiated by ubiquitin ligases, which play a prominent role in several aspects of DNA damage signaling. MDM2 is a DNA damage regulated ubiquitin ligase that targets p53 for degradation under normal growth conditions and can also ubiquitinate RPS27A (Sun et al., 2011). However, we found that siRNA knockdown of MDM2 had no effect on the early loss of RPS27A caused by etoposide or Cas9 (**Figure S3C**). In contrast, we found that stabilizing p53 with the MDM2 inhibitor nutlin (Vassilev et al., 2004) rescued RPS27A

levels at later time points after DSB formation, and this rescue was p53 dependent (**Figure 3I**). Recovery of RPS27A expression occurred at the transcriptional level (**Figure 3J**), consistent with *RPS27A* being a direct transcriptional target of p53 (Nosrati et al., 2015). We also found that nutlin rescued RPL40 levels after dsDNA damage and that this recovery is transcription dependent (**Figures S3D-E**). Overall, our data indicate that *depletion* of RPL40 and RPS27A is independent of p53 pathways, but the *reset* of levels of these proteins after DNA damage can be stimulated by p53.

We next turned towards a candidate approach to identify the ubiquitin ligase that regulates RPS27A. We first tested ZNF598, a mono-ubiquitin ligase known to ubiqutinate small ribosome subunit proteins RPS10 and RPS20 as part of the ribosome quality control pathway (Garzia et al., 2017; Sundaramoorthy et al., 2017). Knockdown of ZNF598 stabilized RPS27A in the presence of etoposide-induced DSBs, but had no effect on levels of RPL40 or other ribosome proteins, including the known ZFN598 target RPS10 (**Figure S3F**). In order to directly monitor RPS27A ubiquitination, we transiently expressed an epitope-tagged ubiquitin, immunoprecipitated this ubiquitin under denaturing conditions, and blotted for RPS27A. We observed ubiquitinated RPS27A under basal growth conditions, and its abundance increased upon proteasome inhibition and induction of DSBs with etoposide. Importantly, ZNF598 knockdown eliminated RPS27A ubiquitination, suggesting that ZNF598 is required for RPS27A ubiquitination (**Figure S3G**).

ZNF598 is a mono-ubiquitin ligase, but proteasomal degradation usually requires polyubiquitin Lys48 chains. As we previously found Lys48 polyubiquitin chains attached to RPS27A (**Figure S3B**), we postulated that another ubiquitin ligase extends the ZNF598-added monoubiquitin. This strategy of priming-and-extending by ubiquitin ligases has been previously described for other proteasomal substrates (Pierce et al., 2009; Wu et al., 2010). Given that MDM2 is not responsible for degradation of RPS27A, we tested the involvement of β-TRCP, which targets CReP, a eukaryotic initiation factor eIF2α phosphatase, for destruction after DNA damage (Loveless et al., 2015). We found that etoposide-induced RPS27A degradation is indeed rescued by knockdown of *β-TRCP* (**Figure S3H**). However, we found that depletion of ZNF598 or β-TRCP reduced etoposide-stimulated polyubiquitination of RPS27A to basal levels but did not eliminate ubiquitination(**Figure S3I**). Our data therefore cannot exclude regulation of RPS27A by ligases other than ZNF598 and β-TRCP. However, our data together with prior work on the molecular activities of ZNF598 and β-TRCP suggest a dual role for these ligases. We propose a 'prime-and-extend' model (Wu et al., 2010) in which RPS27A is first monoubiquitinated by ZNF598 and that this monoubiquitin is subsequently extended to Lys48-linked polyubiquitin chains by β-TRCP to signal proteasomal degradation of RPS27A.

Figure 3. RPS27A is proteasomally degraded after dsDNA breaks

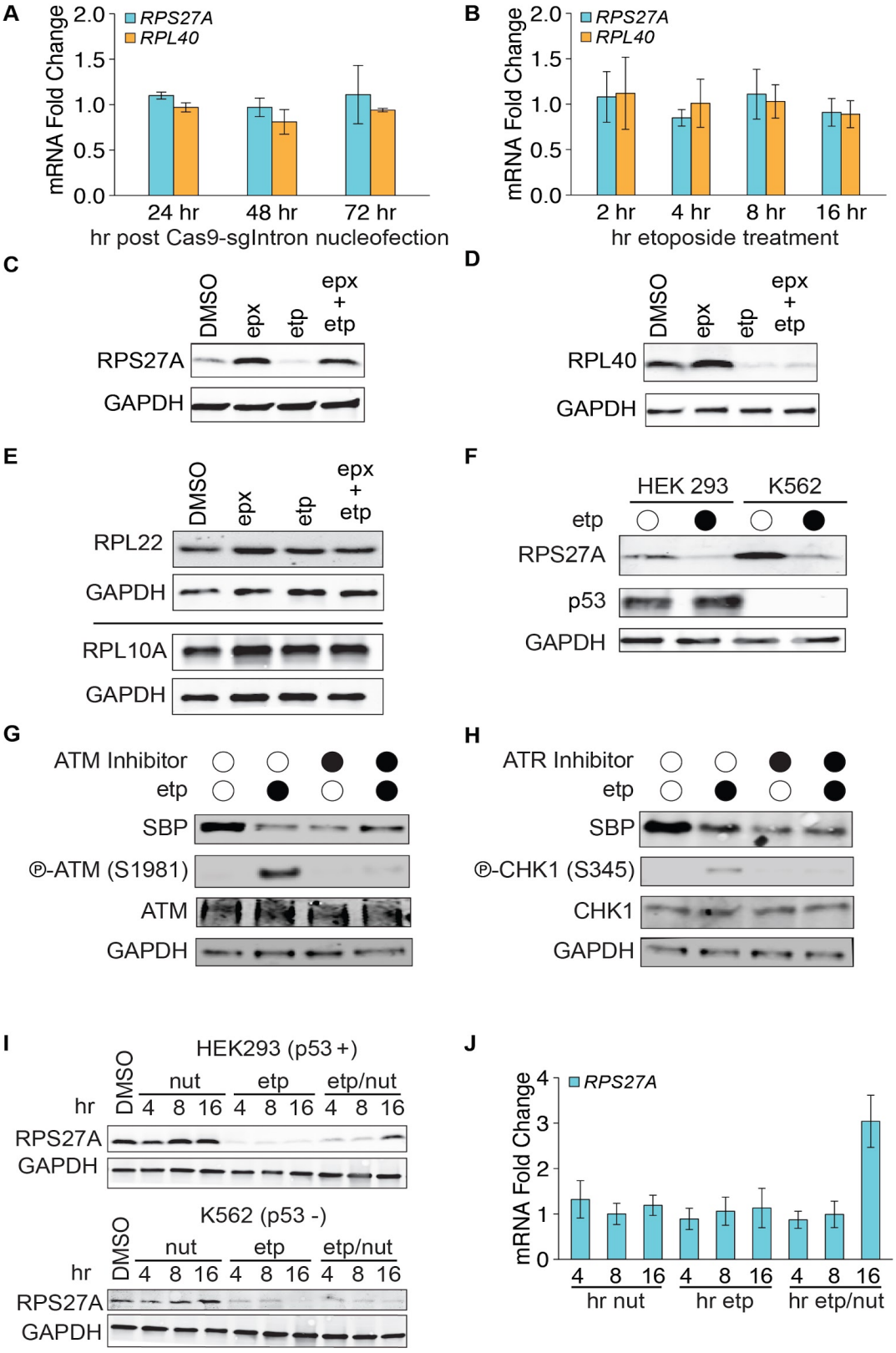

Figure 3. RPS27A is proteasomally degraded after dsDNA damage

(A) Abundance of *RPS27A* and *RPL40* transcripts does not change after Cas9 RNP nucleofection. Fold changes were calculated using the $2^{-\Delta\Delta Ct}$ method with Cas9 without sgIntron (apo Cas9) as the control and *GAPDH* as the reference gene (n = 3, error bars = standard deviation).

(B) As (A), showing abundance of *RPS27A* and *RPL40* transcripts does not change after 5 μM etoposide treatment for 16 hours.

(C) Western blots demonstrate that proteasome inhibition with epoxomicin rescues RPS27A depletion.

(D) As in (C), revealing that proteasome inhibition does not block DNA damage induced RPL40 depletion.

(E) Western blots show that neither DNA damage nor proteasome inhibition affect levels of ribosomal proteins RPL22 or RPL10A.

(F) Western blots confirm the p53 null status of K562 cells and demonstrate that loss of RPS27A is p53-independent.

(G) ATM inhibition does not rescue RPS27A degradation. Transgenic RPS27A with a C-terminal SBP tag was followed by Western blotting after treatment with 5 μM etoposide and/or 10 μM ATM inhibitor, KU 55933. Phospho-ATM served as a positive control for ATM inhibition.

(H) As in (G), showing that ATR inhibition (10 μM AZ 20 for 16 hours) does not rescue RPS27A degradation. Phospho-CHK1 served as a positive control for ATR inhibition.

(I) Western blotting reveals a partial rescue of RPS27A levels in p53-positive HEK cells but not p53-null K562 cells when p53 degradation is inhibited with 10 μM nutlin.

(J) *RPS27A* transcript abundance increases after DNA damage when p53 is stabilized by nutlin treatment (n = 4, error bars = SD).

Figure S3 (Rel. to Fig. 3). RPS27A is proteosomally degraded after dsDNA breaks

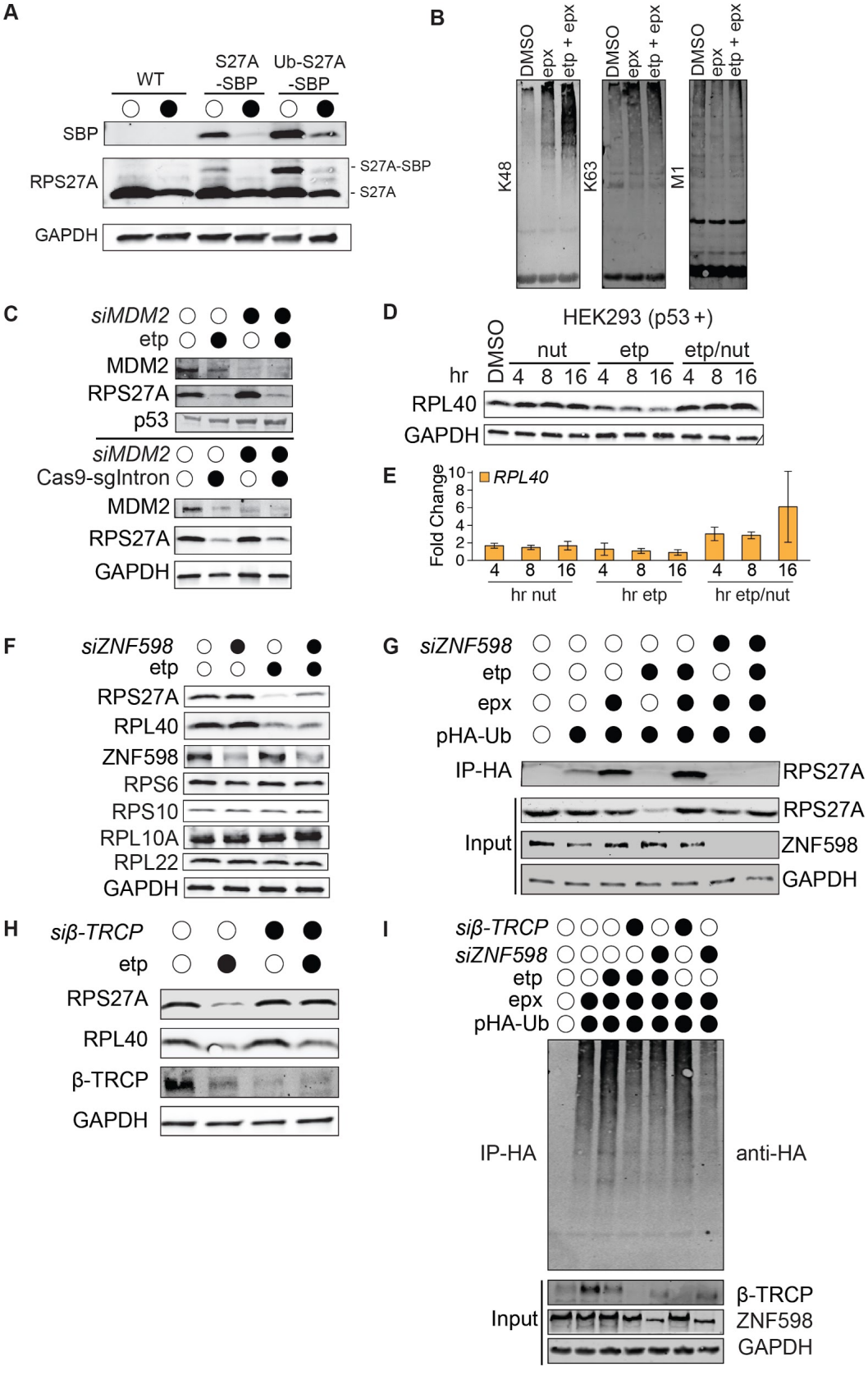

Figure S3 (Related to Fig. 3). RPS27A is proteasomally degraded after dsDNA damage

(A) Western blotting of RPS27A and SBP tag in HEK Flp-In cell lines with stable, single-copies of *pCMV-Ub-RPS27A-SBP* or *pCMV-RPS27A-SBP* transgenes after 5 μM etoposide or DMSO treatment for 16 hours. Note that *RPS27A* transgenes lack the endogenous promoter and UTR sequences.

(B) Western blotting for K48, K63, and M1 ubiquitin linkages on affinity-purified RPS27A-SBP indicates constitutive and etoposide-induced K48-linked ubiquitin chains. HEK Flp-In cell lines expressing *pCMV-RPS27A-SBP* were treated with epoxomicin (50 nM, 17 hours) and etoposide (5 μM, 16 hours).

(C) Western blotting demonstrates RPS27A depletion is insensitive to *MDM2* knock-down 16 hours after 5 μM etoposide treatment or 72 hours after Cas9-sgIntron nucleofection. Non-targeting siRNAs, DMSO, and Cas9 without a guide served as negative controls.

(D) Western blotting of RPL40 shows that nutlin (10 μM) treatment rescues RPL40 depletion induced by etoposide (5 μM) in HEK cells.

(E) Abundance of *RPL40* transcripts increases after co-administration of nutlin and etoposide.

(F) Western blotting to monitor RPS27A and RPL40 after *ZNF598* knock-down relative to a non-targeting control siRNA.

(G) Western blotting against RPS27A protein following anti-HA immunoprecipitations from HEK cell lysates transfected with a plasmid expressing HA-Ub. Cells were transfected with siRNAs and, after 24 hours, with the HA-Ub plasmid. Lysates were prepared 48 hours after the second transfection.

(H) Western blotting against RPS27A protein following siRNA knockdown of *β-TRCP* (or a non-targeting control siRNA) and etoposide treatment.

(I) As in (G), using an HEK cell line expressing a single-copy *pCMV-RPS27A-SBP* transgene.

Double-strand DNA breaks lead to eIF2α phosphorylation and reduced translation initiation

Given the loss of RPS27A and RPL40 after dsDNA damage, we asked if cells exhibit a translation phenotype in response to DSBs. Consistent with our prior data (**Figure 1F**), polysome profiles of HEK293 cells treated with etoposide showed a sharp increase in 80S monosomes and a concordant reduction in polysomes (**Figure 4A**), demonstrating that etoposide-treated cells have fewer ribosomes per transcript. Etoposide-treated cells exhibited an imbalance in small (40S) and large (60S) ribosome subunits compared to DMSO-treated samples (40S:60S peak height ratio of 2:7 etoposide versus 1:1 DMSO), suggesting a deficiency in 40S subunits. Because the accumulation of monosomes is a hallmark of reduced protein synthesis, we wanted to gauge how nascent chain translation changes after DSBs. We used incorporation of L-azidohomoalanine (AHA), a methionine mimic that can be labeled with alkyne-conjugated probes, to track protein synthesis (Wang et al., 2017). Induction of multiple DSBs with etoposide led to a marked reduction in translation, consistent with accumulation of 80S monosomes (**Figure 4B**; **Figures S4A**). Surprisingly, induction of a single DSB with Cas9 led to reduced translation output as well (**Figure 4B**). Polysome profiling of Cas9 nucleofected cells revealed a modest increase in 80S, decrease in 40S, and shift from heavy to light polysomes (**Figure S4B**). Thus both chemically-induced DSBs and Cas9-mediated genome editing lead to a global reduction in protein synthesis.

We next asked if dsDNA-damaged cells regulate translation through either of two canonical mechanisms: the phosphorylation of eukaryotic initiation factor 2α (eIF2α) or the de-phosphorylation of 4E binding protein (4E-BP). Phosphorylation of eIF2α prevents eIF2 from recruiting the initiator methionine tRNA to the mRNA while de-phosphorylation of 4E-BP inhibits eIF4E from associating with the 5' cap of transcripts (Jackson et al., 2010; Sonenberg and Hinnebusch, 2009). We found that multiple, non-specific etoposide-induced DSBs and a single, targeted Cas9-induced DSB both cause phosphorylation of eIF2α (**Figure 4C**). In contrast, we observed no changes in phosphorylation of 4E-BP (**Figure 4D**).

Phosphorylation of eIF2α translationally activates a group of transcripts collectively known as the integrated stress response (Sidrauski et al., 2013). We confirmed that etoposide increases expression of ATF4, a key integrated stress response transcription factor (**Figure S4C**). We also observed that co-administration with ISRIB, a small molecule that mitigates the downstream effects of eIF2α phosphorylation (Sidrauski et al., 2013), rescued the etoposide-induced accumulation of 80S monosomes, depletion of polysomes, and 40S:60S imbalance (**Figure 4A**), and restored bulk protein synthesis (**Figure 4B**). Our data indicate that both drug- and Cas9-induced dsDNA breaks lead to the inhibition of translation initiation through eIF2α phosphorylation.

We previously found that the etoposide-induced loss of RPL40 is not mediated through transcription or proteasomal degradation (**Figure 3A**, **D**), and we therefore asked whether RPL40 is regulated at the translational level by eIF2α signaling. We found that co-administration of ISRIB with etoposide completely prevented the loss of RPL40 caused by DSBs (**Figure 4E**). RPS27A levels were slightly increased by ISRIB in the presence of DSBs, but were far from completely rescued. Thus RPL40 is regulated at the translation level through a phosho-eIF2α dependent mechanism.

We next used Cas9 targeted to different genomic locations to explore whether eIF2α phosphorylation is a general response to genome editing. We tested guide RNAs that target the

JAK2 intron (sgIntron, see **Figure 1C** for editing efficiency), the AAVS1 safe harbor site (sgAAVS1, (Richardson et al., 2016)) or a blue fluorescent protein (BFP) single-copy transgene (sgBFP, (Richardson et al., 2018)). All Cas9 RNPs caused eIF2α phosphorylation (Figure 4F). Nucleofecting Cas9 without a guide RNA (apo Cas9) had no effect on eIF2α phosphorylation, nor did nucleofection of guide RNAs complexed with catalytically inactive dCas9. Genomic nicking induced by the Cas9 D10A nickase (nCas9) also did not induce eIF2α phosphorylation. We confirmed that Cas9-induced eIF2α phosphorylation was specific to the dsDNA damage itself, as Cas9 RNP complexes only induced eIF2α phosphorylation when the guide RNA had a genomic target. When we nucleofected Cas9-sgBFP into parental HEK293 cells we found no evidence of eIF2α phosphorylation (**Figure 4F**), but nucleofecting the same RNP into HEK293 cells harboring a BFP transgene led to phosphorylation of eIF2α.

We also verified that eIF2α phosphorylation is a general response that occurs after Cas9 RNP editing in a range of primary cell types. Neither T-cells, hematopoietic stem and progenitor cells (HSPCs), nor fibroblasts exhibited high levels of eIF2α phosphorylation when nucleofected with negative control apo Cas9 or dCas9-sgRNA **(Figure 4G**; see **Figures S4D-E** for T-cell sgRNA target validation). However, nucleofection with catalytically active Cas9 complexed with multiple different targeting guide RNAs caused increased eIF2α phosphorylation in each of these primary cells. Primary cells are p53-positive, but we found that eIF2α phosphorylation also occurs in K562 p53-negative cells, much like RPS27A degradation (**Figure S4F**). Hence, a single locus Cas9-induced DSB triggers eIF2α phosphorylation in a wide range of cell types.

Figure 4. Double-strand DNA breaks lead to eIF2α phosphorylation and reduced translation initiation

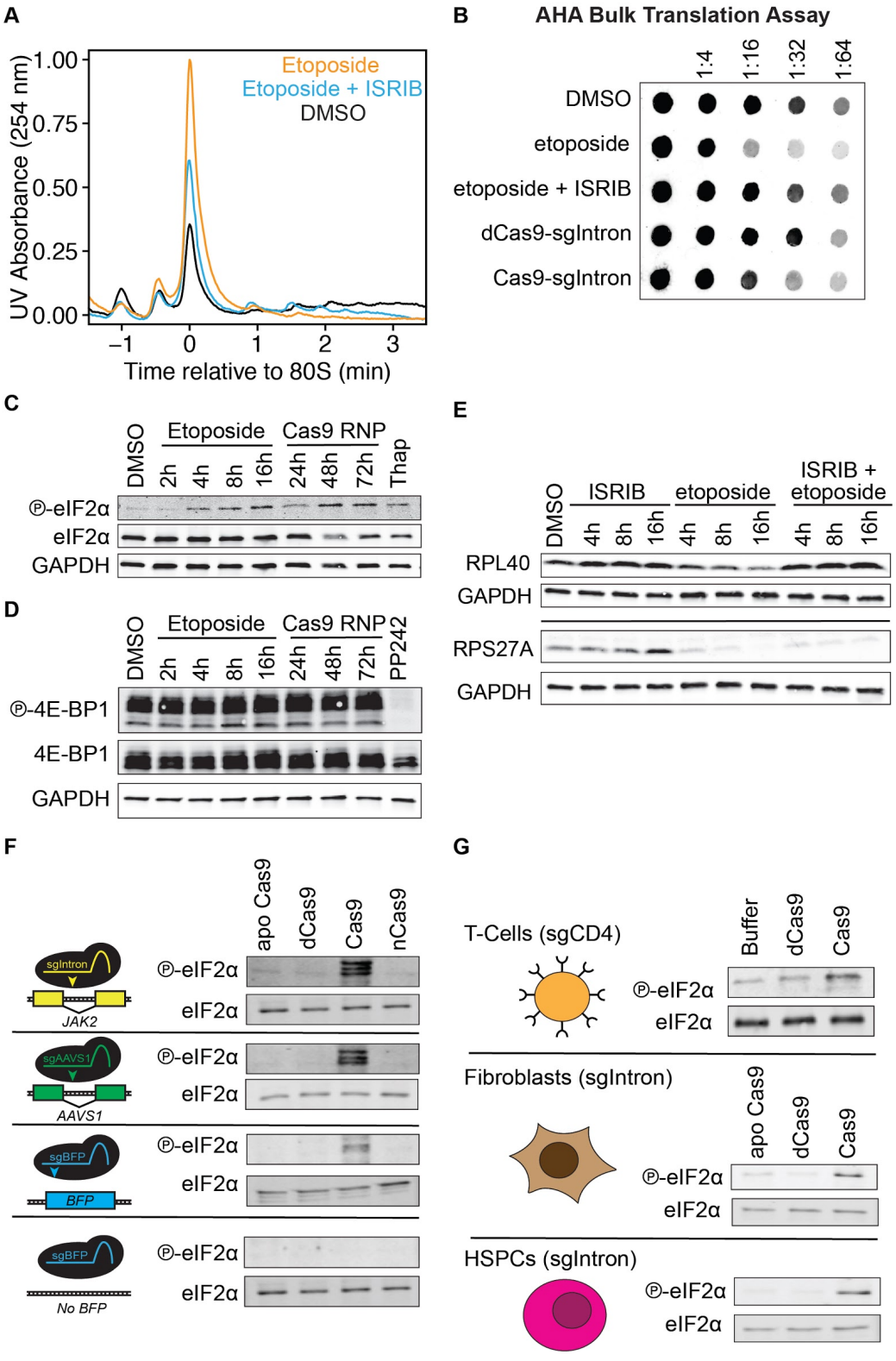

Figure 4. Double-strand DNA damaged leads to eIF2α phosphorylation and reduced translation initiation

(A) Polysome profiles of HEK cells treated with 5 μM etoposide or 5 μM etoposide, 200 nM ISRIB for 16 hours.

(B) AHA bulk translation assay demonstrates that dsDNA damage reduces protein synthesis. HEK cells were lysed after 16 hours after drug treatment or 72 hours after nucleofections with RNPs. Two hours before lysis, growth media replaced with methionine-free media containing a methionine mimic, L-azidohomoalanine (L-AHA). Lysates were normalized by protein content, labeled with IRDye 800CW-DBCO Infrared Dye, blotted on a nitrocellulose membrane, and imaged with a LI-COR Odyssey CLx Imager.

(C) Levels of eIF2α (S51) phosphorylation increase in HEK cells treated with 5 μM etoposide or nucleofected with Cas9-sgRNA RNPs targeting a *JAK2* intron. Treatment with 1 μM thapsigargin (Thap) for 30 minutes served as a positive control for eIF2α phosphorylation.

(D) As in (C), showing that levels of 4E-BP1 (T37/47) phosphorylation do not change after DNA damage. Treatment with 2.5 μM PP242 for 30 minutes served as a positive control for 4E-BP1 hypo-phosphorylation.

(E) Western blotting indicates that phospho-eIF2α inhibitor ISRIB rescues loss of RPL40 but not RPS27A after DNA damage.

(F) Only active Cas9 with a targeting gRNA triggers eIF2α phosphorylation. HEK or HEK-BFP cells were nucleofected with Cas9 without guide (apo Cas9), dCas9, Cas9, or nickase Cas9 and guides against a *JAK2* intron (sgIntron), the *AAVS1* locus (sgAAVS1), or a *BFP* transgene (sgBFP).

(G) Western blotting reveals eIF2α phosphorylation in T-cells, fibroblasts, and MPB-CD34+ HSPCs 24 hours after nucleofection with sgCD4 or sgIntron RNPs.

Figure S4 (rel to Fig 4). Double-strand DNA breaks lead to eIF2α phosphorylation and reduced translation initiation

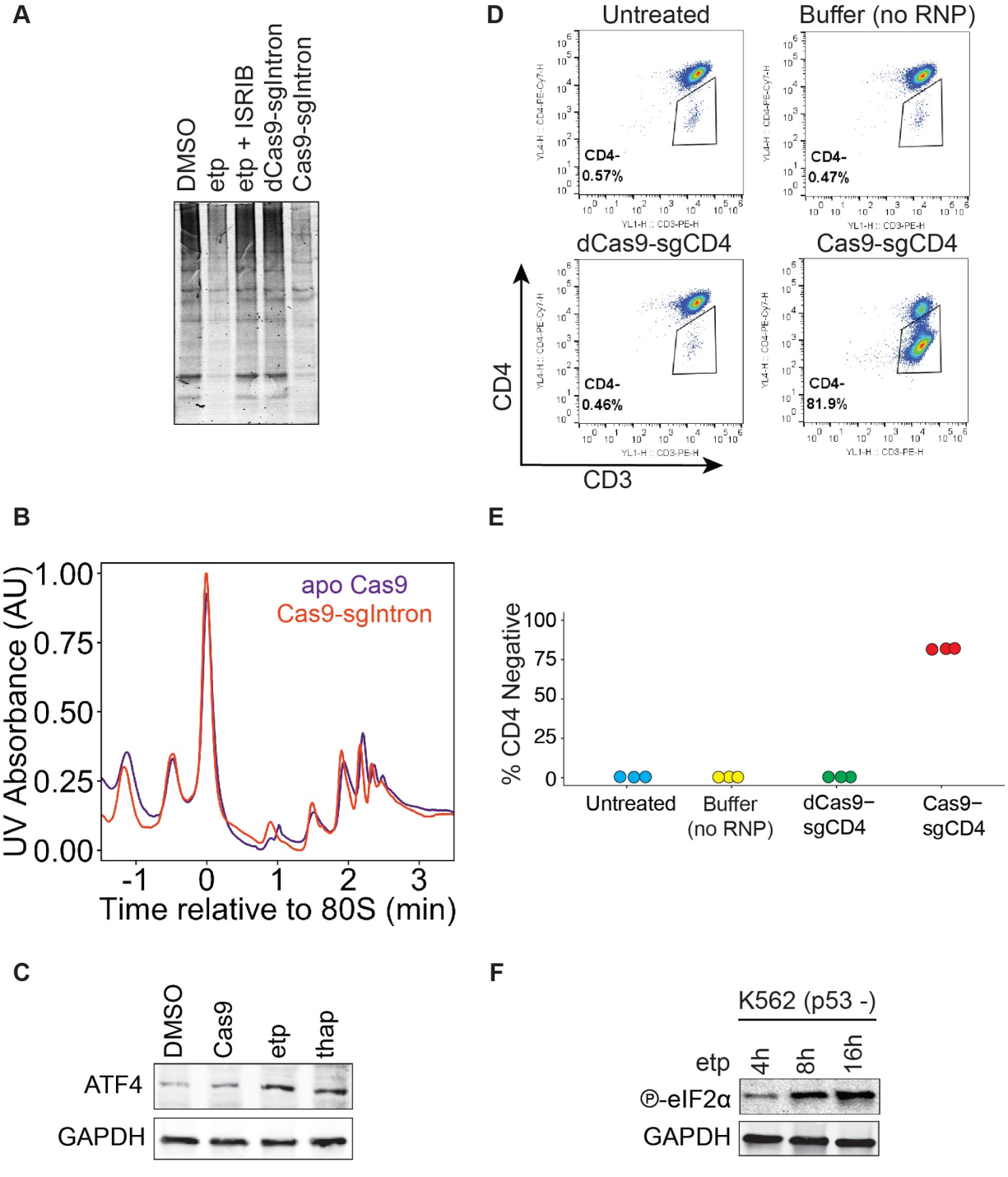

Figure S4 (Related to Fig. 4) Double-strand DNA breaks lead to eIF2α phosphorylation and reduced translation initiation

(A) IR800 LI-COR-image of SDS-PAGE gel with L-AHA labeled lysates depicted in (**Figure 4H**).

(B) Polysome profiles of HEK cells 72 hours after nucleofection with active Cas9-sgIntron RNP, or Cas9 without guide (apo Cas9).

(C) Western blotting of ATF4 induction. Cells were harvested 72 hours after nucleofection with Cas9-sgIntron or 16 hours after treatment with 5 μM etoposide. Cells treated with DMSO for 16 hours or 1 μM thapsigargin for 30 minutes served as negative and positive controls respectively.

(D) Examples of flow cytometry editing efficiency analysis of T-cells nucleofected with Cas9-sgCD4 in tandem with cells depicted in **Figure 4F**. T-cells were stained with anti-CD3-PE, anti-CD4-PE-Cy7, and GhostDye780 (to mark dead cells).

(E) Average percentage of edited, CD4 negative T-cells three days after Cas9-sgCD4 electroporation as determined by FACS (n = 3).

(F) Western blotting of eIF2α (S51) phosphorylationin K562 cells treated with 5 μM etoposide.

Modulating eIF2α phosphorylation alters genome editing outcomes

Given that eIF2α phosphorylation is induced by DSBs, we wondered whether downstream eIF2α signaling influenced genome editing outcomes. We altered the eIF2α response using two small molecule drugs: ISRIB to bypass eIF2α signaling and salubrinal to increase eIF2α phosphorylation (**Figure S5A**, (Boyce et al., 2005)). We performed editing experiments with HEK293 or K562 cells treated with ISRIB or salburinal, targeting a single-copy BFP transgene in each cell line to introduce insertions and deletions (indels) via error-prone DNA repair. We monitored genome editing using both T7 endonuclease I (T7E1) heteroduplex assays and next-generation sequencing of PCR amplicons of the edited transgene. Strikingly, increasing phospho-eIF2α signaling with salubrinal decreased the frequency of indels during Cas9-sgBFP editing. Bypassing phospho-eIF2α signaling with ISRIB, on the other hand, resulted in an increased fraction of indels (**Figure 5A-B**). Increasing eIF2α phosphorylation with salubrinal while simultaneously bypassing this phosphorylation with ISRIB overcame the salubrinal-induced decrease in editing (**Figure 5A-B**). Perturbing eIF2α signaling affected editing levels in both p53-positive (HEK) and p53-negative cells (K562) (**Figure 5A**, **S5B**). From next-generation sequencing of edited alleles, we found that modulating eIF2α phosphorylation changed the relative frequency of edited alleles rather than introducing new types of indels (**Figure 5C**, **Figure S5C**). These data indicate that DSB-induced eIF2α signaling affects DNA repair to reduce the error-prone formation of indels.

Figure 5. Modulating eIF2α phosphorylation alters genome editing outcomes

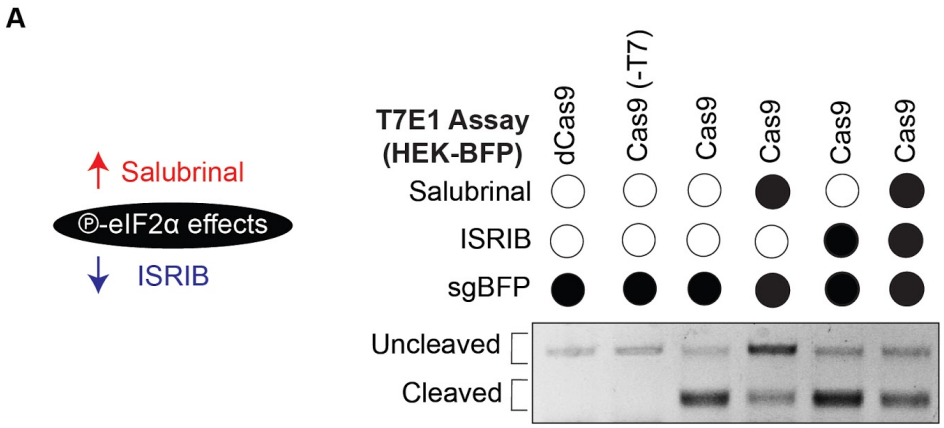

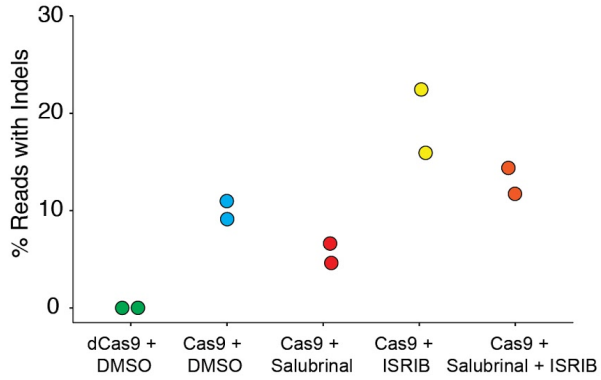

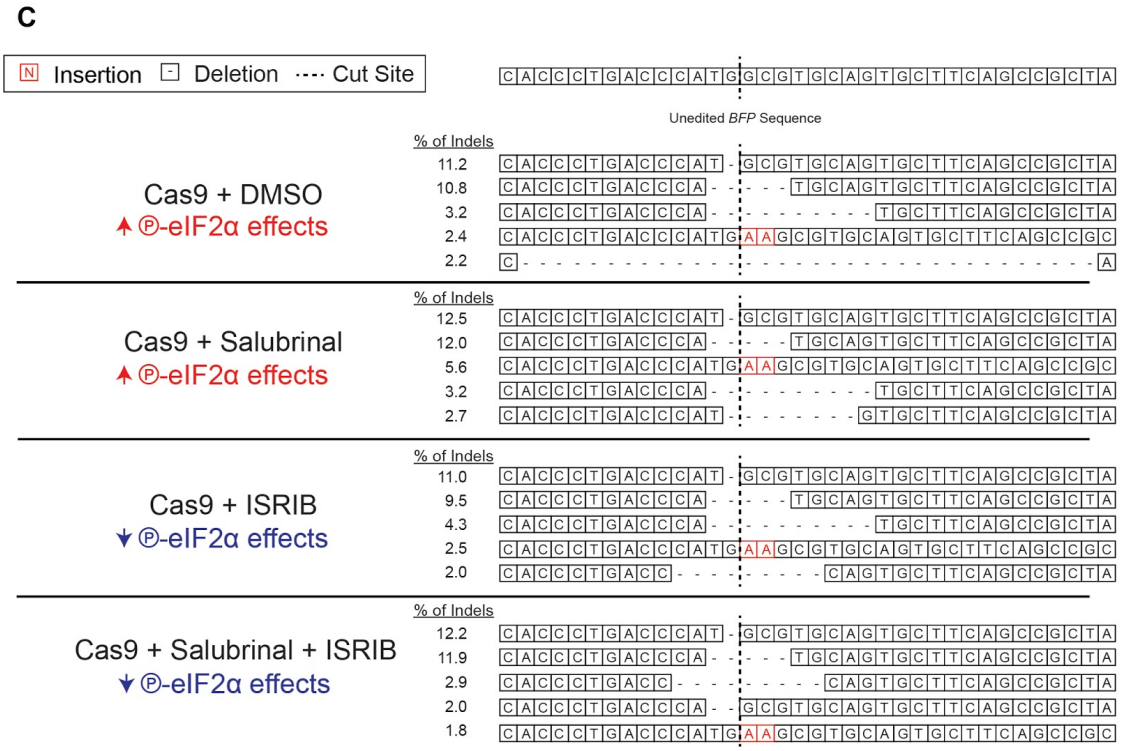

Figure 5. Modulating eIF2α phosphorylation alters genome editing outcomes

(A) T7 Endonuclease 1 assay for genome editing of the transgenic *BFP* locus in HEK-BFP cells nucleofected with sgBFP-Cas9 (or dCas9) RNPs and treated with 75 μM salubrinal or 200 nM ISRIB for 16 hours. (Image analyzed as in **Figure 3A**).

(B) Percentage of next generation sequencing (NGS) reads with insertions or deletions after genome editing, as in (A). Reads were aligned using NEEDLE (Li et al., 2015), and a modified version of CRISPResso (Pinello et al., 2016) was used to analyze editing outcomes.

(C) Sequence identity and frequency of the top five *BFP* indel alleles from one of each experimental condition quantified in (B).

Figure S5 (related to Fig.5). Modulating eIF2α phosphorylation alters genome editing outcomes

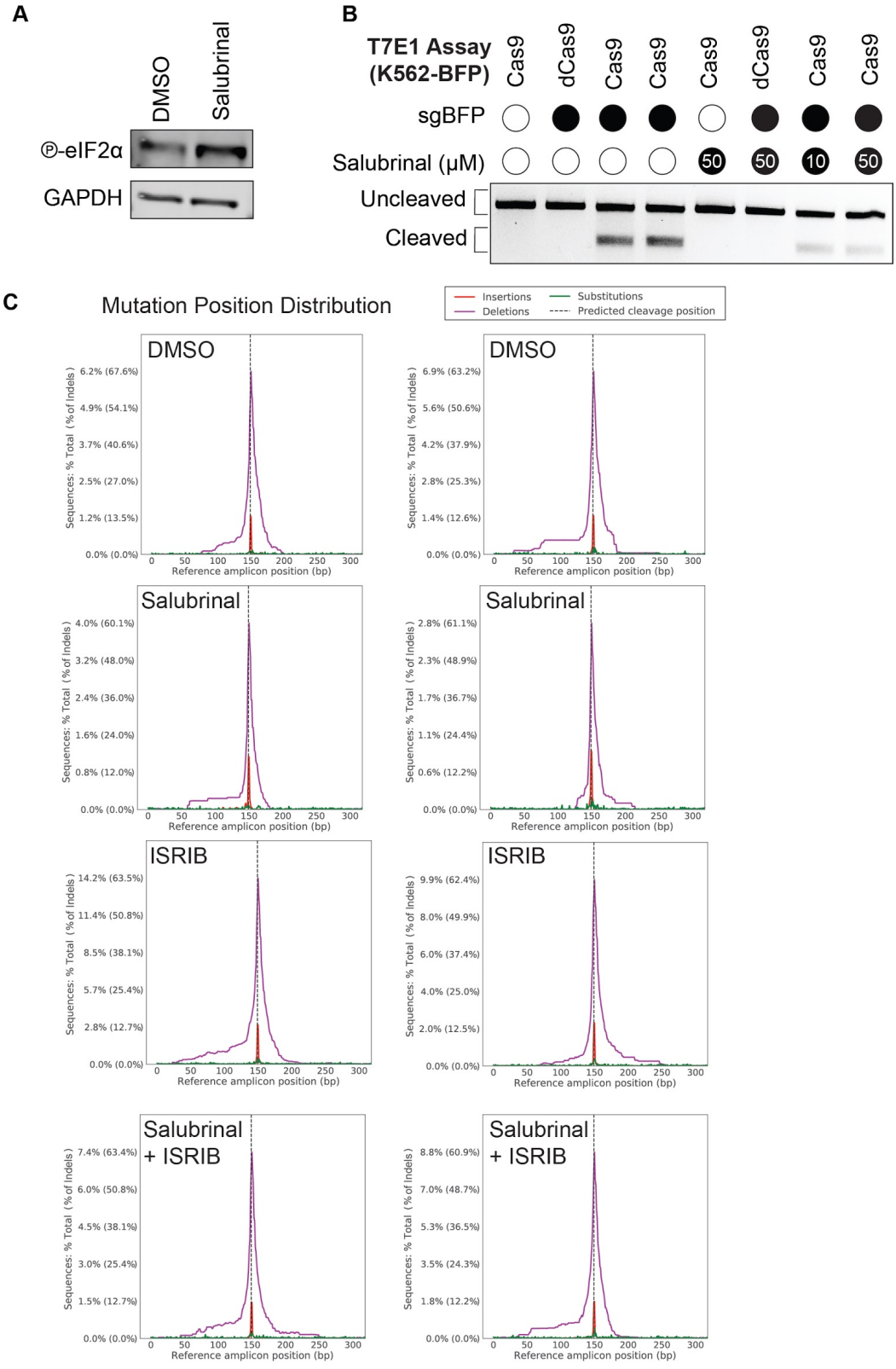

Figure S5 (related to Fig. 5). Modulating eIF2α phosphorylation alters genome editing outcomes

(A) Western blotting of eIF2α (Ser51) phosphorylation in HEK-BFP cells treated with 75 μM salubrinal or DMSO for 24 hours.

(B) T7 Endonuclease 1 cleavage assay. K562-BFP cells were nucleofected with sgBFP-Cas9 (or dCas9) RNPs and treated with 10 or 50 μM salubrinal for 16 hours.

(C) Mutation distribution plots of NGS reads with insertions or deletions (% reads with indels) from gDNA PCRs of HEK-BFP cells nucleofected with sgBFP-Cas9 (or dCas9) RNPs and treated with 75 μM salubrinal or 200 nM ISRIB for 24 hours.

Genome editing initiates a translational response that precedes long-term transcriptional changes

We wanted to measure how the ribosome remodeling and eIF2α phosphorylation induced by Cas9-mediated genome editing globally affect translation. We carried out ribosome profiling and matched mRNA sequencing in HEK293 cells with a single DSB induced by Cas9-sgIntron, with catalytically inactive dCas9-sgIntron serving as our background control (**Figure 6A**). JAK2 mRNA and ribosome footprint levels did not show any significant differences at either 36 or 72 hours, confirming our qPCR data (**Figure S1A**), which indicated that sgIntron-targeted editing does not perturb expression of JAK2. Global profiling of translation and transcription revealed that cells with a single Cas9-DSB activate an early translational program that is replaced by a longer-term transcriptional response. At 36 hours after nucleofection, we found 132 genes that exhibit changes in ribosome footprint abundance while no genes changed in transcript abundance (Wald test, FDR corrected p-value < 0.1, **Figures 6B-C**). By 72 hours, there were changes in mRNA transcript levels but no statistically significant changes in footprint abundance (**Figures 6B&D**). Translational efficiency, the ratio of ribosome footprints to mRNA transcripts, also reflected these differences, with changes in translational efficiency at 36 hours driven by translation and changes at 72 hours driven by mRNA abundance (**Figure S6A**).

Because we found that even a single DSB induces eIF2α phosphorylation, we asked whether genes known to be translationally regulated during the phospho-eIF2α-induced integrated stress response (ISR) also experience changes in translation after a Cas9-induced DSB. At both 36 and 72 hours after Cas9 nucleofection, we found that ISR targets collectively had higher translation ($p< 0.05$, Mann-Whitney-Wilcoxon test, **Figure 6E, 6G**), although individual genes did not rise to the level of significance. This effect was much larger at 36 hours than at 72 hours. Genome editing with Cas9 therefore leads to the induction of the integrated stress response at the translation level. These results provide a global view of cells activating translational and transcriptional responses that persist days after Cas9 is gone from the cell and genome editing is complete (**Figure 1B-C**).

Given that we observed changes in RPS27A and RPL40 levels after Cas9 editing, we asked how the global translation of ribosomal protein genes changes after a Cas9-mediated DSB. We found decreased footprints and mRNA abundance for several ribosomal protein transcripts 36 hours after Cas9 editing ($p< 0.05$, **Figure 6E-F**). eIF2α phosphorylation can lead to modest decreases in ribosome protein translation (Sidrauski et al., 2015), and our data links this eIF2α signaling to the DSB response. Ribosome protein transcript levels increased 72 hours after a Cas9-mediated DSB, suggesting that the cell resets ribosome protein levels through increased transcription (**Figures 6G-H**). Given our previous data that the reset of *RPS27A* and *RPL40* transcripts after DSBs is p53-dependent (**Figure 3I, S3D**), it is tempting to speculate that the global transcriptional increase in ribosomal transcription is the result of p53 signaling.

In the Cas9 ribosome profiling datasets, we found that DSB repair genes are somewhat regulated at the translation level. DSB repair genes showed no significant change in translation at 36 hours (**Figures 6E, S6B**) but showed a small decrease in translation efficiency at 72 hours that was driven by transcript abundance (**Figures S6B**). This decrease in translation may signify that the cell tunes down the production of these proteins as the cell returns to homeostasis. Our data, however, do not exclude early translational control of DSB repair genes that is completed before 36 hours.

In sum, our ribosome profiling and RNA-seq data from Cas9-treated cells demonstrate that even a single DSB can induce small, yet significant changes to the translatome and

transcriptome that persist days after the lesion is formed and repaired. Overall, our data suggest that Cas9 editing leads to changes in signaling, translation, and gene expression that are not only independent of editing a target gene but also inherent to the cellular response to double stranded DNA damage.

Figure 6. Genome editing initiates a translational response that precedes long-term transcriptional changes

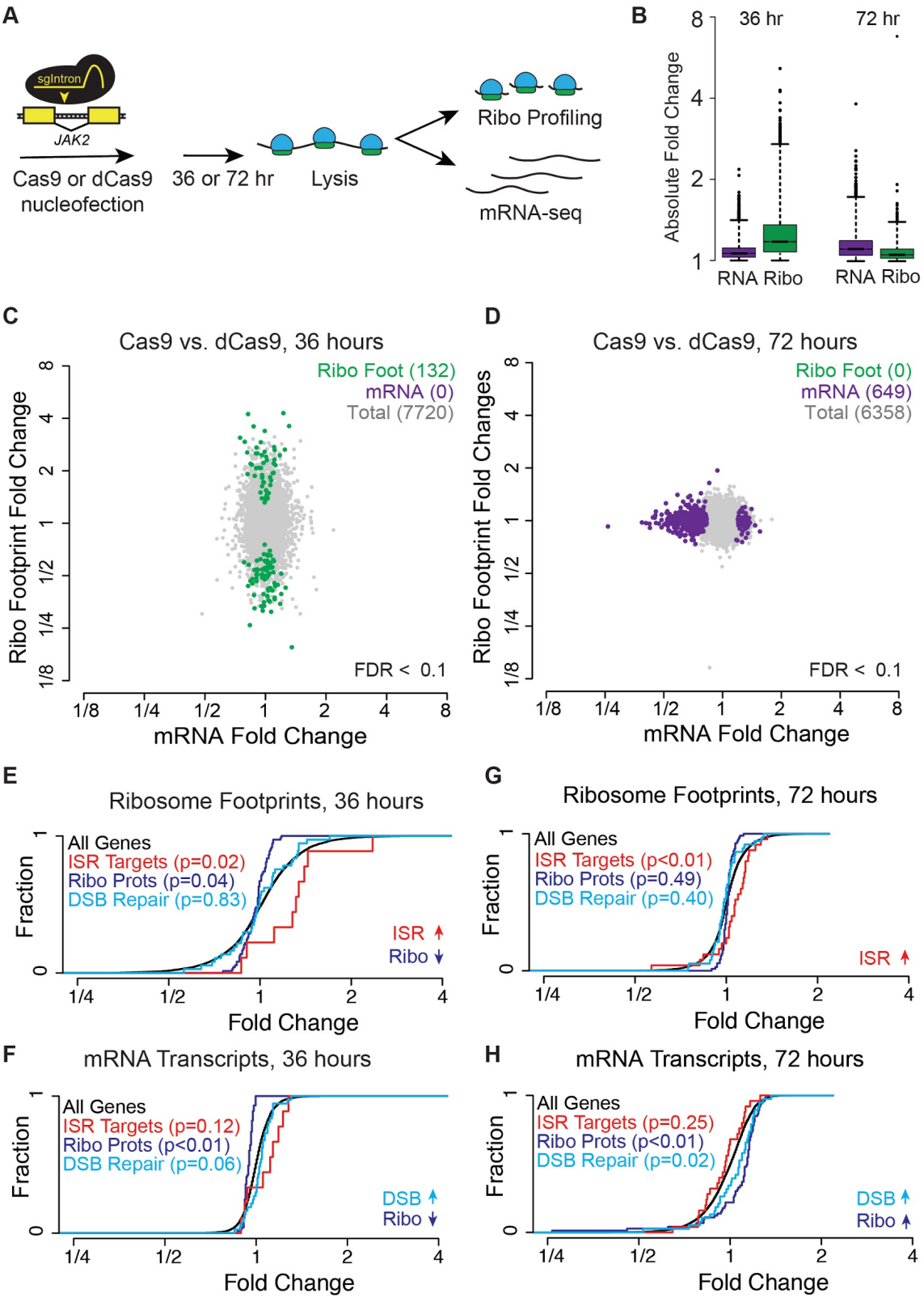

Figure 6. Genome editing initiates a translational response that proceeds long-term transcriptional changes

(A) Experimental design for ribosome profiling and RNA-seq experiments. HEK cells were nucleofected with Cas9-sgIntronand harvested after 36 or 72 hours. Lysates were divided between ribosome profiling and RNA-seq experiments.

(B) Distribution of absolute fold changes on a logarithmic scale, for genes identified in RNA-seq and ribosome profiling experiments at 36 and 72 hours post-editing. Whiskers denote values 1.5 * (the interquartile range).

(C) Changes in ribosome footprint versus mRNA abundance (C) 36 hours or (D) 72 hours after Cas9 or dCas9 nucleofection. Green = genes with significant changes in ribosome footprints. Purple = genes with significant changes in mRNA transcripts (Wald test, FDR < 0.1).

(E) Cumulative distribution function (CDF) plots for ribosomal protein genes (Ribo), integrated stress response targets (ISR), and DSB repair genes observed in the ribosome profiling (E-F) and mRNA-seq (G-H) experiments 36 hours (E and G) or 72 hours (F and H) after Cas9-sgIntron nucleofection. p-values were calculated using the Mann-Whitney-Wilcoxon rank sum test. See **Table S3** for target set gene lists.

Figure S6 (Related to Fig. 6). Genome editing initiates a translational response that precedes long-term transcriptional changes

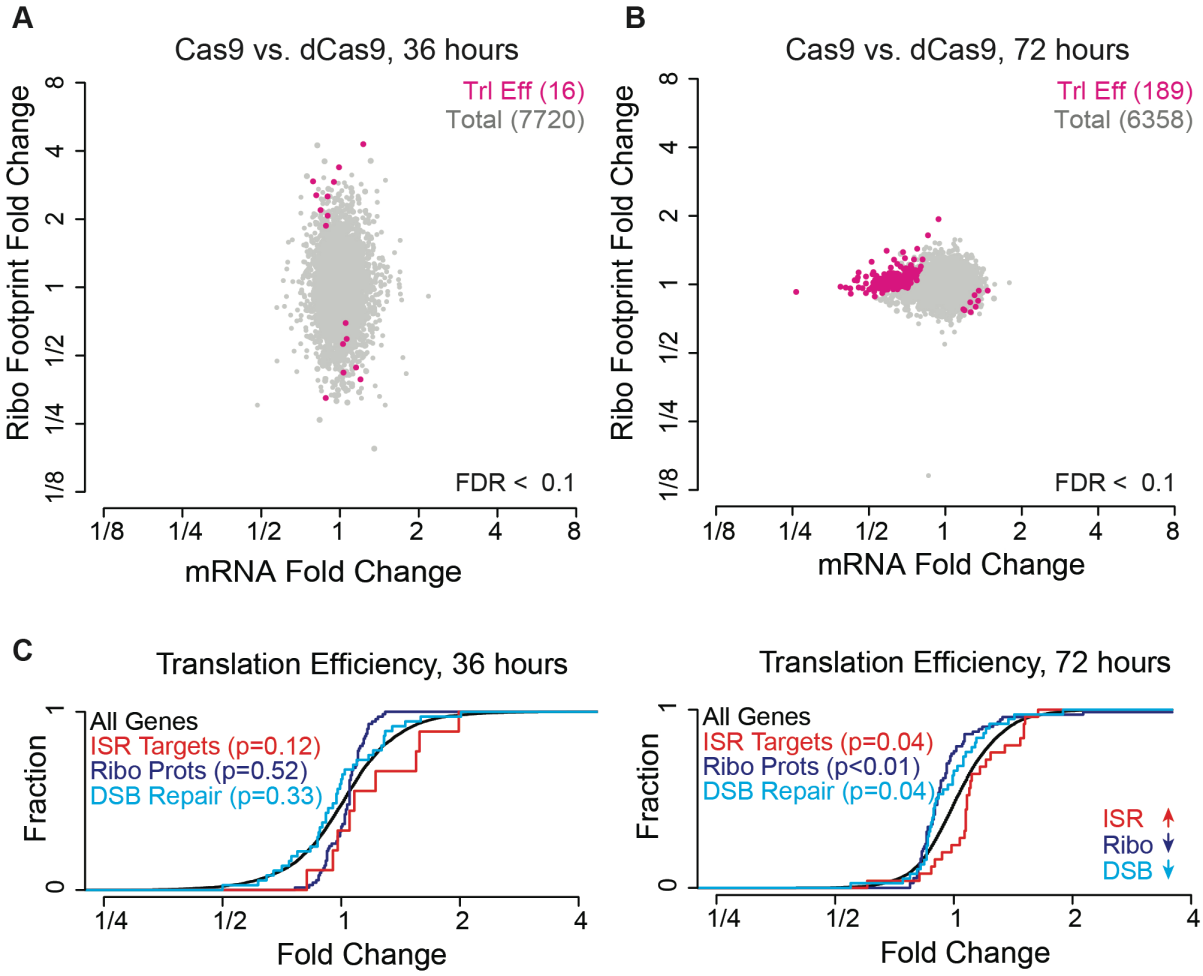

Figure S6 (Related to Fig.6). Genome editing initiates a translational response that proceeds long-term transcriptional changes

(A) As in **Figure 6C**, with pink marking genes with significant changes in translation efficiency, the ratio of ribosome footprints to mRNA transcripts (Wald test, FDR adjusted *p*-value < 0.1).

(B) As in (A) for 72-hour ribosome profiling and RNA sequencing data.

(C) As in Figures 6E through 6H, for translation efficiency.

Discussion

DNA damage poses a serious threat to organisms. Consequently, cells have an array of damage response pathways dedicated to maintaining genome integrity. These responses include cell cycle arrest after moderate levels of damage and apoptosis when the insult becomes too great. One hallmark of the DNA damage response is transcriptional reprogramming, such as the p53 response. Here, we report another, translational layer of DSB response. Even a single DSB caused by Cas9 genome editing can induce potent, p53-independent ribosome remodeling and translational reprogramming that occurs prior to transcriptional changes.

Translational shutdown after DNA damage promotes error-free repair

We found that DSBs introduced during genome editing lead to translational reprogramming in immortalized and primary human cell types. Bulk protein synthesis is reduced after DSBs in part because translation is inhibited by eIF2α phosphorylation. Other types of DNA damage can induce eIF2α phosphorylation (Deng et al., 2002; von Holzen et al., 2007; Jiang and Wek, 2005; Kim et al., 2014; Peidis et al., 2011; Robert et al., 2009; Wu et al., 2002), and we found that multiple DSBs or even a single DSB leads to eIF2α phosphorylation. However, single-strand genomic lesions do not induce this signal (Cas9 vs. nickase Cas9, **Figure 4D**). Ionizing radiation can cause mTOR-mediated dephosphorylation of 4E-BP (Braunstein et al., 2009b; Kumar et al., 2000b; Schneider et al., 2005b), but we found no evidence that cells with chemically- or Cas9-induced DSBs reduce translation through 4E-BP dephosphorylation (**Figure 4C**). This difference may reflect other cellular responses to the collateral damage caused by ionizing radiation to non-DSB DNA lesions or to other macromolecules including RNA and protein. We have found that the DSB translational response does not require canonical DNA damage factors such as p53. Reset of ribosomal protein levels after DSBs can be stimulated by p53-mediated transcription (**Figure 3J, S3E**), but the upstream signaling pathways linking DNA damage to eIF2α phosphorylation remain unclear.

We found that eIF2α phosphorylation may help cells avoid permanent genomic changes after double stranded DNA damage. Notably, bypassing eIF2α phosphorylation increases error-prone repair at a Cas9 DSB, while increasing eIF2α phosphorylation decreases indel formation. Cells have a powerful incentive to avoid error-prone repair, and it has been suggested that nonhomologous end joining (NHEJ) is inherently a fidelitous process (Boulton and Jackson, 1996; Honma et al., 2007; Lin et al., 2013; Rath et al., 2014). In this model, the indels caused by genome editing are products of non-fidelitous alternative end joining (alt-EJ) pathways such as microhomology mediated end joining (MMEJ) or processing of the DNA ends prior to repair (Bae et al., 2014; Bétermier et al., 2014; Guirouilh-Barbat et al., 2007; Nakade et al., 2014). It is tempting to speculate that DSB-induced eIF2α phosphorylation could promote error-free DNA repair as a means to maintain genome fidelity. However, the downstream players that alter the repair profile of a genomic locus after eIF2α phosphorylation remain to be identified.

Translational changes bridge the immediate, post-translational DNA damage response to the long-term transcriptional response

Double stranded DNA breaks elicit an immediate post-translational response that enacts immediate processing of the break. This response includes phosphorylation of proteins such as ATM and H2AX and ubiquitination of proteins such as p53 and histones. DSBs also induce a potent p53-mediated transcriptional response, leading to reprogramming that prioritizes DNA

damage response. We have found that DSBs induce a short-term translational response mediated by eIF2α phosphorylation.

We hypothesize that the translational response to DNA damage enables cells to bridge the immediate post-translational response with longer-term transcriptional reprogramming. Cells increase the translation of integrated stress response genes 36 hours after Cas9 RNP nucleofection, suggesting that cells activate a translational program to cope with DNA damage prior to transcriptional changes. We find that this translational program is shut off by 72 hours, with changes in mRNA levels dominating gene expression.

We observed that RPS27A and RPL40 could be stimulated by p53-mediated transcription after DSBs (**Figures 3J**, **S3E**), consistent with reports that *RPS27A* can be a transcriptional target of p53 (Nosrati et al., 2015). RPS27A was previously described as binding and inhibiting the E3 ligase MDM2 (Sun et al., 2011), thereby promoting p53 expression in the cell. The role of RPS27A in preventing p53 degradation coupled with p53 activation of *RPS27A* transcription suggests an RPS27A-p53 positive feedback loop. Consequently, the degradation of RPS27A may serve to keep this loop inactive or shut it off after repair.

Ribosomes lack core ribosome proteins after dsDNA damage

Non-DSB DNA damage caused by sources such as UV irradiation and cisplatin leads to the inhibition of Pol I transcription (Ciccia et al., 2014; Kruhlak et al., 2007; Larsen et al., 2014), preventing rRNA expression and impacting ribosome biogenesis. Interestingly, Cas9 or I-PpoI-induced DSBs in rDNA triggers this inhibition (van Sluis and McStay, 2015). Our study has revealed that DSBs lead to translation phenotypes beyond impaired ribosome biogenesis regardless of their location in the genome. Our observation that ribosomes lack RPL40 and RPS27A after dsDNA damage is one of the few known instances where ribosome composition is deliberately modulated in response to a specific biological stimulus (Shi and Barna, 2015; Xue and Barna, 2012). While differential expression of ribosomal proteins between tissue types and subpopulations of ribosomes within a cell are emerging themes in ribosome biology, there have been few cases of altered ribosome composition in response to the cellular environment.

While loss of RPS27A and RPL40 may alter ribosome function in a way that is difficult to detect in our ribosome profiling analysis, we cannot rule out that ribosomes lacking RPS27A and RPL40 have different functions. Indeed, ribosomes lacking RPL40 are capable of translation in certain contexts. RPL40 is necessary for vesicular stomatitis virus (VSV) translation but not cap-dependent translation in HeLa cells (Lee et al., 2012). In fact, complete deletion of the paralogous *RPL40A* and *RPL40B* genes in yeast was not lethal, and affected translation of only ~7% of the genome.RPL40 depletion – and perhaps RPS27A depletion as well – may thus act in a regulatory fashion. It is also possible that changes in ribosome composition after DNA damage may serve at least in part to regulate the extra-translational functions of RPS27A, RPL40, or their associated ubiquitins.

Gene editing induces cellular phenotypes

There is growing appreciation that Cas9 genome editing can cause cellular effects that mirror those observed with multiple, non-specific DSBs. The degree of damage may be far less, but the principle is the same. For example, embryonic stem cells are hyper-sensitive to HDR from even a single DSB introduced by Cas9, which can induce a p53 response that compromises cell health (Haapaniemi et al., 2018; Ihry et al., 2018). CRISPR-Cas9 nuclease screening data has also shown that targeting high copy number or repetitive regions of a genome reduces cell

fitness, consistent with a titratable cell cycle arrest that could be caused by p53 signaling (Aguirre et al., 2016; Munoz et al., 2016; Wang et al., 2015a).

We have found that even a single non-coding Cas9-induced DSB elicits ribosome remodeling and translational shutdown. Much of the concern about the safety and efficacy of genome editing had focused on off-target mutagenesis. Our findings highlight how the endogenous DNA damage response can have a days-long impact on the translatome and transcriptome independent of the gene target. These cellular responses should be taken into account when it is impossible to isolate and expand a clonal cell line for long periods of time after genome editing, for example during therapeutic genome editing of primary cells.

Acknowledgements

We thank Gloria Brar and Jamie Cate for their helpful discussions, and we also thank the Rape Lab at UC Berkeley for providing us with the pHA-Ub plasmid and the Cate Lab for supplying us with the thermophilic yeast strain, *Kluyveromyces marxianus.*We would like to acknowledge the QB3 MacroLab at UC Berkeley for purifying Cas9 proteins and the *Kluyveromyces marxianus* deadenylase; the UC Berkeley DNA Sequencing Facility for Sanger sequencing analysis; and the Vincent J. Coates Genomics Sequencing Laboratory for performing our NGS sequencing.

Funding Sources

This work was supported by National Institute Health New Innovator Awards (DP2 HL141006, JEC, and DP2 CA195768, NTI), the Li Ka Shing Foundation (JEC), the Heritage Medical Research Institute (JEC), the National Institute of Health (DP3 DK111914 and P50 GM08225, AM), the Keck Foundation (AM), gifts from Jake Aronov and Galen Hoskin (AM), and a National Multiple Sclerosis Society grant (CA 1074-A-21, AM). CR was supported by fellowships awarded through the The Shurl and Kay Curci Foundation and the National Science Foundation Graduate Research Fellowship Program (DGE 1106400 and DGE 1752814); DNN was supported by the UCSF Infectious Disease Training Program (2T32AI007641-16) and the CIS-CSL Behring Fellowship; PAF by the National Institute Health T32 Training Grant (4T32GM007232-40); and JTV by the California Institute for Regenerative Medicine (TRAN1-09292). AM receives funding from the Innovative Genomics Institute (IGI), holds a Career Award for Medical Scientists from the Burroughs Wellcome Fund, and is a Chan Zuckerberg Biohub Investigator. This work used the Vincent J. Coates Genomics Sequencing Laboratory at UC Berkeley, supported by the NIH S10 OD018174 Instrumentation Grant.

Author Contributions

Conceptualization, JEC, NTI, EZ, and CR; Methodology, JEC, NTI, EZ, CR, SKW, AM, DNN, and JRL; Formal Analysis, NTI, SKW, CR, and EZ; Investigation, EZ, CR, DNN, PAF, JRL, ZAM, and JTV; Writing - Original Draft, CR and JEC; Writing - Review & Editing, CR, JEC, NTI, EZ, DNN, AM, and PAF; Visualization, CR, EZ, SKW, NTI, and DNN; Supervision, JEC, NTI, AM, and CR; Funding Acquisition, JEC, NTI, CR, AM, and DNN.

Conflicts of Interest

AM and JEC are co-founders of Spotlight Therapeutics. AM serves as a scientific advisory board member to PACT Pharma and was previously an advisor to Juno Therapeutics. The Marson laboratory has received a gift from Gilead and sponsored research support from Juno Therapeutics, Epinomics, and Sanofi.

Materials and Methods

CONTACT FOR REAGENT AND RESOURCE SHARING

Further information and requests for resources and reagents should be directed to and will be fulfilled by the Lead Contact, Jacob Corn (jacob.corn@biol.ethz.ch).

EXPERIMENTAL MODEL AND SUBJECT DETAILS

Cell Culture - Immortalized Cell Lines

HEK 293 (ATCC) and HEK Flp-In T-Rex cell lines (Invitrogen) were cultured in DMEM, high glucose, GlutaMAX (Gibco) with 10% FBS (VWR) in a 37°C incubator with 5.0% CO_2 and 20% O_2. K562 cells (ATCC) were cultured in RPMI (Gibco) with 10% FBS (VWR), 10% sodium pyruvate. Human neonatal dermal fibroblasts (ScienCell, Cat# 2310) were cultured in DMEM, high glucose with 10% FBS, 0.01% BME, 1% NEAA, 1% Sodium Pyruvate, 1% Glutamax, 1% HEPES, 1% pen/strep. Mobilized Peripheral Blood CD34+ Stem/Progenitor Cells (AllCells) were cultured in StemSpan™Serum Free Expansion Media II (STEMCELL Technologies), StemSpan™ CC110 (STEMCELL Technologies), 1% Pen/Strep.

Primary T-cell Isolation and Stimulation

Primary human T cells were isolated from two de-identified healthy human donors from Trima Apheresis leukoreduction chamber residuals (Vitalant, formally Blood Centers of the Pacific). Peripheral blood mononuclear cells (PBMCs) were isolated by Ficoll centrifugation using SepMate tubes (STEMCELL, per manufacturer's instructions) then stored frozen in BAMBANKER serum-free freezing medium (Lymphotec Inc, per manufacturer's instructions) until use. PBMCs were thawed and CD4+ T cells were further isolated by magnetic negative selection using an EasySep Human CD4+ Cell Isolation Kit (STEMCELL, per manufacturer's instructions). Immediately following isolation, CD4+ T cells were then stimulated for 2 days by culture at initial concentration 1 x 10^6 cells/mL in XVivo15 medium (STEMCELL) with 5% Fetal Bovine Serum, 50 mM 2-mercaptoethanol, and 10 mM N-Acetyl L-Cystine together with anti-human CD3/CD28 magnetic Dynabeads (ThermoFisher) at a beads to cells ratio of 1:1, along with a cytokine cocktail of IL-2 at 200 U/mL (UCSF Pharmacy), IL-7 at 5 ng/mL (ThermoFisher), and IL-15 at 5 ng/mL (Life Tech).

METHOD DETAILS

Cas9 RNP Nucleofection

gRNAs were in vitro transcribed as previously described (DeWitt et al., 2016; Lingeman et al., 2017). In brief, gRNA transcription template contain a T7 RNA pol promoter followed by target specific region and constant region (T7FwdVar) along with primer that is reverse complement of the invariant region of T7FwdVar (T7RevLong) and amplification primers (T7FwdAmp and T7RevAmp). Transcription templates for gRNA synthesis were PCR amplified

from the primer mix. Phusion high fidelity DNA polymerase was used for assembly (New England Biolabs). Assembled template was used without purification for in vitro transcription by T7 polymerase using the HiScribe T7 High Yield RNA Synthesis Kit (New England Biolabs). RNA was purified with RNeasy kit (Qiagen). Cas9, dCas9, and D10A Cas9 (nCas9) proteins were purified using the protocol detailed in (Lingeman et al., 2017).Cas9, dCas9, and D10A Cas9 ribonucleoproteins (RNPs) were prepared as detailed in (Lingeman et al., 2017)with the exception of the T-cells experiments (see "Cas9 RNP Nucleofections with T-cells"). IVT gRNAs were used in all experiments except for the 36-hour ribosome profiling experiment, which used synthetic gRNA (Synthego), and the T-cell nucleofections, which used synthetic crRNAs and tracrRNAs (Dharmacon).

HEK cells were passaged 2 days before nucleofection and trypsinized at 60-90% confluency. For RNP nucleofections, either 100 pmol Cas9 and 120 pmol gRNA were added to 2.5 x 10^5cells in 20 µl SF Solution (Lonza), or 300 pmol Cas9 and 300 pmol guideRNA were added to 1 x 10^6 cells suspended in 100 µl SF Solution (Lonza). HEK cells were nucleofected using program CM-130 in the X Unit of a Lonza 4D-Nucleofector (AAF-1002X, AAF-1002B) and pre-warmed media was immediately added to the cuvettes to increase cell viability. K562 cells were nucleofected with Cas9 RNPs as described for HEK cells using buffer SF and program FF-120; fibroblasts were nucleofected using buffer P3 and program DT-130. For HSPC nucleofections, 3,000 cells were nucleofected 30 pmol Cas9 and 36 pmol gRNA in solution P3 using pulse code ER-100 and recovered in 96-well plate.

Cas9 RNP Nucleofections with T-Cells

RNPs were produced by complexing a two-component gRNA to Cas9. A crRNA targeting exon 2 of the human CD4 gene (UUGCUUCUGGUGCUGCAACU, (Hultquist et al., 2016)) and tracrRNA were chemically synthesized (Edit-R, Dharmacon). Lyophilized RNA was resuspended in 10 mM Tris-HCL (7.4 pH) with 150 mM KCl at a concentration of 160 µM, and stored in aliquots at -80 ºC. Recombinant Cas9-NLS or dCas9-NLS were purified as detailed in (Lingeman et al., 2017) and stored at 40 µM in 20 mM HEPES-KOH pH 7.5, 150 mM KCl, 10% glycerol, 1 mM DTT. crRNA and tracrRNA aliquots were thawed, mixed 1:1 by volume, and annealed by incubation at 37 ºC for 30 min to form an 80 µM gRNA solution. Cas9 or dCas9 was then mixed with freshly-annealed gRNA at a 1:1 volume ratio (2:1 gRNA to Cas9 molar ratio) then incubated at 37 ºC for 15 min to form a ribonucleoprotein (RNP) at 20 µM. RNPs were electroporated immediately after complexing.

Stimulated CD4+ T cells were harvested from their culture vessels and magnetic anti-CD3/anti-CD28 Dynabeads were removed by placing cells on an EasySep cell separation magnet (STEMCELL) for 4 minutes. Immediately prior to electroporation, cells were centrifuged for 10 minutes at 90 x g, then resuspended in the Lonza electroporation buffer P3 at a concentration of 5.0 x 10^7cells per mL. One million CD4+ T cells (20 µL) and 3 µL of Cas9-NLS RNP, dCas9-NLS RNP, or Tris buffer were added to each well of a 96-well electroporation plate (Lonza) in three replicates for each condition for each of two cell donors. Electroporation was performed with a Lonza 4D 96-well electroporation system with pulse code EH115. 15 minutes following electroporation, each well was split between three replicate 96-well plates and cultured in XVivo15-base growth medium (as above) supplemented with 500 U/mL IL-2 at an approximate density of 1 x 10^6cells per mL of media.

Approximately 20 hours after electroporation, lysates were prepared for Western blot analysis from samples from one replicate plate of edited T-cells. Cells were collected and

centrifuged at 300 x g for 5 minutes. Culture media was aspirated off the cells, and cells were resuspended in PBS. This was repeated for a total of 2 PBS washes. After the final wash, cells were resuspended in 1X RIPA Lysis buffer (Cell Signaling Technologies) with Protease Inhibitor and Phosphatase inhibitor (Cell Signaling Technologies), incubated 10 minutes on ice, then stored at -80 ºC.

Three days after electroporation, samples from a second replicate of edited T cells was collected and stained with Anti-CD3-PE (clone UCHT1, Biolegend), Anti-CD4-PECy7 (clone OKT4, Biolegend), and GhostDye780 (Tonbo). Fluorescence was measured on an Attune NxT Flow Cytometer (Thermo Fisher Scientific) and analyzed using FlowJo (Treestar, Inc) for presence or knockdown of surface expression of CD4.

Western Blotting

Cells were pelleted at 400 x g for 5 minutes then washed twice with PBS before being lysed in RIPA buffer (1% SDS, 50 mM Tris HCl, pH 8.0 with 1X Halt Protease Inhibitor Cocktail or 1X Halt Protease and Phosphatase Inhibitor Cocktail, (Thermo Scientific). Lysates were incubated for 30 minutes on ice, vortexed for 30 seconds, and spun at 18,000 x g for 10 minutes at 4°C. Lysates were normalized using either BCA Assay (Pierce) or a Bradford Assay (Proteomics Grade, VWR) before being boiled at 97°C for 5 minutes with Laemmli buffer or Novex LDS Sample Buffer (Thermo Fisher Scientific). Samples were loaded onto NuPAGE 4-12% Bis-Tris Gels (Invitrogen) or Mini-Protean TGX precast gels (Bio-Rad) and run for 200V for 40 minutes.

Proteins were transferred onto nitrocellulose membranes using the Trans-Blot Turbo Blotting System (Bio-Rad) according to the manufacturer's protocol. Membranes were blocked in 5% milk in TBST, washed 3 x 5 minutes in TBST, and incubated with primary antibodies in TBST with 5% BSA overnight at 4°C. Membranes were washed 3 x 5 minutes in TBST and incubated with either IRDye 800CW (LI-COR), IRDye 680RD (LI-COR), or HRP-conjugated secondary antibodies in 5% milk for 40 minutes before 2 x 5 minute washes with TBST and 1 x 5 minute wash with PBS. Blots were imaged by a LI-COR Odyssey CLx Imager or Pierce ECL reagents (Thermo Fisher) and X-ray film. All primary antibodies were used at a 1:1000 dilution except for anti-p53 (1:500, Santa Cruz Biotechnology, Cat# sc-126) and anti-phospho-ATM (1:50,000, Abcam, Cat# ab81292).See Key Resources Table for the complete list of antibodies.

T7 Endonuclease 1 Assay

Edited cells were gathered off of plates with a pipette, spun at 10,000 x g for 1 min, washed once with PBS, and lysed in QuickExtract^{TM} DNA Extraction Solution (Lucigen). Lysates were incubated at 65°C for 6 minutes and 98°C for 2 minutes in a thermocycler. Edited regions were PCR amplified in 100 ul reactions with AmpliTaq Gold 360 Master Mix (Thermo Fisher Scientific). PCR products were purified using MinElute PCR Purification Kit (Qiagen). PCR products were hybridized and digested with T7 endonuclease 1 (NEB) according to the NEB protocol for determining genome targeting efficiency. Digests were run on a 2% agarose gel. Relative intensities from DNA bands were quantified using ImageJ (Schindelin et al., 2015)with % edited = 100 x (1-(1-fraction cleaved)$^{1/2}$) where fraction cleaved = (sum of cleavage product intensities)/(sum of uncleaved and cleaved product intensities).

Inducing DNA Damage

For chemically inducing double-strand DNA damage, HEK cells were grown to 70% confluency then treated for 16 hours with 5 μM etoposide (Sigma-Aldrich) or 10 μM doxorubicin (Sigma-Aldrich). For chemically inducing other forms of DNA damage, HEK cells were treated with 0.03% methyl methanesulfonate (MMS) for 1 hour, 500 μM hydrogen peroxide for 1 hour, or 10 mM hydroxyurea for 16 hours. To damage cells using ultraviolet light, cells were irradiated at 20 J/$m^2$with a FB-UVXL-1000 UV Crosslinker (Fisher Scientific) and recovered for 6 or 24 hours before lysis. Cells were treated with DMSO for 16 hours as a negative control unless otherwise noted.

Polysome Profiling

HEK cells cultured in 10 cm plates were washed with 10 ml DPBS before lysis with ice cold 100-400 μl polysome buffer (20 mM Tris pH 7.4, 150 mM NaCl, 5 mM $MgCl_2$, 1 mM DTT, 100 μg/mL cycloheximide) with 1% Triton X-100 and 25 U/ml TURBO DNase (Thermo Fisher Scientific). When polysome profiling fractions were collected for protein analysis, 2X protease inhibitor cocktail (P1860, Sigma) was added to the lysis buffer and sucrose gradients. The amount of cells varied between experiments but was generally between 1-8 x 10^6 cells per biological condition. Cells were scraped off plates in lysis buffer and incubated on ice in microcentrifuge tubes for 10 minutes. Lysates were spun at 10 minutes at 20,000xg, and the supernatants were normalized using the Quant-iT RiboGreen RNA Assay Kit (Thermo Fisher Scientific).6 ml 50% (w/v) sucrose in polysome buffer was layered under 6 ml 10% sucrose solution in 14 x 89 mm ultracentrifuge tubes (VWR), and 10-50% sucrose gradients were created using a Gradient Master (BioComp Instruments) with rotation set at 81.5°, speed 16 for 1:58. 200 μl normalized cell lysate (with RNA concentrations generally between 50-250 ng/μl) was layered on top of the gradients, and the gradients were loaded into Beckman Sw41 Ti rotor buckets and spun at 36,000 rpm (~250,000xg) for 2.5 or 3 hours at 4°C in a Beckman L8-M Ultracentrifuge. Sucrose gradients were pumped through the Gradient Master at 0.2 mm/s, and UV absorbance at 254 nm was measured using a BioRad EM-1 Econo UV Monitor connected to a laptop running the Logger Lite software package (Vernier). Depending on the downstream experiment, fractions were manually collected every 20 to 24 seconds for a total of 15-18 fractions per sucrose gradient. Proteins were extracted for Western blots using methanol/chloroform extraction as detailed in Click-it Metabolic Labeling Reagents for Proteins (Invitrogen), and pellets were boiled at 95°C in 1X Laemmli buffer before SDS-PAGE.

RT-qPCR

RNA was extracted from cells using the Direct-zol^{TM}RNA MiniPrep Kit (Zymo) according the manufacturer's instructions. 1 μg total RNA was used for reverse transcription with Superscript III First Strand Synthesis SuperMix (Thermo Fisher Scientific). qRT-PCR was performed using Fast SYBR Green Master Mix (Applied Biosystems) on a StepOnePlus Real-Time PCR System (Applied Biosystems). $C_t$values from target genes were normalized to *GAPDH*, and the expression of each gene was represented as $2^{-(\Delta\Delta Ct)}$ relative to the reference sample.

Endogenous Tagging of Ubiquitin Genes

We used Cas9 genome editing to endogenously tag the N-terminal ubiquitins of *RPS27A,RPL40* (also known as *UBA52*), and *UBC* genes with the HA, V5, and Myc tags,

respectively. We designed gRNA sequences upstream of the *RPS27A, RPL40,* and *UBC* ubiquitin sequences using the CRISPR Design Tool (Hsu et al., 2013)(See "Key Resources Table" for guide RNA sequences). To construct the *Myc-UBC* cell line, a gene block (Dharmacon) containing the Myc-tag sequence flanked by 1000 bp homology arms on both ends was Gibon-assembled into a SmaI-digested pUC19 vector backbone (Addgene) to make pUC19-Myc-UBC. Single-stranded oligodeoxynucleotides (ssODN, IDT) were designed to introduce the HA-tag and V5-tag at the *RPS27A*and *RPL40* loci, respectively. Plasmid and ssODN donors contained mutations in the PAM sequences at each cut site to prevent Cas9 from cutting the edited loci.

Using a Lonza 4D nucleofector, 2×10^5HEK 293 cells were nucleofected with preassembled Cas9 RNP complex together with 100 pmol donor ssODN or 750 ng donor plasmid (see "gRNA and Cas9 Preparation" and "Cas9 RNP Nucleofection" above for more details). 48 hours after nucleofection, single cells were dispersed into four 96-well plates to isolate clones. To genotype clones, cells were lysed in QuickExtract™DNA Extraction Solution (Lucigen, see "T7 Endonuclease 1 Assay" for more details), and the edited region was PCR amplified. PCR fragments were TOPO cloned (Thermo Fisher Scientific), and plasmids were analyzed by Sanger sequencing.

Chemical Genetics

We used a variety of chemical inhibitors to identify the pathways regulating RPS27A and RPL40 depletion. To prevent proteasomal degradation during DNA damage, cells were treated with 50 nM epoxomicin (Calbiochem) for 1 hour before cells were treated with 5 μM etoposide or 50 nM epoxomicin for 16 hours. 10 μM KU 55933 (Tocris) or 10 μM AZ 20 (Tocris) was co-administered with etoposide for 16 hours to inhibit the ATM and ATR pathways, respectively. MDM2-mediated degradation of p53 was prevented after DNA damage with co-administration of 10 μM nutlin (Sigma-Aldrich) and 5 μM etoposide over a 16-hour time course.
To rescue downstream effects of eIF2α phosphorylation after DNA damage, 200 nM ISRIB (Sigma-Aldrich) was added at the same time as etoposide. Cells were treated with 1 μM thapsigargin (Sigma-Aldrich) or 2.5 μM PP242 (Sigma-Aldrich) for 30 minutes as controls for eIF2α phosphorylation or 4E-BP1 hypo-phosphorylation, respectively. To determine the effects of modulating eIF2α phosphorylation on genome editing, HEK-BFP or K562-BFP cells were treated with 10, 50, or 75 μM salubrinal (Tocris) or 200 nM ISRIB (Sigma-Aldrich) for 16 or 24 hours post Cas9 RNP nucleofection.

Generating RPS27A-SBP Flp-In Cell Lines

RNA from HEK cells was isolated using the DirectZol RNA MiniPrep Kit (Zymo) according to the manufacturer's protocol. cDNA was generated using SuperScript II Reverse Transcriptase (Thermo Fisher Scientific), and coding regions of RPS27A with and without the N-terminal ubiquitin sequence was PCR amplified and cloned into a pcDNA5/FRT/TO vector backbone (Invitrogen) that had been previously modified to have a constitutive CMV promoter and C-terminal SBP-tag.

To generate stable transgenic cell lines, 1 x 10^6 HEK Flp-In T-Rex Cells (Invitrogen) were nucleofected using a Lonza 4D nucleofector in according to the Amaxa 4D-Nucleofector™ Protocol for HEK293 (Lonza) for large cuvettes with 1.8 μg pOG44 Flp-Recombinase Expression Vector and 0.2 μg pCMV-RPS27A-SBP or pCMV-Ub-RPS27A-SBP. Two days after nucleofection, cells were passaged and placed on media containing 5 μg/ml blasticidin

(Invitrogen) and 10 µg/ml Hygromycin B (Thermo Fisher Scientific) until all cells from a control plate nucleofected with pmaxGFP™ Vector (Lonza) were dead. Flp-In cell lines were validated using anti-SBP Westerns and Sanger sequencing of the transgenic insert.

Ubiquitin Blots of Denatured RPS27A-SBP

RPS27A-SBP Flp-In HEK cells were lysed in binding buffer (300 mM NaCl, 0.5% NP-40, 50 mM Na_2HPO_4, 50 mM Tris pH 8) with 8M urea using the protocol detailed in "Western Blotting." Samples were diluted 1:3 with binding buffer, and normalized lysates were incubated at 4 ºC for 30 minutes with 60 µl buffer-equilibrated Dynabeads™M-270 Streptavidin (Invitrogen). Beads were washed 5 times with 200-500 µl binding buffer containing 1M NaCl. To elution proteins, beads were boiled in 25 µl 1X NuPAGE loading buffer at 97 ºC for 5 minutes. Westerns were performed as detailed in "Western Blotting."

siRNA Knockdowns

siRNA oligonucleotides (see "Key Resources Table" below) were transiently transfected into cells using RNAiMAX (Invitrogen) according to manufacturer instructions. For each well in 12-well plate, 120 pmol siRNA and 3.6 µl RNAiMAX were used. Cells were transfected with siRNAs 24 hours prior to drug treatment or Cas9 nucleofection.

pHA-Ub Immunoprecipitations

10 cm plates HEK293 or RPS27A-SBP Flp-In cells were transiently transfected with 10 µg of HA-UB plasmid (gift from Rape lab) with Lipofectamine 3000 (Thermo Fisher Scientific) for 48 hours. Immunoprecipitation was performed using Pierce Anti-HA Magnetic Beads Kit (Thermo Fisher) according to the manufacturer. 1 mg of cell lysate and 50 µl beads were used to perform each immunoprecipitation. After overnight incubation at 4 ºC, the beads were washed twice with IP buffer supplemented with 500 mM NaCl and twice with regular IP buffer and proteins were eluted by boiling samples at 98°C in 1X NuPAGE LDS sample buffer (Thermo Fisher) for 5 min. When siRNA was used, cells were first transfected with siRNAs and after 24 hours, with the HA-Ub plasmid. Lysates were prepared 48 hours after the second transfection with drug treatment with epoxomicin and etoposide occuring 17 hours and 16 hours before lysis, respectively.

Bulk Translation Assays

10 cm plates of HEK cells were washed with PBS then placed in 25 µM Click-IT L-Azidohomoalanine (Thermo Fisher Scientific) in DMEM, high glucose, no glutamine, no methionine, no cysteine (Gibco) with 10% FBS for 2 hours. Cells were trypsinized then pelleted at 400 x g for 5 minutes. Cells were washed three times with PBS before being lysed in 200 µl lysis buffer (1% SDS, 50 mM Tris HCl, pH 8.0, 1X Halt Protease Inhibitor Cocktail, Thermo Scientific) with 150 U/ml benzonase nuclease to digest DNA and RNA. Lysates were incubated for 30 minutes on ice, vortexed for 5 seconds, and spun at 18,000 x *g* for 10 minutes at 4 ºC. Protein content of the supernatants was normalized using the Pierce BCA Protein Assay (Thermo Fisher Scientific). 1 µl 10 mM IRDye 800CW DBCO Infrared Dye was added to the lysates, and the lysates were incubated for 2 hours atRT. Unbound IR Dye was removed using a Zeba Column, 7K MWCO, 0.5 mL (Thermo Fisher Scientific). For dot blot analysis, a Bio-Dot Microfiltration Apparatus (Bio-Rad) was used according to the manufacturer's protocol and 20 µl sample dilutions were added to wells. Membranes were imaged on a LI-COR Odyssey CLx

Imager. For protein gel analysis, lysates were combined with 2X Laemmli Buffer,incubated at 97 ºC for 5 min, then run on aNupage 4-12% Bis-Tris Gel (Invitrogen) at 200V fro 40 min. The gel was washed with PBS (3 x 5 minutes) before imaging with a LI-COR Odyssey CLx Imager.

NGS Analysis of Editing Outcomes

HEK cells carrying a single copy of a BFP transgene were nucleofected with Cas9-sgBFP or dCas9-sgBFP and recovered in media containing 75 µM salubrinal or 200 nM ISRIB for 24 hours. gDNA extraction and 50 µl PCRs (PCR1, see "Key Resources Table" for sequences) of the edited genomic loci were prepared as detailed in "T7 Endonuclease 1 Assay."

PCR1 reactions were cleaned up using SPRI bead purification. A 50 mL stock solution of SPRI beads was prepared in advance: 1 ml SPRI beads (Sera-Mag SpeedBeads® Carboxyl Magnetic Beads) were brought to room temperature and washed three times with TE buffer before suspended to 50 ml in 18% PEG-8000, 1 M NaCl, 10 mM Tris-Cl (pH 8.0), 1 mM EDTA, and 0.055% Tween-20. To purify PCR products, 90 µl SPRI bead suspension solution was added to 50 µl PCR reactions in a 96 well plate. The solution was mixed 10 times with a pipette and incubated at room temperature for 1 minute. The plates were placed on a magnetic stand for 2 minutes, and the supernatant was discarded. 200 µl 80% ethanol was added then removed after 2 minutes while the plate remained on the magnetic stand. The ethanol wash and removal steps were repeated one more time for a total of two washes. The beads were left to air dry for 3-10 minutes. To elute the purified PCR1 products from the beads, beads were resuspended in 20 µl ultra-pure water and incubated for 2 minutes. The plate was placed on a magnetic stand for 1 minute, and the supernatant was collected. Concentrations of purified PCR1 products were quantified using the Qubit™1X dsDNA HS Assay with the Invitrogen Qubit™4 Fluorometer (Thermo Fisher Scientific) as per the manufacturer's instructions.

To add Illumina adaptors to the PCR1 products, a second PCR reaction was performed with PrimeSTAR GXL DNA Polymerase (Takara) in a 25 µl reaction with 10 ng PCR1 product and 0.5 µM adaptor according to the manufacturer's instructions. We used adaptors from a custom set of 960 unique combinatorial Illumina TruSeq indices (IDT) supplied by the Vincent J. Coates Genomics Sequencing Laboratory at UC Berkeley. The samples were amplified for 12 cycles consisting of: 95 ºC for 10 seconds, 57 ºC for 15 seconds, and 65 ºC for 30 seconds. PCR2 products were purified and quantified as detailed above. A Biomek FXp Liquid Handler (Beckman Coulter) was used to pool 50 ng of each PCR product, and a 5300 Fragment Analyzer (Advanced Analytical) was used to assess the concentration and quality of the pool before sequencing.

Samples were deep sequenced on an Illumina MiSeq at 300 bp paired-end reads to a depth of at least 10,000 reads. A modified version of CRISPResso (Pinello et al., 2016) was used to analyze editing outcomes and to plot mutation position distributions. Briefly, reads were adapter trimmed then joined before performing a global alignment between sequence reads and the *BFP* reference sequences using NEEDLE (Li et al., 2015). Indel rates were calculated as any reads where an insertion or deletion overlaps the cut site or occurs within three base pairs of either side of the cut site divided by the total number of reads.

Ribosome Profiling and RNA-seq

Paired ribosome profiling and RNA-seq experiments were conducted on HEK 293 cells lysed 36 and 72 hours after Cas9 or dCas9 RNP nucleofection. Cas9 and dCas9 complexed with sgIntron, a guide targeting intron 12 of *JAK2,* were nucleofected using the protocols detailed in

"Cas9 RNP Nucleofections" above. Four small-scale nucleofections were pooled directly into one 10 cm plate to create one biological replicate with each experimental condition having two biological replicates. Due to recent reports about IVT guide RNAs inducing interferon responses in cells (Kim et al., 2018; Wienert et al., 2018), synthetic gRNAs (Synthego) were used at the 36 hour time point.

Ribosome profiling was conducted as detailed in (McGlincy and Ingolia, 2017)with the following modifications. Since Epicentre discontinued the yeast 5′-deadenylase (Cat# DA11101K) we used in our published protocol, we cloned a 5′-deadenylase (*HNT3*) from the thermotolerant yeast *Kluyveromyces marxianus* into the pET His6 TEV LIC cloning vector (2B-T) backbone (gift from Scott Gradia to Addgene). Recombinant 6xHis-TEV-Km-HNT3 was purified from *E. coli*using a Nickel column purification (HisTrap FF Crude column, GE Life Sciences). Protein eluted from the column with imidazole was cleaved with TEV protease, and the residual His tag was removed using a Nickel column. The recombinant protein subsequently purified using size exclusion chromatography (Sephacryl S-300 16/60 column, GE Life Sciences). 0.5 µl of purified protein was added in place of the yeast 5′-deadenylase during ribosome profiling, and the reaction was incubated at 37 ºC instead of 30 ºC.

We also deviated from the McGlincy and Ingolia 2017 protocol by using CircLigase I instead of CircLigase II. We made this change after concerns about the nucleotide bias of CircLigase II were reported in (Tunney et al., 2018). Therefore, we reverted to using CircLigase I as previously detailed in (Ingolia et al., 2012) with a 2 hour incubation step.

Total RNA for mRNA-seq was isolated from 50 µl cell lysate using the DirectZol^{TM}RNA MiniPrep Kit (Zymo) according to the manufacturer's protocol. Sequencing libraries were prepared using the TruSeq Stranded Total RNA Library Kit with Ribo-Zero Gold (Illumina). Ribosome profiling and RNA-seq libraries were sequenced as 50 nt single-end reads on an Illumina HiSeq 4000.

Reads from ribosome profiling were processed as detailed in (McGlincy and Ingolia, 2017). Ribosome profiling and RNA-seq reads from the 36 hour time point were aligned with HiSat2 (Kim et al., 2015)to the Human GENCODE Gene Release GRCh38.p2 (release 22); reads from the 72 hour time point were aligned with TopHat (Trapnell et al., 2009)to GRCH38.p7 (release 25). Alignments were indexed using Samtools (Li et al., 2009), and the number of reads per transcript was tabulated using fp-count (Ingolia et al., 2014)with the basic gene annotations from GRC38.p2 (36 hr) and GRCh38.p7 (72 hr). Differential changes in gene expression were calculated using DESeq2 (Love et al., 2014)with a cutoff of FDR < 0.1 for per-gene significance. Translational efficiency (the ratio of ribosome footprints to mRNA-seq transcripts) calculations and significance tests were made in DESeq2 using a design matrix that tests the ratio of ratios (design = ~ A + B + A:B, where A is Cas9 type and B is library type) with FDR < 0.1.

Cumulative distribution functions and Mann-Whitney-Wilcoxon tests with ribosome profiling and RNA-seq data were calculated in RStudio. Three gene lists were used for this analysis: ISR targets, ribosome proteins, and DSB break repair genes. ISR (Integrated Stress Response) targets are the 78 genes identified by (Sidrauski et al., 2015)to have a statistically significant, greater than twofold change in translational efficiency after tunicamycin treatment. (6 of the 78 genes were removed from analysis because we were unable to identify corresponding GRCh38 Ensembl gene IDs from the original GRCh37 UCSC gene IDs listed in Sidrauski et al., 2015.) Ribosome proteins are the 80 core ribosomal protein genes expressed in humans. DSB break repair genes are 44 genes from the union of genes annotated as DSB repair

genes from (Chae et al., 2016)and on the University of Pittsburgh Cancer Institute's DNA Repair Database website (https://dnapittcrew.upmc.com/db/index.php).

QUANTIFICATION AND STATISTICAL ANALYSIS

Bar graphs, scatterplots, stripcharts, and cumulative distribution function plots were created with RStudio version 1.0.136 running R version 3.3.2. Standard statistical analyses such as standard deviation calculations and Mann-Whitney-Wilcoxon tests were conducted in R. FDR values for RNA-seq and ribosome profiling were calculated using the Wald test in DESeq2 as described in (Love et al., 2014). Statistical details of experiments such as sample size (n) can be found in the figures and figure legends. For this paper, n = number of biological replicates and SD = standard deviation assuming a normal distribution.

DATA AND SOFTWARE AVAILABILITY

Ribosome profiling and mRNA-Seq data are available from NCBI GEO, Accession #GSE122615.

KEY RESOURCES TABLE

REAGENT or RESOURCE	SOURCE	IDENTIFIER
Antibodies		
4E-BP1 Rabbit Polyclonal Ab	Cell Signaling Technology	Cat# 9452, RRID:AB_331692
Phospho-4E-BP1 (T37/46) Rabbit Monoclonal Ab, Clone 236B4	Cell Signaling Technology	Cat# 2855, RRID:AB_560835
GAPDH Rabbit Monoclonal Ab, Clone 14C10	Cell Signaling Technology	Cat# 2118, RRID:AB_561053
eIF2α Rabbit Polyclonal Ab	Cell Signaling Technology	Cat# 9722, RRID:AB_2230924
Phospho-eIF2α (S51) XP Rabbit Monoclonal Ab, Clone D9G8	Cell Signaling Technology	Cat# 3398, RRID:AB_2096481
RPS27A Mouse Monoclonal Ab, Clone 3E2-E6	Abcam	Cat# ab57646, RRID:AB_2180587
γ-Tubulin Rabbit Polyclonal Ab	Santa Cruz Biotechnology	Cat# sc-7396-R, RRID:AB_1120814
Cas9 Mouse Monoclonal Ab, Clone 7A9-3A3	Active Motif	Cat# 61578, RRID: none

UBA52 (RPL40) Rabbit Polyclonal Ab	Thermo Fisher Scientific	Cat# PA5-23685, RRID:AB_2541185
RPS10 Rabbit Polyclonal Ab	Novus Biological	Cat# NBP1-98599, RRID: none
RPL10A Rabbit Polyclonal Ab	Bethyl	Cat# A305-062A, RRID:AB_2631457
V5-Tag Rabbit Monoclonal Ab, Clone D3H8Q	Cell Signaling Technology	Cat# 13202, RRID:AB_2687461
Myc-Tag Mouse Monoclonal Ab, Clone 9B11	Cell Signaling Technology	Cat# 2276, RRID:AB_331783
HA-Tag Rabbit Monoclonal Ab, Clone C29F4	Cell Signaling Technology	Cat# 3724, RRID:AB_1549585
Human HA Mouse Monoclonal Ab, Clone HA-7	Sigma-Aldrich	Cat# H3663, RRID:AB_262051
Ubiquitin Mouse Monoclonal Ab, Clone P4D1	Cell Signaling Technology	Cat# 3936S, RRID:AB_10691572
RPL22 Rabbit Polyclonal Ab	Abcam	Cat# ab77720, RRID:AB_1952492
P53 Mouse Monoclonal Ab, Clone DO-1	Santa Cruz Biotechnology	Cat# sc-126, RRID:AB_628082
SBP Tag Mouse Monoclonal Ab, Clone SB19-C4	Santa Cruz Biotechnology	Cat# sc-101595, RRID:AB_1128239

Phospho-ATM (S1981) Rabbit Monoclonal Ab, Clone EP1890Y	Abcam	Cat# ab81292, RRID:AB_1640207
ATM Rabbit Monoclonal Ab, Clone D2E2	Cell Signaling Technology	Cat# 2873S, RRID:AB_2062659
MDM2 Mouse Monoclonal Ab, Clone SMP14	Santa Cruz Biotechnology	Cat# sc-965, RRID:AB_627920
Ubiquitin Linkage-Specific K48 Rabbit Monoclonal Ab, Clone EP8589	Abcam	Cat# ab140601, RRID: None
Ubiquitin Linkage-Specific K63 Rabbit Monoclonal Ab, Clone EPR8590-448	Abcam	Cat# ab179434, RRID: None
Linear (M1) Polyubiquitin Mouse Monoclonal Ab, Clone LUB9	LifeSensors	Cat# AB130, RRID:AB_2576211
ZNF598 Rabbit Polyclonal Ab	Bethyl	Cat# A305-108A, RRID:AB_2631503
RPS6 Rabbit Polyclonal Ab	Bethyl	Cat# A300-557A, RRID:AB_477988
β-TRCP Rabbit Monoclonal Ab, Clone D13F10	Cell Signaling Technology	Cat# 4394S, RRID:AB_10545763
CREB-2 (ATF4) Rabbit Polyclonal Ab	Santa Cruz Biotechnology	Cat# sc-200, RRID:AB_2058752
PKR Rabbit Polyclonal Ab	Cell Signaling Technology	Cat# 3072, RRID:AB_10693467

CHK1 Mouse Monoclonal Ab, Clone 2G1D5	Cell Signaling Technology	Cat# 2360, RRID:AB_2080320
Phospho-CHK1 (Ser345) Rabbit Polyclonal Ab	Cell Signaling Technology	Cat# 2341, RRID:AB_330023
Human CD3 PE-Conjugated Mouse Monoclonal Ab, Clone UCHT1	Biolegend	Cat# 300407, RRID:AB_314061
Human CD4 PE/Cy7-Conjugated Mouse Monoclonal Ab, Clone OKT4	Biolegend	Cat# 317414, RRID:AB_571959
Biological Samples		
Human Peripheral Blood Mononuclear Cells (PBMCs)	Vitalant	https://vitalant.org/Home.aspx
Chemicals, Peptides, and Recombinant Proteins		
Etoposide	Sigma-Aldrich	Cat# E1383, CAS# 33419-42-0
Methyl methanesulfonate	Sigma-Aldrich	Cat# 129925, CAS# 66-27-3
Hydroxyurea	Sigma-Aldrich	Cat# H8627, CAS# 127-07-1
Thapsigargin	Sigma-Aldrich	Cat# T9033, CAS# 67526-95-8
PP242 hydrate	Sigma-Aldrich	Cat# P0037, PubChem 329819988

Doxorubicin hydrochloride	Sigma-Aldrich	Cat# D1515, CAS# 25316-40-9
Epoxomicin	Calbiochem	Cat# 324800, CAS# 134381-21-8
KU 55933	Tocris	Cat# 3544, CAS# 587871-26-9
AZ 20	Tocris	Cat# 5198, CAS# 1233339-22-4
Nutlin-3	Sigma-Aldrich	Cat# N6287, CAS# 548472-68-0
ISRIB	Sigma-Aldrich	Cat# SML0843, PubChem SID 329825607
Salubrinal	Tocris	Cat# 2347, CAS#405060-95-9
Click-IT AHA (L-Azidohomoalanine)	Thermo Fisher Scientific	Cat# C10102
DMEM, high glucose, no glutamine, no methionine, no cystine	Thermo Fisher Scientific	Cat# 21013024
IRDye 800CW DBCO Infrared Dye	LI-COR	Cat# 929-50000
T7 Endonuclease I	NEB	Cat# M0302L

IL-2	UCSF Pharmacy	N/A
IL-7 Recombinant Human Protein	Thermo Fisher Scientific	Cat# PHC0073
IL-15 Recombinant Human Protein	Thermo Fisher Scientific	Cat# PHC9153
Ghost Dye™ Red 780	Tonbo Biosciences	Cat# 13-0865
Experimental Models: Cell Lines		
HEK 293 Cell Line	ATCC	Cat# CRL-1573, RRID:CVCL_0045
V5-RPL40 HEK Cell Line	This Paper	None
HA-RPS27A HEK Cell Line	This Paper	None
Myc-UBC HEK Cell Line	This Paper	None
Flp-In-T-REx-293 Cell Line	Invitrogen	Cat# R78007, RRID:CVCL_U427

pCMV-RPS27A-SBP Flp-In-T-REx-293 Cell Line	This Paper	None
pCMV-Ub-RPS27A-SBP Flp-In-T-REx-293 Cell Line	This Paper	None
HEK 293T-BFP Cells	(Richardson et al., 2018)	None
K562-BFP Cells	(Richardson et al., 2018)	None
Mobilized Peripheral Blood CD34+ Stem/Progenitor Cells	AllCells	Cat# mPB015F, RRID: none
K-562 Cell Line	ATCC	Cat# CCL-243, RRID:CVCL_0004
Human Dermal Fibroblasts-Neonatal	ScienCell	Cat# 2310, RRID: none
Oligonucleotides		
T7FwdAmp, forward oligo for sgRNA production: GGATCCTAATACGACTCACTATAG	(Lingeman et al., 2017)	N/A
T7RevAmp, reverse oligo for sgRNA production: AAAAAAGCACCGACTCGG	(Lingeman et al., 2017)	N/A
T7RevLong, oligo for sgRNA production: AAAAAAGCACCGACTCGGTGCCACTTTTTC AAGTTGATAACGGACTAGCCTTATTTTAAC TTGCTATTTCTAGCTCTAAAAC	(Lingeman et al., 2017)	N/A

T7FwdVar oligo for *sgJAK2* production (guide sequence in **bold**)*:* GGATCCTAATACGACTCACTATAG**TCAGTTTCAGGATCACAGCT**GTTTTAGAGCTAGAA	This Paper	N/A
T7FwdVar oligo for *sgRPS27A* production: GGATCCTAATACGACTCACTATA**GACCATCACCCTCGAGGTAC**GTTTTAGAGCTAGAA	This Paper	N/A
T7FwdVar oligo for *sgRPL40* production: GGATCCTAATACGACTCACTATAG**TCCTCCTGCAGACGCAAAC**GTTTTAGAGCTAGAA	This Paper	N/A
T7FwdVar oligo for *sgUBC* production: GGATCCTAATACGACTCACTATA**GGTTTTGAACTATGCGCTCG**GTTTTAGAGCTAGAA	This Paper	N/A
T7FwdVar oligo for *sgBFP* production : GGATCCTAATACGACTCACTATA**GCTGAAGCACTGCACGCCAT**GTTTTAGAGCTAGAA	(Richardson et al., 2018)	N/A
T7FwdVar oligo for *sgAAVS1* production: GGATCCTAATACGACTCACTATAG**TGTCCCTAGTGGCCCCACTG**GTTTTAGAGCTAGAA	(Richardson et al., 2016)	N/A
JAK2 T7E1 Assay forward primer: CCTCAGAACGTTGATGGCAGTT	This Paper	N/A
JAK2 T7E1 Assay reverse primer: CTCTATTGTTTGGGCATTGTAACC	This Paper	N/A
JAK2 RT-qPCR forward primer: AACTGCATGAAACAGAAGTTCTT	This Paper	N/A
JAK2 RT-qPCR reverse primer: GCATGGCCCATGCCAACTGT	This Paper	N/A

ssODN donor for *HA-RPS27A* editing: ACCTGTCTCTTCCTTTTCCTCAACCTCAGGT GGAGCCGCCACCAAAATGTACCCATACGAT GTTCCAGATTACGCTGGTGGATCTGGAGGT TCTGGTGGAATGCAGATTTTCGTGAAAACC CTTACGGGGAAGACCATCACCCTCGAGGTA CGAGCCGGGTGGTCATGAGGAAGCCAAGG TCCGAATAAGGTCCTGAGGT	This Paper	N/A
ssODN donor for *V5-RPL40* editing: GCACCTGAGCTTGTGCTACTCAGGCATGCA TTGCTCACCAGTCTATCCTGCCTCACTTCCT CCTGCAGACGCAAACATGGGGAAGCCCAT ACCAAACCCACTACTAGGTCTGGATTCTAC GGGTGGATCTGGAGGTTCTGGTGGAATGCA GATCTTTGTGAAGACCCTCACTGGCAAAAC CATCACCCTTGAGGTCGAGC	This Paper	N/A
Forward primer for TOPO cloning *V5-RPL40*: CCAGGGTGTGTGAGAAGCCTA	This paper	N/A
Reverse primer for TOPO cloning *V5-RPL40*: CAACCCACACAGGACTGAGACTC	This paper	N/A
Forward primer for TOPO cloning *HA-RPS27A*: GGTGCCTTCTCTTGTGATCCCT	This paper	N/A
Reverse primer for TOPO cloning *HA-RPS27A*: CTAAGACATGGAAAGCAGCGCC	This paper	N/A
Forward primer for TOPO cloning *Myc-UBC*: AAGACCCGTCCATCTCGCAG	This paper	N/A
Reverse primer for TOPO cloning *Myc-UBC*: GATGTTGTAGTCAGACAGGGTGC	This paper	N/A
Forward genotyping primer for pCMV-RPS27A-SBP and pCMV-Ub-RPS27A-SBP Flp-In-T-REx-293 Cell Lines (pCMV): CGCAAATGGGCGGTAGGCGTG	UC Berkeley DNA Sequencing Facility	N/A

Reverse genotyping primer for pCMV-RPS27A-SBP and pCMV-Ub-RPS27A-SBP Flp-In-T-REx-293 Cell Lines (BGH PolyA Signal): TAGAAGGCACAGTCGAGG	UC Berkeley DNA Sequencing Facility	N/A
RPL40 qPCR forward primer: GGTGGCATTATTGAGCCTTCT	(Vihervaara et al., 2013)	N/A
RPL40 qPCR reverse primer: GTGAAGGCGAGCATAGCACT	(Vihervaara et al., 2013)	N/A
RPS27A qPCR forward primer: TGTCTCTTCCTTTTCCTCAACC	(Vihervaara et al., 2013)	N/A
RPS27A qPCR reverse primer: CTATCGTATCCGAGGGTTCAA	(Vihervaara et al., 2013)	N/A
ON-TARGETplus Non-Targeting siRNA Pool	Dharmacon	Cat# D-001810-10-05
Human ON-TARGETplus SMARTpool *siMDM2*	Dharmacon	Cat# L-003279-00
siZNF598: GAAAGGUGUACGCAUUGUAUU	(Sundaramoorthy et al., 2017)	Dharmacon A4 Custom siRNA
siβ-TRCP: GUGGAAUUUGUGGAACAU	(Loveless et al., 2015)	Dharmacon A4 Custom siRNA
siPKR: GAGAAUUUCCAGAAGGUGA	(Watanabe et al., 2013)	Dharmacon A4 Custom siRNA

Edit-R custom *CD34 crRNA,* guide sequence: UUGCUUCUGGUGCUGCAACU	(Hultquist et al., 2016)	Dharmacon
Edit-R CRISPR-Cas9 Synthetic tracrRNA	Dharmacon	Cat# U-002005-20
PCR1 forward primer for NGS Analysis of *sgBFP* editing: GCTCTTCCGATCTAGCTGGAC GGCGACGTAAAC	(Richardson et al., 2018)	N/A
PCR1 reverse primer for NGS Analysis of *sgBFP* editing: GCTCTTCCGATCTATGCGGTTCAC CAGGGTGTC	(Richardson et al., 2018)	N/A
Recombinant DNA		
pHA-Ub	Gift from Rape Lab, UC Berkeley	N/A
pUC19	Addgene; (Norrander et al., 1983)	Cat# 50005#5000 #50005
pUC19-Myc-UBC	This paper	N/A
pcDNA5/FRT/TO	Invitrogen	Cat# V652020
pcDNA5/FRT/pCMV-RPS27A-SBP	This paper	N/A
pcDNA5/FRT/pCMV-Ub-RPS27A-SBP	This paper	N/A
pOG44 Flp-Recombinase Expression Vector	Invitrogen	Cat# V600520

pET His6 TEV LIC cloning vector (2B-T)	Addgene	Cat# 29666
pET His-TEV-Km-HNT3	This paper	N/A
Software and Algorithms		
DESeq2	(Love et al., 2014)	http://bioconductor.org/packages/release/bioc/html/DESeq2.html; RRID:SCR_015687
TopHat	(Trapnell et al., 2009)	RRID:SCR_013035
HiStat2	(Kim et al., 2015)	RRID:SCR_015530
Samtools	(Li et al., 2009)	http://samtools.sourceforge.net/, RRID:SCR_002105
ImageJ	(Schindelin et al., 2015)	https://imagej.net/, RRID:SCR_003070
R (Version 3.3.2)	r-project	RRID:SCR_001905
RStudio (Version 1.0.136)	RStudio	RRID:SCR_000432
Logger Lite (Version 1.8)	Vernier Software & Technology	RRID: None

FlowJo	Treestar Inc.	RRID:SCR_008520
NEEDLE	(Li et al., 2015).	N/A
CRISPResso	(Pinello et al., 2016)	N/A
Other		
TruSeq Stranded Total RNA Library Kit with Ribo-Zero Gold	Illumina	Cat# RS-122-2301
Pierce Anti-HA Magnetic Beads Kit	Thermo Fisher Scientific	Cat# 88836
Dynabeads M-270 Streptavidin Beads	Thermo Fisher Scientific	Cat# 65305
EasySep Human CD4+ Cell Isolation Kit	STEMCELL Technologies	Cat# 17952
Dynabeads™ Human T-Activator CD3/CD28 for T Cell Expansion and Activation	Thermo Fisher Scientific	Cat# 11131D
Sera-Mag SpeedBeads® Carboxyl Magnetic Beads	GE Healthcare	Cat# 09-981-123

Chapter 6: Conclusions and Future Directions

The three studies presented in this dissertation clearly demonstrate that the ribosome is a hub for gene regulation in the cell. In our first study, we showed that proteins with unknown functions associate with the ribosome. These unknown proteins may have key roles in regulating the process of protein production in the cell, such as guiding the ribosome to a particular organelle. In our second study, we demonstrated that removing a ribosomal post-translational modification at the ER led to global changes in transcript levels, particularly for extracellular matrix mRNAs. This suggests that specific post-translational modifications of the ribosome inform global gene expression in the cell. Lastly, we show that the composition of the ribosome changes in response to DNA damage, illustrating that the cell can modify the core composition of the ribosome in response to stimuli.

A key limitation of our studies is that we fall short of describing the functional relevance of the changes in ribosome composition we observe. In our proteomics screen (*Chapter 3*), we generated lists of ribosome-associated proteins, but we did uncover functions for any novel ribosome-associated proteins. To do so, we would need to interrogate candidate genes by expressing tagged proteins and identifying their associated proteins or mRNAs, or by generating deletion cell lines and assaying their translation phenotypes. In our UFMylation study (*Chapter 4*), we see that ribosomes are ufmylated at the ER surface, but we have yet to understand why cells evolved this post-translational modification. In our DNA damage response study (*Chapter 5*), we observe that the two core ribosomal proteins disappear after DNA damage, but we do not understand how this depletion impacts translation or the life cycle of the ribosome. Furthermore, we have not identified the mechanism that triggers the depletion of RPS27A and RPL40 or the phosphorylation of eIF2α. In the following section, we will touch upon some of the outstanding questions from our UFMylation and DNA damage response studies.

Outstanding Questions: Ribosomal protein RPL26 is the principal target of UFMylation

What is the function of UFMylation?

Despite our work to characterize the UFMylation pathway in human cell lines, we have yet to understand the function of UFMylation. Due to the proximity of RPL26 to the translocon and the decrease in ECM transcript levels in our $UFM1^{KO}$ cell lines, we hypothesize that this protein is involved with directing the translation and folding of secreted proteins like extracellular matrix proteins as they enter the ER. Recently, (Liang et al.) noted that one of the UFMylation pathway components, DDRGK1, was necessary for ER-autophagy in human cells. Consequently, we hypothesize that the UFMylation of ribosomes at the ER may play a role in directing ER-autophagy machinery.

What types of transcripts are associated with UFMylated ribosomes?

It still remains unclear if UFMylation is a general feature of the ER-associated ribosome, or a post-translational modification that is necessary for directing the translation of a select number of transcripts. To differentiate between these two models, we will need to identify the mRNA transcripts that associate with UFMylated ribosomes to see if there are specific classes of mRNAs that co-localize with the modification.

Outstanding Questions: Double Stranded DNA Damage triggers ribosome remodeling and translational shutdown

What happens to other ribosomal proteins after dsDNA damage?

In our work, we found that RPS27A and RPL40 are lost after double-stranded DNA damage. As controls, we assayed the protein levels of four other ribosomal proteins, RPS6, RPL10A, RPL22, and RPS10, to gauge whether or not the loss of RPS27A and RPL40 represented a specific change in protein levels or a general loss in ribosomes. We found that none of these proteins changed in expression after dsDNA damage, suggesting that the loss of RPS27A and RPL40 is unique to these two proteins.

We made several attempts to analyze the composition of the ribosome after dsDNA breaks using proteomics. As the ribosome is made up of small basic proteins, we were concerned that trypsin would not yield as many unique peptides as another protease. Therefore, we performed *in silico* digests of ribosome proteins with different proteases (trypsin, chymotrypsin, LysC, ArgC, GluC, LysN, AspN), and we found that trypsin and chymotrypsin are the proteases that yield the highest average number of unique peptides (23 and 21 peptides per ribosomal protein, respectively). Chymotrypsin, however, created the greatest number of unique peptides mapping to RPS27A and RPL40, so we used that protease for our first round of mass spectrometry analysis.

We first performed a TMT labeling experiment with polysome profiling fractions from DMSO, etoposide, etoposide/ISRIB, epoxomicin, and etoposide/epoxomicin treated cells; however, this experiment failed because of poor peptide yield. Our second proteomics experiment used data independent acquisition (DIA) analysis on chymotrypsin-digested ribosomal pellets from DMSO, etoposide, and etoposide/ISRIB treated lysates. During a standard shotgun proteomics experiment (data dependent acquisition, or DDA), a fixed number of peptides are selected and fragmented for MS2 analysis. During data independent acquisition (DIA), however, peptides of a particular *m/z* range are fragmented and analyzed. DIA data are highly multiplexed, so we built a precursor library by running DDA analysis on all of our samples and compiling a library from all of the peptides we identified. Although a peptide for RPL40 showed up in the DDA analysis, we did not observe this protein in any of the DIA datasets. Furthermore although we had high correlation at the protein level between biological replicates for our experimental conditions, we did not see any differences in protein level for RPS27A. We checked unique peptides that mapped to the ribosome protein portion alone, but we still saw no changes. Although we were able to check for DNA damage in etoposide-treated samples with an anti-phospho-ATM antibody, we were unable to check protein levels of RPS27A because Abcam discontinued production of our antibody and we were unable to locate another functional antibody. We thus could not conclude if we could not see changes RPS27A because of our mass spectrometry technique or because our experimental conditions failed to trigger the protein's depletion.

In our third mass spectrometry experiment, we repeated the DIA experiment in the RPS27A-SBP HEK cell line, making sure that we could observe RPS27A depletion via anti-SBP Western blots prior to sample submission. We also wanted to see if we could get better results for DIA analysis with trypsin rather than chymotrypsin, so we split the samples in half and digested with chymotrypsin or trypsin. We found that there were no significant difference in

RPS27A levels, and we still did not observe RPL40 peptides. (RPL40 is a 6 kDa protein with few uniquely mapping peptides. This protein is often spuriously identified in MS datasets when the ubiquitin portion of the protein is mapped.) Because we could not find a technical or biological reason why the mass spectrometry data did not align with our Western data, we did not include these proteomics datasets in our bioRxiv manuscript. These data, however, merit re-visiting, as DIA analysis with ScaffoldDIA revealed that there were many ribosome proteins that changed in abundance in these datasets. The downside of these ribosome pelleting experiments is that they contain all ribosomal species--40S, 60S, 80S, and polysomes--and thus the results cannot tell us how the composition of translating ribosomes changes in response to DNA damage. To get at that question, we will likely need to revisit the TMT-polysome profiling experiments with a new technique for protein and peptide isolation.

What happens to the structure of the ribosome after dsDNA damage?

Once we have a better handle of the overall changes to ribosome composition in the cell after double-stranded DNA damage, we want to understand how these changes in protein levels alter the structure of the ribosome. We plan to submit ribosomes isolated from polysome profiling experiments for cryogenic electron microscopy analysis to understand how the ribosomes changes structure after double stranded DNA damage. We hope that this structural analysis of ribosomes will help inform why the cell decreases RPL40 and RPS27A levels in the ribosomes after double stranded DNA damage.

Why do RPS27A and RPL40 decrease after dsDNA damage?

Despite our efforts to characterize translation phenotypes after dsDNA damage, the reason why RPS27A and RPL40 decrease after dsDNA damage still remains a mystery. We were were surprised that our ribosome profiling data at the 36 and 72 hour timepoints had modest changes to the translatome, and the footprints exhibited no discernible changes to footprint length or 5' UTR, start codon, stop codon, or 3'UTR occupancy. It follows that the depletion of RPS27A and RPL40 may not impact the process of protein production in the cell. For example, RPS27A and RPL40 may play a role in ribosome biogenesis that would not impact the translational output of fully-formed ribosomes. Although we have evidence that total ubiquitin levels remain unchanged in the cell after dsDNA damage, we cannot rule out the possibility that ubiquitins translated from RPS27A and RPL40 specifically ubiquitinate a subset of the proteome and that depleting RPS27A and RPL40 prevents the turnover of this subset of proteins. For example, (Kobayashi et al., 2016) reported that ubiquitins translated from *RPL40* specifically associate with the ribosome. We thus speculate that cells may decrease the amount of ribosome ubiqutination from RPL40 after dsDNA damage as a means of regulating ribosomal levels in the cell.

Are the ubiquitins associated with RPL40 and RPS27A regulated translationally or post-translationally after dsDNA damage?

Because ubiquitins translated from *RPL40* and *RPS27A* are thought to be co-translationally processed, we hypothesized that the decrease that we observe in these ubiquitins is due to transcriptional or translational repression of these genes. We found that there were no changes in transcript levels via qPCR or RNA-seq. However, we observed that neither *RPL40* nor *RPS27A* exhibited changes in translation in our Cas9 ribosome profiling experiments. Since the ubiquitin sequences from these genes have high sequence homology, we isolated and

quantified changes only in the ribosome protein portions of these genes, yet we still found no changes in translation or transcription. Our Cas9 ribosome profiling data appear to contradict our etoposide data that suggests that RPL40 is regulated translationally. This discrepancy between the etoposide and Cas9 data leads us to propose that during severe dsDNA damage, RPL40 is regulated at the translation level and cannot be rescued by epoxomicin, but in the case of mild Cas9-induced DNA damage, RPL40 is translated and post-translationally degraded. It follows that the loss of ubiquitins translated from these genes observed after Cas9 treatment is due to degradation of the ubiquitin-RP fusion protein not translational repression.

What are the DNA damage response pathways that trigger the decrease of RPS27A and RPL40 and the phosphorylation of eIF2α?

One shortcoming of our DNA damage work is that we were unable to identify the pathways that trigger the decrease of RPS27A and RPL40 or that promote eIF2α phosphorylation after dsDNA damage. In our work with RPS27A, we found that neither ATM or ATR was responsible for transducing the signal for RPS27A's degradation, and we have yet to test if the third DNA damage transducer, DNA-PKcs, is responsible. It was also unclear if beta-TRCP and ZNF598 were the E3 ligases that directly ubiquitinated RPS27A or if their knockdown rescued RPS27A indirectly. We also wish to see if there is any relation between RPS27A depletion and eIF2α phosphorylation during the DNA damage response. Since ISRIB rescues RPL40 but does not rescue RPS27A, we hypothesize that depletion of RPS27A is either upstream or in different pathway that governing eIF2α phosphorylation and depletion of RPL40.

We are also interested in identifying the upstream kinase that phosphorylates eIF2α after dsDNA damage. There are three eIF2α kinases expressed in HEK cells (GCN2, PERK, PKR), and all three have been implicated in the dsDNA damage response. We assayed PKR, as it was previously identified as the kinase that phosphorylated eIF2α after doxorubicin treatment (von Holzen et al., 2007), however, we did not observe any change in phosphorylation levels with this treatment. We thus wish to determine if GCN2 or PERK is responsible for the phosphorylation of eIF2 alpha, or if two kinases have redundant functions after double-stranded DNA damage.

What happens when we modulate the effects of eIF2 alpha phosphorylation during HDR?

In our editing efficiency experiments with ISRIB and salubrinal, we found that ISRIB increased indel frequency while salubrinal decreased indel frequency. We performed these experiments in K562-BFP and HEK-BFP cell lines that contain single alleles for BFP, and thus we could not gauge how these drugs impact HDR, as there is no genomic template to repair the BFP gene in these cells. Consequently, we wish to perform editing efficiency experiments in HEK-BFP and K562-BFP cells that are nucleofected with ssODN GFP donors that contain 4 point mutations that convert BFP to GFP. Consequently, we will dose the BFP cells with salubrinal and ISRIB after nucleofection with Cas9, sgRNA, and an ssODN donor then assay HDR efficiency using NGS analysis of the edited locus.

Does modulating the effect of eIF2 alpha phosphorylation change editing efficiency in primary cell lines?

Our results with ISRIB suggest that dosing cells with ISRIB may help increase the percentage of indels in experiments that use guides that have low editing efficiency. We are also

curious to know if dosing with ISRIB and salubrinal has any implications the viability or editing efficiency of primary cells.

Conclusions

Our work with ribosome-associated proteins shows that the ribosome is a dynamic center for gene regulation in the cell, yet we are still working towards understanding the functional relevance of the modifications to the ribosome composition we observe. Thus the future of these projects will focus on uncovering the mechanisms regulating these changes to ribosome composition. All and all, our findings have opened up exciting new avenues for the translation, genome editing, and DNA damage fields to pursue.

Acknowledgements

To Nicholas Ingolia – for taking me on as a graduate student when I needed a new scientific home.

To Jacob Corn – for giving me a chance to turn a collaboration into an outstanding thesis project.

To Matt Welch and Gloria Brar – for pragmatic optimism. Thank you for helping me navigate everything from changing thesis labs to applying to post-doctoral positions.

To Chris Walczak and Ron Kopito – for letting me work on an awesome project with awesome people.

To Deborah Benedict – for believing in me and my voice.

To Anna McGeachy – for overzealous parties, a shoulder to cry on, and the Brain Cake.

To Lisa Anne Hendricks - for taking care of me under the same roof for the last ten years. Who knew that sitting next to each other in freshman Mechanics would have resulted in us completing two degrees together.

To Russell and Diana Riepe - for patiently listening to six years of science, music, and life.

To the Ingolia Lab – for being a wonderful scientific family. You guys are amazing!

References

Aguirre, A.J., Meyers, R.M., Weir, B.A., Vazquez, F., Zhang, C.-Z., Ben-David, U., Cook, A., Ha, G., Harrington, W.F., Doshi, M.B., et al. (2016). Genomic Copy Number Dictates a Gene-Independent Cell Response to CRISPR/Cas9 Targeting. Cancer Discov. *6*, 914–929.

Akutsu, M., Dikic, I., and Bremm, A. (2016). Ubiquitin chain diversity at a glance. Journal of Cell Science *129*, 875–880.

Andreassi, C., Zimmermann, C., Mitter, R., Fusco, S., De Vita, S., Saiardi, A., and Riccio, A. (2010). An NGF-responsive element targets myo-inositol monophosphatase-1 mRNA to sympathetic neuron axons. Nat. Neurosci. *13*, 291–301.

Andreev, D.E., O'Connor, P.B.F., Fahey, C., Kenny, E.M., Terenin, I.M., Dmitriev, S.E., Cormican, P., Morris, D.W., Shatsky, I.N., and Baranov, P.V. (2015). Translation of 5′ leaders is pervasive in genes resistant to eIF2 repression. Elife *4*.

Armistead, J., Khatkar, S., Meyer, B., Mark, B.L., Patel, N., Coghlan, G., Lamont, R.E., Liu, S., Wiechert, J., Cattini, P.A., et al. (2009). Mutation of a gene essential for ribosome biogenesis, EMG1, causes Bowen-Conradi syndrome. Am. J. Hum. Genet. *84*, 728–739.

Bae, S., Kweon, J., Kim, H.S., and Kim, J.-S. (2014). Microhomology-based choice of Cas9 nuclease target sites. Nat. Methods *11*, 705–706.

Baker, R.T., Tobias, J.W., and Varshavsky, A. (1992). Ubiquitin-specific proteases of Saccharomyces cerevisiae. Cloning of UBP2 and UBP3, and functional analysis of the UBP gene family. J. Biol. Chem. *267*, 23364–23375.

Barakat, A., Szick-Miranda, K., Chang, I.F., Guyot, R., Blanc, G., Cooke, R., Delseny, M., and Bailey-Serres, J. (2001). The organization of cytoplasmic ribosomal protein genes in the Arabidopsis genome. Plant Physiol. *127*, 398–415.

Bee, A., Ke, Y., Forootan, S., Lin, K., Beesley, C., Forrest, S.E., and Foster, C.S. (2006). Ribosomal protein l19 is a prognostic marker for human prostate cancer. Clin. Cancer Res. *12*, 2061–2065.

Ben-Shem, A., Jenner, L., Yusupova, G., and Yusupov, M. (2010). Crystal Structure of the Eukaryotic Ribosome. Science *330*, 1203–1209.

Bétermier, M., Bertrand, P., and Lopez, B.S. (2014). Is Non-Homologous End-Joining Really an Inherently Error-Prone Process? PLoS Genet. *10*, e1004086.

Binns, D., Dimmer, E., Huntley, R., Barrell, D., O'Donovan, C., and Apweiler, R. (2009). QuickGO: a web-based tool for Gene Ontology searching. Bioinformatics *25*, 3045–3046.

Blackford, A.N., and Jackson, S.P. (2017). ATM, ATR, and DNA-PK: The Trinity at the Heart of the DNA Damage Response. Mol. Cell *66*, 801–817.

Bortoluzzi, S., d'Alessi, F., Romualdi, C., and Danieli, G.A. (2001). Differential expression of genes coding for ribosomal proteins in different human tissues. Bioinformatics *17*, 1152–1157.

Boulton, S.J., and Jackson, S.P. (1996). Saccharomyces cerevisiae Ku70 potentiates illegitimate DNA double-strand break repair and serves as a barrier to error-prone DNA repair pathways. EMBO J. *15*, 5093–5103.

Boyce, M., Bryant, K.F., Jousse, C., Long, K., Harding, H.P., Scheuner, D., Kaufman, R.J., Ma, D., Coen, D.M., Ron, D., et al. (2005). A selective inhibitor of eIF2alpha dephosphorylation protects cells from ER stress. Science *307*, 935–939.

Braunstein, S., Badura, M.L., Xi, Q., Formenti, S.C., and Schneider, R.J. (2009a). Regulation of Protein Synthesis by Ionizing Radiation. Mol. Cell. Biol. *29*, 5645–5656.

Braunstein, S., Badura, M.L., Xi, Q., Formenti, S.C., and Schneider, R.J. (2009b). Regulation of Protein Synthesis by Ionizing Radiation. Mol. Cell. Biol. *29*, 5645–5656.

Carlile, T.M., Rojas-Duran, M.F., Zinshteyn, B., Shin, H., Bartoli, K.M., and Gilbert, W.V. (2014). Pseudouridine profiling reveals regulated mRNA pseudouridylation in yeast and human cells. Nature *515*, 143–146.

Chae, Y.K., Anker, J.F., Carneiro, B.A., Chandra, S., Kaplan, J., Kalyan, A., Santa-Maria, C.A., Platanias, L.C., and Giles, F.J. (2016). Genomic landscape of DNA repair genes in cancer. Oncotarget *7*, 23312–23321.

Chen, D., Zhang, Z., Li, M., Wang, W., Li, Y., Rayburn, E.R., Hill, D.L., Wang, H., and Zhang, R. (2007). Ribosomal protein S7 as a novel modulator of p53–MDM2 interaction: binding to MDM2, stabilization of p53 protein and activation of p53 function. Oncogene *26*, 5029–5037.

Ciccia, A., Huang, J.-W., Izhar, L., Sowa, M.E., Harper, J.W., and Elledge, S.J. (2014). Treacher Collins syndrome TCOF1 protein cooperates with NBS1 in the DNA damage response. Proc. Natl. Acad. Sci. U. S. A. *111*, 18631–18636.

Cloix, C., Tutois, S., Yukawa, Y., Mathieu, O., Cuvillier, C., Espagnol, M.-C., Picard, G., and Tourmente, S. (2002). Analysis of the 5S RNA pool in Arabidopsis thaliana: RNAs are heterogeneous and only two of the genomic 5S loci produce mature 5S RNA. Genome Res. *12*, 132–144.

Colin, E., Daniel, J., Ziegler, A., Wakim, J., Scrivo, A., Haack, T.B., Khiati, S., Denommé, A.-S., Amati-Bonneau, P., Charif, M., et al. (2016). Biallelic Variants in UBA5 Reveal that Disruption of the UFM1 Cascade Can Result in Early-Onset Encephalopathy. Am. J. Hum. Genet. *99*, 695–703.

Dai, M.-S., and Lu, H. (2004). Inhibition of MDM2-mediated p53 ubiquitination and degradation by ribosomal protein L5. J. Biol. Chem. *279*, 44475–44482.

Deng, J., Harding, H.P., Raught, B., Gingras, A.-C., Berlanga, J.J., Scheuner, D., Kaufman, R.J.,

Ron, D., and Sonenberg, N. (2002). Activation of GCN2 in UV-irradiated cells inhibits translation. Curr. Biol. *12*, 1279–1286.

Deusser, E. (1972). Heterogeneity of ribosomal populations in Escherichia coli cells grown in different media. Mol. Gen. Genet. *119*, 249–258.

Deusser, E., and Wittmann, H.-G. (1972). Biological Sciences: Ribosomal Proteins: Variation of the Protein Composition in Escherichia coli Ribosomes as Function of Growth Rate. Nature *238*, 269–270.

DeWitt, M.A., Magis, W., Bray, N.L., Wang, T., Berman, J.R., Urbinati, F., Heo, S.-J., Mitros, T., Muñoz, D.P., Boffelli, D., et al. (2016). Selection-free genome editing of the sickle mutation in human adult hematopoietic stem/progenitor cells. Sci. Transl. Med. *8*, 360ra134.

Dimarco, E., Cascone, E., Bellavia, D., and Caradonna, F. (2012). Functional variants of 5S rRNA in the ribosomes of common sea urchin Paracentrotus lividus. Gene *508*, 21–25.

Duan, R., Shi, Y., Yu, L., Zhang, G., Li, J., Lin, Y., Guo, J., Wang, J., Shen, L., Jiang, H., et al. (2016). UBA5 Mutations Cause a New Form of Autosomal Recessive Cerebellar Ataxia. PLoS One *11*, e0149039.

Eisenberg, A.R., Higdon, A., Keskin, A., Hodapp, S., Jovanovic, M., and Brar, G.A. (2018). Precise Post-translational Tuning Occurs for Most Protein Complex Components during Meiosis. Cell Rep. *25*, 3603–3617.e2.

FANTOM Consortium and the RIKEN PMI and CLST (DGT), Forrest, A.R.R., Kawaji, H., Rehli, M., Baillie, J.K., de Hoon, M.J.L., Haberle, V., Lassmann, T., Kulakovskiy, I.V., Lizio, M., et al. (2014). A promoter-level mammalian expression atlas. Nature *507*, 462–470.

Fisher, E.M.C., Beer-Romero, P., Brown, L.G., Ridley, A., McNeil, J.A., Lawrence, J.B., Willard, H.F., Bieber, F.R., and Page, D.C. (1990). Homologous ribosomal protein genes on the human X and Y chromosomes: Escape from X inactivation and possible implications for turner syndrome. Cell *63*, 1205–1218.

Fleischer, T.C., Weaver, C.M., McAfee, K.J., Jennings, J.L., and Link, A.J. (2006). Systematic identification and functional screens of uncharacterized proteins associated with eukaryotic ribosomal complexes. Genes Dev. *20*, 1294–1307.

Garzia, A., Jafarnejad, S.M., Meyer, C., Chapat, C., Gogakos, T., Morozov, P., Amiri, M., Shapiro, M., Molina, H., Tuschl, T., et al. (2017). The E3 ubiquitin ligase and RNA-binding protein ZNF598 orchestrates ribosome quality control of premature polyadenylated mRNAs. Nat. Commun. *8*, 16056.

Genuth, N.R., and Barna, M. (2018). The Discovery of Ribosome Heterogeneity and Its Implications for Gene Regulation and Organismal Life. Mol. Cell *71*, 364–374.

Gressner, A.M., and Wool, I.G. (1974). The phosphorylation of liver ribosomal proteins in vivo.

Evidence that only a single small subunit protein (S6) is phosphorylated. J. Biol. Chem. *249*, 6917–6925.

Grou, C.P., Pinto, M.P., Mendes, A.V., Domingues, P., and Azevedo, J.E. (2015). The de novo synthesis of ubiquitin: identification of deubiquitinases acting on ubiquitin precursors. Sci. Rep. *5*.

Guimaraes, J.C., and Zavolan, M. (2016). Patterns of ribosomal protein expression specify normal and malignant human cells. Genome Biol. *17*, 236.

Guirouilh-Barbat, J., Rass, E., Plo, I., Bertrand, P., and Lopez, B.S. (2007). Defects in XRCC4 and KU80 differentially affect the joining of distal nonhomologous ends. Proc. Natl. Acad. Sci. U. S. A. *104*, 20902–20907.

Gunderson, J.H., Sogin, M.L., Wollett, G., Hollingdale, M., de la Cruz, V.F., Waters, A.P., and McCutchan, T.F. (1987). Structurally distinct, stage-specific ribosomes occur in Plasmodium. Science *238*, 933–937.

Guo, X., Shi, Y., Gou, Y., Li, J., Han, S., Zhang, Y., Huo, J., Ning, X., Sun, L., Chen, Y., et al. (2011). Human ribosomal protein S13 promotes gastric cancer growth through down-regulating p27(Kip1). J. Cell. Mol. Med. *15*, 296–306.

Haapaniemi, E., Botla, S., Persson, J., Schmierer, B., and Taipale, J. (2018). CRISPR–Cas9 genome editing induces a p53-mediated DNA damage response. Nat. Med. *24*, 927–930.

Halim, V.A., García-Santisteban, I., Warmerdam, D.O., van den Broek, B., Heck, A.J.R., Mohammed, S., and Medema, R.H. (2018). Doxorubicin-induced DNA Damage Causes Extensive Ubiquitination of Ribosomal Proteins Associated with a Decrease in Protein Translation*. Molecular & Cellular Proteomics *17*, 2297–2308.

Hamilton, E.M.C., Bertini, E., Kalaydjieva, L., Morar, B., Dojčáková, D., Liu, J., Vanderver, A., Curiel, J., Persoon, C.M., Diodato, D., et al. (2017). founder mutation in the Roma population causes recessive variant of H-ABC. Neurology *89*, 1821–1828.

Heiss, N.S., Knight, S.W., Vulliamy, T.J., Klauck, S.M., Wiemann, S., Mason, P.J., Poustka, A., and Dokal, I. (1998). X-linked dyskeratosis congenita is caused by mutations in a highly conserved gene with putative nucleolar functions. Nature Genetics *19*, 32–38.

Henry, J.L., Coggin, D.L., and King, C.R. (1993). High-level expression of the ribosomal protein L19 in human breast tumors that overexpress erbB-2. Cancer Res. *53*, 1403–1408.

Higa-Nakamine, S., Suzuki, T., Uechi, T., Chakraborty, A., Nakajima, Y., Nakamura, M., Hirano, N., Suzuki, T., and Kenmochi, N. (2012). Loss of ribosomal RNA modification causes developmental defects in zebrafish. Nucleic Acids Res. *40*, 391–398.

Higgins, R., Gendron, J.M., Rising, L., Mak, R., Webb, K., Kaiser, S.E., Zuzow, N., Riviere, P., Yang, B., Fenech, E., et al. (2015). The Unfolded Protein Response Triggers Site-Specific

Regulatory Ubiquitylation of 40S Ribosomal Proteins. Mol. Cell *59*, 35–49.

von Holzen, U., Pataer, A., Raju, U., Bocangel, D., Vorburger, S.A., Liu, Y., Lu, X., Roth, J.A., Aggarwal, B.B., Barber, G.N., et al. (2007). The double-stranded RNA-activated protein kinase mediates radiation resistance in mouse embryo fibroblasts through nuclear factor kappaB and Akt activation. Clin. Cancer Res. *13*, 6032–6039.

Honma, M., Sakuraba, M., Koizumi, T., Takashima, Y., Sakamoto, H., and Hayashi, M. (2007). Non-homologous end-joining for repairing I-SceI-induced DNA double strand breaks in human cells. DNA Repair *6*, 781–788.

Hsu, P.D., Scott, D.A., Weinstein, J.A., Ran, F.A., Konermann, S., Agarwala, V., Li, Y., Fine, E.J., Wu, X., Shalem, O., et al. (2013). DNA targeting specificity of RNA-guided Cas9 nucleases. Nat. Biotechnol. *31*, 827–832.

Hultquist, J.F., Schumann, K., Woo, J.M., Manganaro, L., McGregor, M.J., Doudna, J., Simon, V., Krogan, N.J., and Marson, A. (2016). A Cas9 Ribonucleoprotein Platform for Functional Genetic Studies of HIV-Host Interactions in Primary Human T Cells. Cell Rep. *17*, 1438–1452.

Ihry, R.J., Worringer, K.A., Salick, M.R., Frias, E., Ho, D., Theriault, K., Kommineni, S., Chen, J., Sondey, M., Ye, C., et al. (2018). p53 inhibits CRISPR-Cas9 engineering in human pluripotent stem cells. Nat. Med. *24*, 939–946.

Ingolia, N.T., Brar, G.A., Rouskin, S., McGeachy, A.M., and Weissman, J.S. (2012). The ribosome profiling strategy for monitoring translation in vivo by deep sequencing of ribosome-protected mRNA fragments. Nat. Protoc. *7*, 1534–1550.

Ingolia, N.T., Brar, G.A., Stern-Ginossar, N., Harris, M.S., Talhouarne, G.J.S., Jackson, S.E., Wills, M.R., and Weissman, J.S. (2014). Ribosome profiling reveals pervasive translation outside of annotated protein-coding genes. Cell Rep. *8*, 1365–1379.

Ishikawa, Y., and Bächinger, H.P. (2013). A molecular ensemble in the rER for procollagen maturation. Biochimica et Biophysica Acta (BBA) - Molecular Cell Research *1833*, 2479–2491.

Jackson, R.J., Hellen, C.U.T., and Pestova, T.V. (2010). The mechanism of eukaryotic translation initiation and principles of its regulation. Nat. Rev. Mol. Cell Biol. *11*, 113–127.

Jiang, H.-Y., and Wek, R.C. (2005). GCN2 phosphorylation of eIF2alpha activates NF-kappaB in response to UV irradiation. Biochem. J *385*, 371–380.

Jin, A., Itahana, K., O'Keefe, K., and Zhang, Y. (2004). Inhibition of HDM2 and Activation of p53 by Ribosomal Protein L23. Molecular and Cellular Biology *24*, 7669–7680.

Joerger, A.C., and Fersht, A.R. (2016). The p53 Pathway: Origins, Inactivation in Cancer, and Emerging Therapeutic Approaches. Annu. Rev. Biochem. *85*, 375–404.

Kim, D., Langmead, B., and Salzberg, S.L. (2015). HISAT: a fast spliced aligner with low

memory requirements. Nat. Methods *12*, 357–360.

Kim, E.J., Lee, Y.-J., Kang, S., and Lim, Y.-B. (2014). Ionizing radiation activates PERK/eIF2α/ATF4 signaling via ER stress-independent pathway in human vascular endothelial cells. Int. J. Radiat. Biol. *90*, 306–312.

Kim, H.-L., Song, W.-S., Kim, K., and Lee, K. (2008). Characterization of heterogeneous LSU rRNA profiles in Streptomyces coelicolor under different growth stages and conditions. Curr. Microbiol. *57*, 537–541.

Kim, J.-H., You, K.-R., Kim, I.H., Cho, B.-H., Kim, C.-Y., and Kim, D.-G. (2004). Over-expression of the ribosomal protein L36a gene is associated with cellular proliferation in hepatocellular carcinoma. Hepatology *39*, 129–138.

Kim, S., Koo, T., Jee, H.-G., Cho, H.-Y., Lee, G., Lim, D.-G., Shin, H.S., and Kim, J.-S. (2018). CRISPR RNAs trigger innate immune responses in human cells. Genome Res.

Kobayashi, M., Oshima, S., Maeyashiki, C., Nibe, Y., Otsubo, K., Matsuzawa, Y., Nemoto, Y., Nagaishi, T., Okamoto, R., Tsuchiya, K., et al. (2016). The ubiquitin hybrid gene UBA52 regulates ubiquitination of ribosome and sustains embryonic development. Sci. Rep. *6*, 36780.

Komili, S., Farny, N.G., Roth, F.P., and Silver, P.A. (2007). Functional specificity among ribosomal proteins regulates gene expression. Cell *131*, 557–571.

Kondrashov, N., Pusic, A., Stumpf, C.R., Shimizu, K., Hsieh, A.C., Ishijima, J., Shiroishi, T., and Barna, M. (2011). Ribosome-mediated specificity in Hox mRNA translation and vertebrate tissue patterning. Cell *145*, 383–397.

Kruhlak, M., Crouch, E.E., Orlov, M., Montaño, C., Gorski, S.A., Nussenzweig, A., Misteli, T., Phair, R.D., and Casellas, R. (2007). The ATM repair pathway inhibits RNA polymerase I transcription in response to chromosome breaks. Nature *447*, 730–734.

Kumar, V., Sabatini, D., Pandey, P., Gingras, A.C., Majumder, P.K., Kumar, M., Yuan, Z.M., Carmichael, G., Weichselbaum, R., Sonenberg, N., et al. (2000a). Regulation of the rapamycin and FKBP-target 1/mammalian target of rapamycin and cap-dependent initiation of translation by the c-Abl protein-tyrosine kinase. J. Biol. Chem. *275*, 10779–10787.

Kumar, V., Sabatini, D., Pandey, P., Gingras, A.C., Majumder, P.K., Kumar, M., Yuan, Z.M., Carmichael, G., Weichselbaum, R., Sonenberg, N., et al. (2000b). Regulation of the rapamycin and FKBP-target 1/mammalian target of rapamycin and cap-dependent initiation of translation by the c-Abl protein-tyrosine kinase. J. Biol. Chem. *275*, 10779–10787.

Kurylo, C.M., Parks, M.M., Juette, M.F., Zinshteyn, B., Altman, R.B., Thibado, J.K., Vincent, C.T., and Blanchard, S.C. (2018). Endogenous rRNA Sequence Variation Can Regulate Stress Response Gene Expression and Phenotype. Cell Rep. *25*, 236–248.e6.

Larsen, C.N., Krantz, B.A., and Wilkinson, K.D. (1998). Substrate Specificity of

Deubiquitinating Enzymes: Ubiquitin C-Terminal Hydrolases†. Biochemistry *37*, 3358–3368.

Larsen, D.H., Hari, F., Clapperton, J.A., Gwerder, M., Gutsche, K., Altmeyer, M., Jungmichel, S., Toledo, L.I., Fink, D., Rask, M.-B., et al. (2014). The NBS1-Treacle complex controls ribosomal RNA transcription in response to DNA damage. Nat. Cell Biol. *16*, 792–803.

Lee, A.S.-Y., -Y. Lee, A.S., Burdeinick-Kerr, R., and Whelan, S.P.J. (2012). A ribosome-specialized translation initiation pathway is required for cap-dependent translation of vesicular stomatitis virus mRNAs. Proceedings of the National Academy of Sciences *110*, 324–329.

Li, H., Handsaker, B., Wysoker, A., Fennell, T., Ruan, J., Homer, N., Marth, G., Abecasis, G., Durbin, R., and 1000 Genome Project Data Processing Subgroup (2009). The Sequence Alignment/Map format and SAMtools. Bioinformatics *25*, 2078–2079.

Li, W., Cowley, A., Uludag, M., Gur, T., McWilliam, H., Squizzato, S., Park, Y.M., Buso, N., and Lopez, R. (2015). The EMBL-EBI bioinformatics web and programmatic tools framework. Nucleic Acids Res. *43*, W580–W584.

Liang, J.R., Lingeman, E., Luong, T., Ahmed, S., Nguyen, T., Olzmann, J., and Corn, J.E. A genome-wide screen for ER autophagy highlights key roles of mitochondrial metabolism and ER- resident UFMylation.

Lin, W.Y., Wilson, J.H., and Lin, Y. (2013). Repair of chromosomal double-strand breaks by precise ligation in human cells. DNA Repair *12*, 480–487.

Lingeman, E., Jeans, C., and Corn, J.E. (2017). Production of Purified CasRNPs for Efficacious Genome Editing. Curr. Protoc. Mol. Biol. *120*, 31.10.1–31.10.19.

Llanos, S., and Serrano, M. (2010). Depletion of ribosomal protein L37 occurs in response to DNA damage and activates p53 through the L11/MDM2 pathway. Cell Cycle *9*, 4005–4012.

Lohrum, M.A.E., Ludwig, R.L., Kubbutat, M.H.G., Hanlon, M., and Vousden, K.H. (2003). Regulation of HDM2 activity by the ribosomal protein L11. Cancer Cell *3*, 577–587.

Lopes, A.M., Miguel, R.N., Sargent, C.A., Ellis, P.J., Amorim, A., and Affara, N.A. (2010). The human RPS4 paralogue on Yq11.223 encodes a structurally conserved ribosomal protein and is preferentially expressed during spermatogenesis. BMC Mol. Biol. *11*, 33.

López-López, A., Benlloch, S., Bonfá, M., Rodríguez-Valera, F., and Mira, A. (2007). Intragenomic 16S rDNA divergence in Haloarcula marismortui is an adaptation to different temperatures. J. Mol. Evol. *65*, 687–696.

Love, M.I., Huber, W., and Anders, S. (2014). Moderated estimation of fold change and dispersion for RNA-seq data with DESeq2. Genome Biol. *15*, 550.

Loveless, T.B., Topacio, B.R., Vashisht, A.A., Galaang, S., Ulrich, K.M., Young, B.D., Wohlschlegel, J.A., and Toczyski, D.P. (2015). DNA Damage Regulates Translation through β-

TRCP Targeting of CReP. PLoS Genet. *11*, e1005292.

Maréchal, A., and Zou, L. (2013). DNA damage sensing by the ATM and ATR kinases. Cold Spring Harb. Perspect. Biol. *5*.

Martin, K.C., and Ephrussi, A. (2009). mRNA localization: gene expression in the spatial dimension. Cell *136*, 719–730.

Martin, I., Kim, J.W., Lee, B.D., Kang, H.C., Xu, J.-C., Jia, H., Stankowski, J., Kim, M.-S., Zhong, J., Kumar, M., et al. (2014). Ribosomal Protein s15 Phosphorylation Mediates LRRK2 Neurodegeneration in Parkinson's Disease. Cell *157*, 472–485.

McGlincy, N.J., and Ingolia, N.T. (2017). Transcriptome-wide measurement of translation by ribosome profiling. Methods *126*, 112–129.

Meyuhas, O. (2015). Ribosomal Protein S6 Phosphorylation: Four Decades of Research. Int. Rev. Cell Mol. Biol. *320*, 41–73.

Mi, H., Muruganujan, A., Casagrande, J.T., and Thomas, P.D. (2013). Large-scale gene function analysis with the PANTHER classification system. Nat. Protoc. *8*, 1551–1566.

Mi, H., Huang, X., Muruganujan, A., Tang, H., Mills, C., Kang, D., and Thomas, P.D. (2017). PANTHER version 11: expanded annotation data from Gene Ontology and Reactome pathways, and data analysis tool enhancements. Nucleic Acids Res. *45*, D183–D189.

Munoz, D.M., Cassiani, P.J., Li, L., Billy, E., Korn, J.M., Jones, M.D., Golji, J., Ruddy, D.A., Yu, K., McAllister, G., et al. (2016). CRISPR Screens Provide a Comprehensive Assessment of Cancer Vulnerabilities but Generate False-Positive Hits for Highly Amplified Genomic Regions. Cancer Discov. *6*, 900–913.

Muona, M., Ishimura, R., Laari, A., Ichimura, Y., Linnankivi, T., Keski-Filppula, R., Herva, R., Rantala, H., Paetau, A., Pöyhönen, M., et al. (2016). Biallelic Variants in UBA5 Link Dysfunctional UFM1 Ubiquitin-like Modifier Pathway to Severe Infantile-Onset Encephalopathy. Am. J. Hum. Genet. *99*, 683–694.

Nahorski, M.S., Maddirevula, S., Ishimura, R., Alsahli, S., Brady, A.F., Begemann, A., Mizushima, T., Guzmán-Vega, F.J., Obata, M., Ichimura, Y., et al. (2018). Biallelic UFM1 and UFC1 mutations expand the essential role of ufmylation in brain development. Brain *141*, 1934–1945.

Nakade, S., Tsubota, T., Sakane, Y., Kume, S., Sakamoto, N., Obara, M., Daimon, T., Sezutsu, H., Yamamoto, T., Sakuma, T., et al. (2014). Microhomology-mediated end-joining-dependent integration of donor DNA in cells and animals using TALENs and CRISPR/Cas9. Nat. Commun. *5*, 5560.

Natori, Y., Nanamiya, H., Akanuma, G., Kosono, S., Kudo, T., Ochi, K., and Kawamura, F. (2007). A fail-safe system for the ribosome under zinc-limiting conditions in Bacillus subtilis.

Mol. Microbiol. *63*, 294–307.

Newton, K., Matsumoto, M.L., Wertz, I.E., Kirkpatrick, D.S., Lill, J.R., Tan, J., Dugger, D., Gordon, N., Sidhu, S.S., Fellouse, F.A., et al. (2008). Ubiquitin chain editing revealed by polyubiquitin linkage-specific antibodies. Cell *134*, 668–678.

Norrander, J., Kempe, T., and Messing, J. (1983). Construction of improved M13 vectors using oligodeoxynucleotide-directed mutagenesis. Gene *26*, 101–106.

Nosrati, N., Kapoor, N.R., and Kumar, V. (2015). DNA damage stress induces the expression of ribosomal protein S27a gene in a p53-dependent manner. Gene *559*, 44–51.

Özbek, S., Balasubramanian, P.G., Chiquet-Ehrismann, R., Tucker, R.P., and Adams, J.C. (2010). The Evolution of Extracellular Matrix. Mol. Biol. Cell *21*, 4300–4305.

Parenteau, J., Durand, M., Morin, G., Gagnon, J., Lucier, J.-F., Wellinger, R.J., Chabot, B., and Elela, S.A. (2011). Introns within ribosomal protein genes regulate the production and function of yeast ribosomes. Cell *147*, 320–331.

Parks, M.M., Kurylo, C.M., Dass, R.A., Bojmar, L., Lyden, D., Theresa Vincent, C., and Blanchard, S.C. (2018). Variant ribosomal RNA alleles are conserved and exhibit tissue-specific expression. Science Advances *4*, eaao0665.

Peidis, P., Papadakis, A.I., Muaddi, H., Richard, S., and Koromilas, A.E. (2011). Doxorubicin bypasses the cytoprotective effects of eIF2α phosphorylation and promotes PKR-mediated cell death. Cell Death Differ. *18*, 145–154.

Pierce, N.W., Kleiger, G., Shan, S.-O., and Deshaies, R.J. (2009). Detection of Sequential Polyubiquitylation on a Millisecond Time-Scale. Nature *462*, 615.

Pinello, L., Canver, M.C., Hoban, M.D., Orkin, S.H., Kohn, D.B., Bauer, D.E., and Yuan, G.-C. (2016). Analyzing CRISPR genome-editing experiments with CRISPResso. Nat. Biotechnol. *34*, 695–697.

Pogue-Geile, K., Geiser, J.R., Shu, M., Miller, C., Wool, I.G., Meisler, A.I., and Pipas, J.M. (1991). Ribosomal protein genes are overexpressed in colorectal cancer: isolation of a cDNA clone encoding the human S3 ribosomal protein. Mol. Cell. Biol. *11*, 3842–3849.

Rabl, J., Leibundgut, M., Ataide, S.F., Haag, A., and Ban, N. (2011). Crystal Structure of the Eukaryotic 40S Ribosomal Subunit in Complex with Initiation Factor 1. Science *331*, 730–736.

Ramagopal, S., and Ennis, H.L. (1981). Regulation of synthesis of cell-specific ribosomal proteins during differentiation of Dictyostelium discoideum. Proc. Natl. Acad. Sci. U. S. A. *78*, 3083–3087.

Rath, A., Hromas, R., and De Benedetti, A. (2014). Fidelity of end joining in mammalian episomes and the impact of Metnase on joint processing. BMC Mol. Biol. *15*, 6.

Reschke, M., Clohessy, J.G., Seitzer, N., Goldstein, D.P., Breitkopf, S.B., Schmolze, D.B., Ala, U., Asara, J.M., Beck, A.H., and Pandolfi, P.P. (2013). Characterization and analysis of the composition and dynamics of the mammalian riboproteome. Cell Rep. *4*, 1276–1287.

Richardson, C.D., Ray, G.J., DeWitt, M.A., Curie, G.L., and Corn, J.E. (2016). Enhancing homology-directed genome editing by catalytically active and inactive CRISPR-Cas9 using asymmetric donor DNA. Nat. Biotechnol. *34*, 339–344.

Richardson, C.D., Kazane, K.R., Feng, S.J., Zelin, E., Bray, N.L., Schäfer, A.J., Floor, S.N., and Corn, J.E. (2018). CRISPR–Cas9 genome editing in human cells occurs via the Fanconi anemia pathway. Nat. Genet. *50*, 1132–1139.

Robert, F., Williams, C., Yan, Y., Donohue, E., Cencic, R., Burley, S.K., and Pelletier, J. (2009). Blocking UV-induced eIF2alpha phosphorylation with small molecule inhibitors of GCN2. Chem. Biol. Drug Des. *74*, 57–67.

Ruvinsky, I., Sharon, N., Lerer, T., Cohen, H., Stolovich-Rain, M., Nir, T., Dor, Y., Zisman, P., and Meyuhas, O. (2005). Ribosomal protein S6 phosphorylation is a determinant of cell size and glucose homeostasis. Genes Dev. *19*, 2199–2211.

Saal, L., Briese, M., Kneitz, S., Glinka, M., and Sendtner, M. (2014). Subcellular transcriptome alterations in a cell culture model of spinal muscular atrophy point to widespread defects in axonal growth and presynaptic differentiation. RNA *20*, 1789–1802.

Sauert, M., Temmel, H., and Moll, I. (2015). Heterogeneity of the translational machinery: Variations on a common theme. Biochimie *114*, 39–47.

Schindelin, J., Rueden, C.T., Hiner, M.C., and Eliceiri, K.W. (2015). The ImageJ ecosystem: An open platform for biomedical image analysis. Mol. Reprod. Dev. *82*, 518–529.

Schleich, S., Strassburger, K., Janiesch, P.C., Koledachkina, T., Miller, K.K., Haneke, K., Cheng, Y.-S., Küchler, K., Stoecklin, G., Duncan, K.E., et al. (2014). DENR–MCT-1 promotes translation re-initiation downstream of uORFs to control tissue growth. Nature *512*, 208–212.

Schneider, R., Braunstein, S., Xi, Q., and Formenti, S. (2005a). Ionizing Radiation Controls Protein Synthesis Through a Novel Akt-independent Pathway Involving Regulation of mTOR and 4E-BP1 Stability. International Journal of Radiation Oncology*Biology*Physics *63*, S146.

Schneider, R., Braunstein, S., Xi, Q., and Formenti, S. (2005b). Ionizing Radiation Controls Protein Synthesis Through a Novel Akt-independent Pathway Involving Regulation of mTOR and 4E-BP1 Stability. International Journal of Radiation Oncology*Biology*Physics *63*, S146.

Schosserer, M., Minois, N., Angerer, T.B., Amring, M., Dellago, H., Harreither, E., Calle-Perez, A., Pircher, A., Gerstl, M.P., Pfeifenberger, S., et al. (2015). Methylation of ribosomal RNA by NSUN5 is a conserved mechanism modulating organismal lifespan. Nat. Commun. *6*, 6158.

Shi, Z., and Barna, M. (2015). Translating the genome in time and space: specialized ribosomes,

RNA regulons, and RNA-binding proteins. Annu. Rev. Cell Dev. Biol. *31*, 31–54.

Shi, Z., Fujii, K., Kovary, K.M., Genuth, N.R., Röst, H.L., Teruel, M.N., and Barna, M. (2017). Heterogeneous Ribosomes Preferentially Translate Distinct Subpools of mRNAs Genome-wide. Mol. Cell *67*, 71–83.e7.

Shigeoka, T., Koppers, M., Wong, H.H.-W., Lin, J.Q., Dwivedy, A., de Freitas Nascimento, J., Cagnetta, R., van Tartwijk, F., Strohl, F., Cioni, J.-M., et al. On-site ribosome remodeling by locally synthesized ribosomal proteins in axons.

Sidrauski, C., Acosta-Alvear, D., Khoutorsky, A., Vedantham, P., Hearn, B.R., Li, H., Gamache, K., Gallagher, C.M., Ang, K.K.-H., Wilson, C., et al. (2013). Pharmacological brake-release of mRNA translation enhances cognitive memory. Elife *2*, e00498.

Sidrauski, C., McGeachy, A.M., Ingolia, N.T., and Walter, P. (2015). The small molecule ISRIB reverses the effects of eIF2α phosphorylation on translation and stress granule assembly. Elife *4*.

Silva, G.M., Finley, D., and Vogel, C. (2015). K63 polyubiquitination is a new modulator of the oxidative stress response. Nat. Struct. Mol. Biol. *22*, 116–123.

Simsek, D., and Barna, M. (2017). An emerging role for the ribosome as a nexus for post-translational modifications. Curr. Opin. Cell Biol. *45*, 92–101.

Simsek, D., Tiu, G.C., Flynn, R.A., Byeon, G.W., Leppek, K., Xu, A.F., Chang, H.Y., and Barna, M. (2017). The Mammalian Ribo-interactome Reveals Ribosome Functional Diversity and Heterogeneity. Cell *169*, 1051–1065.e18.

Slavov, N., Semrau, S., Airoldi, E., Budnik, B., and van Oudenaarden, A. (2015). Differential Stoichiometry among Core Ribosomal Proteins. Cell Rep. *13*, 865–873.

Sloan, K.E., Warda, A.S., Sharma, S., Entian, K.-D., Lafontaine, D.L.J., and Bohnsack, M.T. (2017). Tuning the ribosome: The influence of rRNA modification on eukaryotic ribosome biogenesis and function. RNA Biol. *14*, 1138–1152.

van Sluis, M., and McStay, B. (2015). A localized nucleolar DNA damage response facilitates recruitment of the homology-directed repair machinery independent of cell cycle stage. Genes Dev. *29*, 1151–1163.

Society., B., Biophysical Society., and Roberts, R.B. (1958). Microsomal particles and protein synthesis; papers presented at the First Symposium of the Biophysical Society, at the Massachusetts Institute of Technology, Cambridge, February 5, 6, and 8, 1958. Richard B. Roberts, editor.

Sonenberg, N., and Hinnebusch, A.G. (2009). Regulation of translation initiation in eukaryotes: mechanisms and biological targets. Cell *136*, 731–745.

Song, W., Joo, M., Yeom, J.-H., Shin, E., Lee, M., Choi, H.-K., Hwang, J., Kim, Y.-I., Seo, R.,

Lee, J.E., et al. (2019). Divergent rRNAs as regulators of gene expression at the ribosome level. Nat Microbiol *4*, 515–526.

Sun, X.-X., DeVine, T., Challagundla, K.B., and Dai, M.-S. (2011). Interplay between Ribosomal Protein S27a and MDM2 Protein in p53 Activation in Response to Ribosomal Stress. J. Biol. Chem. *286*, 22730.

Sundaramoorthy, E., Leonard, M., Mak, R., Liao, J., Fulzele, A., and Bennett, E.J. (2017). ZNF598 and RACK1 Regulate Mammalian Ribosome-Associated Quality Control Function by Mediating Regulatory 40S Ribosomal Ubiquitylation. Mol. Cell *65*, 751–760.e4.

Takagi, M., Absalon, M.J., McLure, K.G., and Kastan, M.B. (2005). Regulation of p53 translation and induction after DNA damage by ribosomal protein L26 and nucleolin. Cell *123*, 49–63.

Taoka, M., Nobe, Y., Hori, M., Takeuchi, A., Masaki, S., Yamauchi, Y., Nakayama, H., Takahashi, N., and Isobe, T. (2015). A mass spectrometry-based method for comprehensive quantitative determination of post-transcriptional RNA modifications: the complete chemical structure of Schizosaccharomyces pombe ribosomal RNAs. Nucleic Acids Res. *43*, e115.

Taoka, M., Nobe, Y., Yamaki, Y., Yamauchi, Y., Ishikawa, H., Takahashi, N., Nakayama, H., and Isobe, T. (2016). The complete chemical structure of Saccharomyces cerevisiae rRNA: partial pseudouridylation of U2345 in 25S rRNA by snoRNA snR9. Nucleic Acids Res. *44*, 8951–8961.

Trapnell, C., Pachter, L., and Salzberg, S.L. (2009). TopHat: discovering splice junctions with RNA-Seq. Bioinformatics *25*, 1105–1111.

Tunney, R., McGlincy, N.J., Graham, M.E., Naddaf, N., Pachter, L., and Lareau, L.F. (2018). Accurate design of translational output by a neural network model of ribosome distribution. Nat. Struct. Mol. Biol. *25*, 577–582.

Vassilev, L.T., Vu, B.T., Graves, B., Carvajal, D., Podlaski, F., Filipovic, Z., Kong, N., Kammlott, U., Lukacs, C., Klein, C., et al. (2004). In vivo activation of the p53 pathway by small-molecule antagonists of MDM2. Science *303*, 844–848.

Vihervaara, A., Sergelius, C., Vasara, J., Blom, M.A.H., Elsing, A.N., Roos-Mattjus, P., and Sistonen, L. (2013). Transcriptional response to stress in the dynamic chromatin environment of cycling and mitotic cells. Proc. Natl. Acad. Sci. U. S. A. *110*, E3388–E3397.

Walczak, C.P., Leto, D.E., Zhang, L., Riepe, C., Muller, R.Y., DaRosa, P.A., Ingolia, N.T., Elias, J.E., and Kopito, R.R. (2019). Ribosomal protein RPL26 is the principal target of UFMylation. Proc. Natl. Acad. Sci. U. S. A. *116*, 1299–1308.

Wang, J., Zhang, J., Lee, Y.M., Ng, S., Shi, Y., Hua, Z.-C., Lin, Q., and Shen, H.-M. (2017). Nonradioactive quantification of autophagic protein degradation with L-azidohomoalanine labeling. Nat. Protoc. *12*, 279–288.

Wang, T., Birsoy, K., Hughes, N.W., Krupczak, K.M., Post, Y., Wei, J.J., Lander, E.S., and Sabatini, D.M. (2015a). Identification and characterization of essential genes in the human genome. Science *350*, 1096–1101.

Wang, W., Nag, S., Zhang, X., Wang, M.-H., Wang, H., Zhou, J., and Zhang, R. (2015b). Ribosomal Proteins and Human Diseases: Pathogenesis, Molecular Mechanisms, and Therapeutic Implications. Medicinal Research Reviews *35*, 225–285.

Wang, Y.J., Vaidyanathan, P.P., Rojas-Duran, M.F., Udeshi, N.D., Bartoli, K.M., Carr, S.A., and Gilbert, W.V. (2018). Lso2 is a conserved ribosome-bound protein required for translational recovery in yeast. PLoS Biol. *16*, e2005903.

Watanabe, T., Hiasa, Y., Tokumoto, Y., Hirooka, M., Abe, M., Ikeda, Y., Matsuura, B., Chung, R.T., and Onji, M. (2013). Protein kinase R modulates c-Fos and c-Jun signaling to promote proliferation of hepatocellular carcinoma with hepatitis C virus infection. PLoS One *8*, e67750.

Wegnez, M., Monier, R., and Denis, H. (1972). Sequence heterogeneity of 5 S RNA in Xenopus laevis. FEBS Lett. *25*, 13–20.

Weijers, D., Franke-van Dijk, M., Vencken, R.J., Quint, A., Hooykaas, P., and Offringa, R. (2001). An Arabidopsis Minute-like phenotype caused by a semi-dominant mutation in a RIBOSOMAL PROTEIN S5 gene. Development *128*, 4289–4299.

Wienert, B., Shin, J., Zelin, E., Pestal, K., and Corn, J.E. (2018). In vitro-transcribed guide RNAs trigger an innate immune response via the RIG-I pathway. PLoS Biol. *16*, e2005840.

Wong, Q.W.-L., Li, J., Ng, S.R., Lim, S.G., Yang, H., and Vardy, L.A. (2014). RPL39L is an example of a recently evolved ribosomal protein paralog that shows highly specific tissue expression patterns and is upregulated in ESCs and HCC tumors. RNA Biol. *11*, 33–41.

Wu, K., Kovacev, J., and Pan, Z.-Q. (2010). Priming and extending: an UbcH5/Cdc34 E2 handoff mechanism for polyubiquitination on a SCF substrate. Mol. Cell *37*, 784.

Wu, S., Hu, Y., Wang, J.-L., Chatterjee, M., Shi, Y., and Kaufman, R.J. (2002). Ultraviolet light inhibits translation through activation of the unfolded protein response kinase PERK in the lumen of the endoplasmic reticulum. J. Biol. Chem. *277*, 18077–18083.

Xiong, X., Zhao, Y., He, H., and Sun, Y. (2011). Ribosomal protein S27-like and S27 interplay with p53-MDM2 axis as a target, a substrate and a regulator. Oncogene *30*, 1798–1811.

Xue, S., and Barna, M. (2012). Specialized ribosomes: a new frontier in gene regulation and organismal biology. Nat. Rev. Mol. Cell Biol. *13*, 355–369.

Xue, S., Tian, S., Fujii, K., Kladwang, W., Das, R., and Barna, M. (2015). RNA regulons in Hox 5′ UTRs confer ribosome specificity to gene regulation. Nature *517*, 33–38.

Yang, C., Zang, W., Ji, Y., Li, T., Yang, Y., and Zheng, X. (2019). Ribosomal protein L6

(RPL6) is recruited to DNA damage sites in a poly(ADP-ribose) polymerase–dependent manner and regulates the DNA damage response. Journal of Biological Chemistry *294*, 2827–2838.

Young, D.J., Makeeva, D.S., Zhang, F., Anisimova, A.S., Stolboushkina, E.A., Ghobakhlou, F., Shatsky, I.N., Dmitriev, S.E., Hinnebusch, A.G., and Guydosh, N.R. (2018). Tma64/eIF2D, Tma20/MCT-1, and Tma22/DENR Recycle Post-termination 40S Subunits In Vivo. Mol. Cell *71*, 761–774.e5.

Zhang, Y., Wolf, G.W., Bhat, K., Jin, A., Allio, T., Burkhart, W.A., and Xiong, Y. (2003). Ribosomal protein L11 negatively regulates oncoprotein MDM2 and mediates a p53-dependent ribosomal-stress checkpoint pathway. Mol. Cell. Biol. *23*, 8902–8912.

Zhu, Y., Poyurovsky, M.V., Li, Y., Biderman, L., Stahl, J., Jacq, X., and Prives, C. (2009). Ribosomal Protein S7 Is Both a Regulator and a Substrate of MDM2. Molecular Cell *35*, 316–326.

Zivraj, K.H., Tung, Y.C.L., Piper, M., Gumy, L., Fawcett, J.W., Yeo, G.S.H., and Holt, C.E. (2010). Subcellular profiling reveals distinct and developmentally regulated repertoire of growth cone mRNAs. J. Neurosci. *30*, 15464–15478.